

Petter Leira

Spectroscopic Diversity of Fluorescent Amyloid Ligand Interactions with Native Transthyretin

Master's thesis in Applied Physics and Mathematics

Supervisor: Mikael Lindgren

August 2020

Petter Leira

Spectroscopic Diversity of Fluorescent Amyloid Ligand Interactions with Native Transthyretin

Master's thesis in Applied Physics and Mathematics
Supervisor: Mikael Lindgren
August 2020

Norwegian University of Science and Technology
Faculty of Natural Sciences
Department of Physics



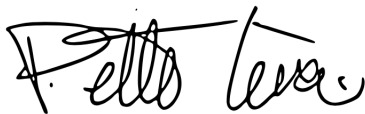
Preface

This thesis is written as a completion of the master education and to obtain the degree of Master of Science at Norwegian University of Science and Technology in Trondheim spring of 2020.

The content of a master report is normally produced in the course of 20 weeks the final semester at department of Physics, and allocates 30 credits in total. Due to the Corona lock-down during spring 2020, there was an intermission of all practical work for almost 6 weeks (March - April). Moreover, initial plans that included a visit to Linköping University to produce *in vitro* amyloid samples, had to be abandoned. Therefore, the content of the original plan was modified as outlined in the presentation of the objectives. The workload have been distributed evenly throughout the semester, with the good help of guidance every week from supervisor.

First, I would like to thank my supervisor Prof. Mikael Lindgren (Department of Physics, NTNU), for great ideas, input and advice on how to handle the problem and objective of the dissertation. Your experience, helpful discussions, and not to mention patience you have shown, is very much appreciated. I would also like to give my gratitude to Prof. Per Hammarström's group at the University of Linköping, who have synthesized and sent samples for me to investigate and do laboratory research on. Leo Juhlin, who is a student under Per Hammarström, was also of great help when it came to the subject of Molecular Docking preparation, simulation and analysis. Also, thank you Thor Bernt Melø for always showing an interest and fascination with my project, as well as contributing to useful discussions. There have also been several other contributors from the department at NTNU that have dedicated time to answer my questions about various investigated topics. Finally, I would like to thank my fiancé Shelby Grimac for your never-ending support and patience.

Trondheim August 3, 2020



Petter Leira

Summary

The protein Transthyretin (TTR) is a transport protein linked to a group of diseases called amyloidosis. Amyloidosis is characterized by protein misfolding forming toxic amyloid fibrils which are highly stable and insoluble. These protein aggregates, or depositions of TTR, are the root of diseases such as a variant of Alzheimer's disease, Carpal Tunnel Syndrome and heart failures. Characterization of the TTR protein is therefore important for better knowledge of the protein itself, and to further use this to be able to diagnose the TTR related diseases at an early stage. By this it is possible to give necessary treatments as early as possible.

Fluorescent binding probes or molecules together with photo-physical processes have shown to be a powerful method of characterization of amyloid structure by staining the protein aggregates. The probes p-FTAA, hx-FTAA, h-FTAA, Py1SA, Py2SA, X-34, BTD-SB, HS-169 and ANS, have shown to be novel amyloid binding probes used to stain the TTR protein under inspection. These probes all have the feature of characterizing the protein structure in terms of fluorescence spectra.

Absorption spectroscopy of the fluorescent binding probes and the TTR protein was performed to determine the wavelength regions accessible for excitation. Fluorescence spectroscopy was then utilized to look at spectral shifts, differences and comparisons of the probes, with and without TTR protein. Quantum efficiency and lifetime measurements were then carried out to further characterize the photo-physical processes and parameters of TTR and potential probes. Furthermore, the FRET effect was used to obtain a qualitative measure of the distance between the fluorescent probes and tryptophans in the TTR protein. From the time-resolved anisotropy it was possible to calculate the rotational diffusion time using probes with long lifetime.

Among the fluorescent probes, h-FTAA, X-34 and HS-169 in PBS showed the largest spectral shift when they are bound to TTR, where the emission spectra are substantially blue-shifted. The rest of the probes also show the trend of blue-shifting when binding to TTR. Py2SA is also showing interesting discrepancies in its emission spectrum.

Quantum efficiency measurements show an increasing trend when the probes are bound to TTR, with X-34 being the most interesting candidate with an increase from 4.7% to 44.3%. Also for lifetime measurements the probes show a general increase of in excited state lifetime when TTR is added. The probe with the longest lifetime is Py2SA with an excited state lifetime of 7.1 ns, and 31.2 ns when bound to TTR. Because of its long lifetime, it was used for calculations of the rotational dynamics of TTR. The rotational correlation time of Py2SA bound to TTR was calculated to be 19 ns. The anisotropy calculations, together with FRET results and molecular docking, show indeed that there is an interaction between the probes and the protein. With all the probes showing optical properties with TTR, they all can be used in characterization, and potentially for diagnosis tools for neurodegenerative diseases linked to TTR.

Sammendrag

Proteinet Transthyretin (TTR) er et transportprotein knyttet til en rekke sykdommer kalt amyloidose. Amyloidose er karakterisert ved at avleiringer av proteiner danner skadelige amyloidfibriller som er svært stabile og uløselige. Disse proteinaggregatene, eller avleiringene av TTR, er forbundet til sykdommer som for eksempel en type Alzheimers sykdom, karpaltunnelsyndrom og hjertesykdom. Karakterisering av TTR-proteinet er derfor viktig for å få en bedre kunnskap om selve proteinet, samt bruke dette videre for å kunne diagnostisere TTR-relaterte sykdommer i en tidlig fase. Dermed vil det være mulig å gi nødvendige behandlinger så tidlig som mulig.

Fluorescerende molekyler, eller prober, sammen med fotofysiske prosesser har vist seg å være en god metode for karakterisering av amyloidstrukturer ved å markere, eller farge, proteinaggregatene. Probene p-FTAA, hx-FTAA, h-FTAA, Py1SA, Py2SA, X-34, BTD-SB, HS-169 og ANS, har vist seg å være nye og interessante amyloidbindende molekyler som ble i denne avhandlingen brukt til å markere TTR-proteinet. Alle disse probene har gitt resultater som kan være med på å karakterisere proteinstrukturen.

Det ble gjennomført absorpsjonsspektroskopi av de fluorescerende probene og TTR-proteinet for å bestemme områdene hvor de forskjellige stoffene eksiterer. Fluorescensspektroskopi ble deretter benyttet for å se på spektrale skift, forskjeller og sammenligninger mellom probene både med og uten TTR-proteinet. Målinger av kvantegrad og levetider ble så utført for å ytterligere karakterisere de fotofysiske prosessene og parametrene til TTR, og potensielle prober. Videre ble FRET brukt for å få et kvalitativt mål på avstanden mellom diverse prober og tryptofanene i TTR-proteinet. Ved å bruke anisotropi, var det mulig å beregne rotasjonsdiffusjonstiden til TTR ved bruk av prober med lang levetid.

Blant de fluorescerende probene, var det h-FTAA, X-34 og HS-169 i PBS som viste de største spektrale skiftene når de ble bundet til TTR, der emisjonsspektrene ble vesentlig blå-skiftet. Resten av probene viste også tendensen til et blå-skiftet spekter når de ble bundet til TTR. I tillegg viste Py2SA noen interessante forandringer og avvik i sitt emisjonsspekter.

For målingene angående kvanteeffekten og kvantegraden, ser vi en økende tendens når probene blir bundet til TTR. Her er X-34 definitivt den mest interessante kandidaten, da den får en økning fra 4.7 % til 44.3 %. For målinger når det gjelder levetid av molekylene, ser vi også en økende trend når TTR tilsettes. Proben med lengst levetid er Py2SA med en eksitert levetid på 7.1 ns, og 31.2 ns når den er bundet til TTR. På grunn av lang levetid, ble denne proben brukt til beregninger av rotasjonsdynamikken til TTR. Rotasjonskorrelasjonstiden for Py2SA bundet til TTR ble beregnet til å være 19 ns. Anisotropiberegningene, sammen med FRET-resultater og molekylær dokking, viser at det faktisk er en interaksjon mellom probene og proteinet. Siden alle probene viser optiske egenskaper med TTR, kan de brukes til karakterisering, og potensielt verktøy til diagnostisering av neurodegenerative sykdommer knyttet til TTR.

Contents

Preface	i
Summary	iii
Sammendrag	v
Table of Contents	ix
List of Tables	xii
List of Figures	xviii
Nomenclature	xx
I BACKGROUND	1
1 Introduction	3
1.1 Motivation	3
1.2 Objectives	4
1.3 Approach	4
1.4 Limitations	5
1.5 Structure overview	5
2 Theoretical Background	7
2.1 Optical Absorption	7
2.2 Emission of Light	8
2.2.1 Luminescence	8
2.2.2 Quenching	12
2.3 The Quantum Efficiency	13
2.4 Excited State Lifetime	14

2.5	Fluorescence Anisotropy	15
2.6	Fluorescence Resonance Energy Transfer (FRET)	18
2.7	Computational Molecular Docking	20
3	Materials and Methods	23
3.1	Fluorescent Probes and Protein	23
3.2	Absorption Spectroscopy	26
3.3	Fluorescence Spectroscopy	27
3.4	Measuring the Quantum Yield	28
3.5	Lifetime measurements	31
3.6	Fluorescence Anisotropy measurements	32
3.7	FRET methods	34
3.8	Docking and Simulation measurements	35
3.9	Treatment of Errors	36
3.9.1	General Propagation of Uncertainty	36
3.9.2	Error calculations for Quantum Yield	37
II	RESULTS	39
4	TTR-Probe Characterization	41
4.1	Absorption Spectroscopy	41
4.2	Fluorescence Spectroscopy	45
4.3	The Quantum Efficiency	47
4.4	Lifetime measurements	51
5	Probe-TTR Interaction	55
5.1	Changes in Spectra	55
5.2	TTR characteristics	57
5.3	FRET analysis	59
6	TTR Dynamics from Fluorescence Anisotropy	63
6.1	Polarized Intensities	63
6.2	Calculated Anisotropy	64
7	Molecular Docking Calculations	67
7.1	Results of Docking	67
7.2	Comparison with X-ray Crystallography	70
III	DISCUSSION	71
8	Discussion and Limitations	73
8.1	Evaluation of the TTR-probe characterization	73
8.1.1	Absorption Spectroscopy	73
8.1.2	Fluorescence properties	74
8.1.3	Quantum Yield properties	75

8.1.4	Excited State Lifetime properties	76
8.2	Evaluation of the Probe-TTR Interaction	77
8.2.1	FRET properties	77
8.2.2	Properties of Molecular Docking	77
8.2.3	The dynamics of TTR	78
9	Conclusion and Suggested Further Work	81
9.1	Suggested Further Work	82
	Bibliography	82
A	Additional Results	89
A.1	Emission and Excitation Spectroscopy	89
A.2	The Quantum efficiency	91
A.3	Lifetime measurements	93
A.4	FRET measurements	95
A.5	Anisotropy	96
A.6	Molecular Docking	97

List of Tables

4.1	Absorption characteristics, and calculated Molar Extinction Coefficient for the fluorescent probes investigated. λ_{abs} is the wavelength where the absorption was maximum, and from which ϵ is calculated.	44
4.2	Photophysical characteristics of the samples under investigation. λ_{abs} is the wavelength of maximum absorption, λ_{ex} is the wavelength of maximum excitation, λ_{em} is the wavelength of maximum emission, and Φ_X is the calculated quantum yield with its uncertainty.	50
4.3	Lifetime characteristics of the samples investigated in this thesis. τ_1 is the first lifetime component of a multi-exponential lifetime decay, α_1 is the first component's preexponential factor, τ_2 is the second component, α_2 its factor, and τ_{avg} is the average lifetime calculated by the components and equation (2.8). For the probes HS-169 and Py2SA, all excitation and emission peaks are considered, and are chronologically specified.	54
5.1	Changes in photo-physical characteristics of the samples under investigation. $\Delta\lambda_{abs}$ is the change in wavelengths of maximum absorption, $\Delta\lambda_{ex}$ is the change in wavelengths of maximum excitation, $\Delta\lambda_{em}$ is the change in wavelengths of maximum emission, ΔSS is the change in the spectra Stokes' Shifts, $\Delta\Phi_X$ is the change in QY, and $\Delta\tau$ is the change in lifetime. Here, the probe is compared with $+/-$ differences against when it is bound to TTR. For example if $\Delta\Phi_X = +5$, the quantum yield increases by 5 when the probe is bound to TTR, compared to when it is not. For the probe HS-169, both excitation peaks are considered, and are chronologically specified. Also, when considering HS-169 (MeOH) it is compared with the TTR in PBS.	56
5.2	Photophysical characteristics of TTR and L-Trp which is a component of TTR. λ_{abs} is the wavelength of maximum absorption, λ_{ex} is the wavelength of maximum excitation, λ_{em} is the wavelength of maximum emission, SS is the Stokes' Shift, Φ_X is the calculated quantum yield with its uncertainty, and τ is the lifetime with its uncertainty.	57

5.3	FRET results for the Oligothiophenes under investigation. c-ratio is the ratio of concentration between the probe and tetrameric TTR, λ_{em} is the wavelength of maximum emission. As in table 4.3, the different components of the multi-exponential lifetime decay are given as τ_i with their respective preexponential factor (α_i) in paranthesis, if applicable. τ_{avg} is the average lifetime calculated by the components and equation (2.8).	61
5.4	Continuation of table 5.3. FRET results for the probes under investigation. c-ratio is the ratio of concentration between the probe and tetrameric TTR, λ_{em} is the wavelength of maximum emission. As in table 4.3, the different components of the multi-exponential lifetime decay are given as τ_i with their respective preexponential factor (α_i) in paranthesis, if applicable. τ_{avg} is the average lifetime calculated by the components and equation (2.8).	62
7.1	Docking results calculated from docking h-FTAA to tetrameric TTR with Autodock Vina (Trott & Olson 2010). Left- and right binding sites relative to what figure 7.1 is showing. Here, nine different binding modes or affinities are calculated, and ranked accordingly. The root-mean-square deviation is also displayed.	68
7.2	Docking results calculated from docking Py1SA to tetrameric TTR with Autodock Vina (Trott & Olson 2010). Left- and right binding sites relative to what figure 7.2 is showing. Here, nine different binding modes or affinities are calculated, and ranked accordingly. The root-mean-square deviation is also displayed.	69
A.1	Docking results calculated from docking ANS (figure A11) to tetrameric TTR.	98
A.2	Docking results calculated from docking p-FTAA (figure A10a) to tetrameric TTR.	99
A.3	Docking results calculated from docking hx-FTAA (figure A10b) to tetrameric TTR.	99
A.4	Docking results calculated from docking Py2SA (figure A10c) to tetrameric TTR.	100
A.5	Docking results calculated from docking X-34 (figure A10d) to tetrameric TTR.	100
A.6	Docking results calculated from docking BTD-SB (figure A10e) to tetrameric TTR.	101
A.7	Docking results calculated from docking HS-169 (figure A10f) to tetrameric TTR.	101

List of Figures

2.1	One typical simplified example of a Jabłoński diagram. The figure shows the different electronic states and the vibrational energy levels within them. The subscripts A , F and P stand for Absorption, Fluorescence and Phosphorescence respectively.	9
2.2	The Franck-Condon principle. This figure shows the vibrational transitions, and how some of these transitions are favored when their wave functions overlap. This is the reason for why the difference between absorbed and emitted energy is observed.	10
2.3	Normalized absorption (excitation) and fluorescence emission spectra of the fluorophore Rhodamine-6G as a function of wavelength. One can easily see the Stokes shift in the figure. Raw data are produced in lab at NTNU and plotted in Python.	11
2.4	Intensity decay figure normalized. The fluorescence lifetime, τ , is the time at which the intensity has decayed to $1/e$ of the original value. The decay of the intensity with time is given by relation (2.7). This figure features the decay of the fluorescent probe Py2SA, which has a lifetime of about 7 ns, and will be discussed in later chapters.	14
2.5	Fluorescence spectra of a donor and acceptor. X stands for the absorption (excitation) spectrum, and M stands for the emission spectrum. One can clearly see the spectra overlap between the donor’s emission spectrum and the acceptor’s excitation spectrum. Here, there is almost a full overlap! The donor in this case is the native protein TTR, and the acceptor is the fluorophore BTD-SB. These will be further discussed in later sections. . .	18
3.1	Structural representation of the native tetrameric TTR used, characterized and investigated on in this thesis. Each monomer chain is colored differently to easily distinguish the monomeric and the tetrameric structure. PDB file of the structure was forwarded from the research group at Linköping University. Figure was generated in the software PyMOL (Schrödinger, LLC 2020).	24

3.2	Chemical representation of the fluorescent probes used and investigated on in this thesis. The sketches were drawn with the chemical editor MarvinSuite (ChemAxon 2020)	25
3.3	A schematic setup of the absorption spectrophotometer. The monitoring wavelength is set by the monochromator. A beamsplitter (BS) and a mirror splits and aligns the lightbeam into two beams going to the reference solution and the sample. The detectors then detect the transmitted optical density.	26
3.4	A schematic setup of the fluorescence spectrometer. For emission spectroscopy, the detection angles are set to 90°. Excitation source is a lamp, laser or similar. Polarizer and monochromators can be used and inserted where shown. The emission intensity is then detected and sent to the computer.	28
3.5	Typical measurements of the quantum efficiency. Here, four different concentrations are measured. The sample under investigation in this figure is the probe h-FTAA together with TTR as on can see from the absorption peak around 280 nm. These data are further analysed.	29
3.6	A schematic setup of the TCSPC measurements. The top part of the setup is pretty similar to the fluorescence setup in figure 3.4 and also works in the same way. What is introduced is the delay due to the different path-lengths of the start and stop signal. See the text for more details.	31
3.7	Prompt, decay curve and model of TTR in PBS, excited at 278 nm using the NanoLED. Emission measured at 340 nm. Single exponential decay fit with a lifetime of $\tau = 3.42$ ns.	32
3.8	Time dependent steady state lifetime measurements for different polarization. These are further used to calculate and plot the anisotropy by equation (3.8). Here, the sample is X-34, excited at 403 nm, emission measured at 460 nm, and the measuring time was pre-set to 600 s.	34
4.1	Absorption spectra of some of the fluorescent probes used and investigated on in this project. All the probes, except the Pyrenes, are diluted in PBS, while the Pyrenes are diluted in MeOH. The absorption spectra have clear peaks for their excitation wavelength. See table 4.1 for more details. It is plotted as the molar extinction coefficient, ϵ , as a function of wavelength, λ	42
4.2	Absorption spectra of the fluorescent Oligothiophenes used and investigated on in this project. All of the probes with PBS as solvent. The absorption spectra have clear peaks for their excitation wavelength. See table 4.1 for more details. It is plotted as the molar extinction coefficient, ϵ , as a function of wavelength, λ	42
4.3	Absorption spectra of all the fluorescent probe HS-169 used and investigated on in this project. Here, two different solvents are used. The absorption spectra have clear peaks for their excitation wavelength, and figure show two distinct peaks for both solvents. See table 4.1 for more details. It is plotted as the molar extinction coefficient, ϵ , as a function of wavelength, λ	43

4.4	Absorption spectrum of tetrameric TTR, the protein investigated on in this project, and L-Tryptophan. The absorption spectra has clear expected peaks at an excitation wavelength around $\lambda_{abs} = 280$ nm. This absorption band is associated with the tryptophans in the protein. It is plotted as the molar extinction coefficient, ϵ , as a function of wavelength, λ	44
4.5	Excitation (green and blue) and emission (yellow and red) spectra of the fluorescent probe X-34, with and without the protein TTR.	45
4.6	Excitation (green and blue) and emission (yellow and red) spectra of the fluorescent probe Py1SA, with and without the protein TTR. Notice how two of the emission maxima around 380 nm and 410 nm disappear when bound to TTR.	46
4.7	Excitation (green and blue) and emission (yellow and red) spectra of the fluorescent probe HS-169, with and without the protein TTR. Here a long-pass filter was used.	46
4.8	Relative quantum efficiency for samples containing the fluorescent probe h-FTAA, with and without the protein TTR. Both samples are diluted in PBS. Here, the highly reliable quantum yield standard for Rhodamine-6G is used as a reference.	47
4.9	Relative quantum efficiency for samples containing the fluorescent probe Py2SA, with and without the protein TTR. The probe without the protein is diluted in MeOH, while with the protein, it is diluted in PBS. Here, the highly reliable quantum yield standard for Coumarin-102 is used as a reference.	48
4.10	Relative quantum efficiency for samples containing the fluorescent probe X-34, with and without the protein TTR. Both samples are diluted in PBS. The probe by itself is here used as the quantum yield standard, where the quantum efficiency is established to be $\Phi_R = 4.70\%$ (Zhang, Sandberg, Kongsno, Wu, Nyström, Nilsson, Konradsson, LeVine III, Lindgren & Hammarström 2018)	48
4.11	Lifetime decay of the fluorescent probe Py2SA, with and without the protein, TTR, in PBS. The samples are excited at 337 nm, and the emission is measured at 420 nm and 445 nm (The two emission maxima). Both single and double exponential decays. The average lifetimes (τ_{avg}) along with the values of its components are given in table 4.3.	51
4.12	Lifetime decay of the fluorescent probe X-34, with and without the protein, TTR, in PBS. The samples are excited at 373 nm, and the emission is measured at 510 nm. Single exponential decays. The average lifetimes (τ_{avg}) are given in table 4.3.	52
4.13	Lifetime decay of the fluorescent probe ANS, with and without the protein, TTR, in PBS. The samples are excited at 373 nm, and the emission is measured at 480 nm. Double exponential decays. The average lifetimes (τ_{avg}) along with the values of its components are given in table 4.3.	52
5.1	Excitation (green and blue) and emission (yellow and red) spectra of TTR and L-Trp	57

5.2	Relative quantum efficiency for the samples TTR and L-Trp. Both samples are diluted in PBS. Here, L-Trp itself is used as the quantum yield standard, where the quantum efficiency is established to be $\Phi_R = 0.15 \pm 0.01$ (Suzuki et al. 2009, Chen 1972).	58
5.3	Lifetime decay of TTR and L-Trp, in PBS. The samples are excited at 278 nm, and the emission is measured at 340 nm. Single exponential decays.	58
5.4	FRET measurements for the acceptor h-FTAA together with the donor TTR, using time-resolved method. The NanoLED with excitation wavelength of 278 nm is used, and the emission is observed at 350 nm.	59
5.5	FRET measurements for the acceptor X-34 together with the donor TTR, using time-resolved method. The NanoLED with excitation wavelength of 278 nm is used, and the emission is observed at 350 nm.	60
5.6	FRET measurements for the acceptor BTD-SB together with the donor TTR, using time-resolved method. The NanoLED with excitation wavelength of 278 nm is used, and the emission is observed at 350 nm.	60
6.1	Time dependent steady state lifetime measurements for different polarization of Py2SA bound to TTR. These are further used to calculate and plot the anisotropy by equation (3.8). Here, the sample is excited at 337 nm, emission measured at 416 nm, and the measuring time was pre-set to 1200 s (20 min).	64
6.2	Results of anisotropy based on the polarization intensities from figure 6.1 and calculations from equation (3.8). There is also calculated a moving average, where the average of 5 points are taken for each point. A single exponential decay was fitted with the data using equation (2.10), yielding the rotational correlation time to be $\tau_r = 19.0 \pm 4.0$, with $r_0 = 0.17$	65
6.3	Results of anisotropy based on the polarization intensities from figure A8 and calculations from equation (3.8). There is also calculated a moving average, where the average of 5 points are taken for each point. A single exponential decay was fitted with the data using equation (2.10), yielding the rotational correlation time to be $\tau_r = 4.0 \pm 0.5$, with $r_0 = 0.17$. A baseline was also fitted, where this was found to be $y_0 = -0.13$	65
6.4	Results of anisotropy based on the polarization intensities from figure A9 and calculations from equation (3.8). There is also calculated a moving average, where the average of 5 points are taken for each point. A single exponential decay was fitted with the data using equation (2.10), yielding the rotational correlation time to be $\tau_r = 0.5 \pm 0.2$, with $r_0 = 0.17$. A baseline was also fitted, where this was found to be $y_0 = -0.07$	66
7.1	Best docking, best conformation and best binding affinity of the probe h-FTAA docked to native tetrameric TTR. Each monomer of TTR is colored differently. Results calculated with Autodock Vina (Trott & Olson 2010). The chemical representation generated in the software PyMOL (Schrödinger, LLC 2020).	68

7.2	Best docking, best conformation and best binding affinity of the probe Py1SA docked to native tetrameric TTR. Results are calculated with Autodock Vina (Trott & Olson 2010). The chemical representation generated in the software PyMOL (Schrödinger, LLC 2020).	69
7.3	Py1SA docking results (blue and pink) with TTR compared with a X-ray crystallography structure of Py1SA bound to TTR, green being the crystallography structure (Full structure: TTR + Py1SA). Crystallography structure made by the research group in Linköping.	70
A1	Excitation (green and blue) and emission (yellow and red) spectra of some additional fluorescent probes characterized, with and without the protein TTR. See table 4.2 for more details on each probe, and table 5.1 for changes when the probes are bound to TTR.	89
A2	Excitation (green and blue) and emission (yellow and red) spectra of some additional fluorescent probes characterized, with and without the protein TTR. See table 4.2 for more details on each probe, and table 5.1 for changes in spectra when the probes are bound to TTR.	90
A3	Relative quantum efficiency for samples containing the fluorescent probe HS-169, with and without the protein TTR. HS-169 is both diluted in PBS and MeOH. HS-169 with the protein is diluted in PBS. C-102 and R6G are used as quantum yield standards, depending on the excitation wavelength. See table 4.2 or each figure for the measured and calculated quantum yield, and table 5.1 for the changes when HS-169 are bound to TTR.	91
A4	Relative quantum efficiency for some samples investigated in this thesis, with and without the protein TTR. C-102 and R6G are used as references. See table 4.2 or each figure for the measured and calculated quantum yield. See table 4.2 for more details on each probe, and table 5.1 for the changes in QY when the probes are bound to TTR.	92
A5	Lifetime decay of some fluorescent probes, with and without the protein, TTR, in PBS. The average lifetimes (τ_{avg}) are given in table 4.3. See table 5.1 for the changes when the probe is bound to TTR.	93
A6	Lifetime decay of the fluorescent probe HS-169 diluted in both MeOH and PBS, with and without the protein, TTR (protein in PBS). The average lifetimes (τ_{avg}) along with the values of its components are given in table 4.3. See table 5.1 for the changes when the probe is bound to TTR.	94
A7	FRET measurements for some of the samples under investigation, using time-resolved method. The donor (D) is TTR and the acceptor (A) is each probe in the figure. The NanoLED with excitation wavelength of 278 nm is used, and the emission is observed at 350 nm. See table 5.3 and table 5.4 for more details regarding the FRET effects for each probe.	95
A8	Time dependent steady state lifetime measurements for different polarization of the probe Py2SA diluted in 75 % Glycerol. These measurements are further used to calculate and plot the anisotropy by equation (3.8). Here, the sample is excited at 337 nm, emission measured at 416 nm, and the measuring time was pre-set to 1500 s (25 min). The results of anisotropy can be seen in figure 6.3.	96

A9	Time dependent steady state lifetime measurements for different polarization of the probe Py2SA diluted in PBS. These measurements are further used to calculate and plot the anisotropy by equation (3.8). Here, the sample is excited at 337 nm, emission measured at 416 nm, and the measuring time was pre-set to 2100 s (35 min).The results of anisotropy can be seen in figure 6.4	96
A10	Best docking, best conformation, and best binding affinity of some of the probes docked to the native tetrameric TTR, taken from some different angles. Results calculated with Autodock Vina (Trott & Olson 2010). The chemical representation generated in the software PyMOL (Schrödinger, LLC 2020).	97
A11	Best docking, best conformation and best binding affinity of the probe ANS docked to native tetrameric TTR. Results gathered and calculated with Autodock Vina (Trott & Olson 2010). The chemical representation generated in the software PyMOL (Schrödinger, LLC 2020).	98

Nomenclature

Acronyms

A	Acceptor
BFGS	Broyden-Fletcher-Goldfarb-Shanno method
BS	Beamsplitter
C-102	Coumarin-102
D	Donor
D-A	Donor-Acceptor
EtOH	Ethanol
FLIM	Fluorescence Lifetime Imaging Microscopy
FRET	Fluorescence (Förster) Resonance Energy Transfer
LCO	Luminescent Conjugated Oligothiophenes
M	Emission
MCA	Multi-Channel Analyzer
MD	Molecular Docking
MeOH	Methanol
NTNU	Norwegian University of Science and Technology
OD	Optical Density
PBS	Phosphate Buffered Saline
PDB	Protein Data Bank
QE	Quantum Efficiency

QY	Quantum Yield
R6G	Rhodamine-6G
S/N	Signal-to-noise ratio
SS	Stokes' Shift
TAC	Time-to-Amplitude Converter
TCSPC	Time-Correlated Single Photon Counting
Trp	Tryptophan
TTR	Transthyretin
UV	Ultra Violet
VH	Vertical-Horizontal
VV	Vertical-Vertical
X	Excitation
Xe	Xenon

Part I

BACKGROUND

Introduction

1.1 Motivation

Many diseases are caused by protein misfolding. The most famous one is the Alzheimer's disease associated with the Amyloid- β protein. Several of these diseases have in common that they are related to amyloid formation of the transport protein Transthyretin (TTR) causing senile systemic amyloidosis, familial amyloid cardiomyopathy, carpal tunnel syndrome, and familial amyloid polyneuropathy (Fikrle et al. 2013). This group of diseases is known as transthyretin amyloidosis. Amyloidosis is classified as a group of diseases where normal soluble proteins are triggered to form conformational changes that causes the protein to aggregate and form toxic amyloid fibrils. This is characterized by protein misfolding, or a destabilization of the protein's structure and can be due to mutations and changes in the physiological conditions. The amyloid fibrils that form are highly stable and insoluble and form at different places in the body. The deposition of TTR fibrils in the extracellular tissues is the root of the diseases mentioned earlier, and are also different diseases depending on where in the body it is located.

TTR is a transportation protein found in the cerebrospinal fluid and carries the thyroid hormone thyroxine, and retinol by binding to a retinol-binding protein, hence the name TTR. Being one of three major transport proteins for the thyroid hormone, along with albumin and thyroxine-binding globulin, the task is to ensure that there are appropriate levels of the hormone all around the body. TTR is also responsible for maintaining a free hormone pool in the blood and the cerebrospinal fluid. TTR is mostly synthesized in the liver and secreted into the blood plasma.

Currently, there is no cure for people affected by TTR amyloidosis. There exist, however, treatments such as liver transplantation to slow down the production of mutated TTR variants. This to prevent further formation of the fibrils caused by the mutated TTR. (Ueda & Ando 2014) There are plenty of ongoing studies and methods to prevent or cure TTR

amyloidosis, but it is also important to look at how we can detect and diagnose TTR amyloidosis. (Rambaran & Serpell 2008)

Many biological tools and techniques have been contributing to understanding the protein and the amyloid fibrils at a molecular level. Studies have shown that using photo-physical processes and small fluorescent binding molecules (or probes) have proven to be a powerful method for characterization of amyloid structure by staining protein aggregates. Here, probes such as Congo Red and Thioflavin T have been used for a long time. (Murphy 2007) More and more studies have shown that the usage of different types of binding probes prove to have a better binding sensitivity and selectivity, but also spectral characterization in fluorescence measurements than other binding probes. (Sjölander et al. 2015, 2016)

1.2 Objectives

The background and aim for this project was originally to acquire more knowledge of the protein (TTR), how it forms amyloid structures and can be characterized using several fluorescent binding probes. Due to the corona pandemic during spring 2020, the spectroscopy lab at NTNU, and the protein lab with our collaboration at Linköping University, were closed, or operating with reduced capacity during most of March until May. The initial objective and project plan was altered. No production of TTR amyloids could be carried out. Instead, the project's focus was shifted towards a more detailed investigation of the native TTR protein because it has been shown that native TTR binds to several amyloid binding probes in a hydrophobic binding site. The objectives therefore include:

- calculations of docking between fluorescent probes and TTR
- investigation of the FRET effect of the tryptophan in TTR with probes bound to the protein
- studies of rotational dynamics of TTR with certain fluorescent ligands

1.3 Approach

Investigations on how TTR interacts with several different binding probes will be characterized by using photo-physical processes. The interactions with the probes and the native protein will be tested *in vitro*. Reliable probes that interacts with the protein (TTR) can be of great importance when it comes to detection. Especially, also if the specific protein unfolds and causes amyloid depositions to be formed which lead to said diseases. Good knowledge on the protein itself, and on the different probes used for detection, are therefore important. By using these methods to characterize the protein and amyloid structure with amyloid and protein binding probes, it is possible to diagnose the diseases at an early stage. This is crucial for the involved patient, where he/she can get the treatment needed as early as possible.

By introducing and characterizing several new fluorescent binding probes to the field, a comparison, grouping and categorizing of the different probes can be done. As said earlier,

different types of binding probes have different binding sensitivity and selectivity, but also spectral characterization. This can be of interest in terms of which probe one wants to use, or which one is best to use for a certain experiment or for specific diagnostics.

1.4 Limitations

The thesis is limited to one semester, and therefore ambitious to have evaluated every aspect in a definite way. There exists countless of fluorescent binding probes that bind to TTR. Because of time limitation, a set of fluorescent probes are chosen, so that solid data and calculations can be gathered for each probe.

As briefly mentioned earlier, due to the corona pandemic during spring 2020, both the labs at NTNU and our collaborating lab at Linköping University were closed. Because the production of TTR amyloid could not be carried out, limitations such as doing comparisons and measurements on the TTR amyloids as for native TTR, are caused. From a medical point of view, the changes and comparisons of the native TTR versus the unfolded TTR are of great interest.

There is therefore room for further work to support the rationale. Further improvements and limitations of the thesis are further explained in the background and the discussion.

1.5 Structure overview

The report is divided into three parts complete with chapters and sections, covering the background, results and discussion. The remainder of the thesis will be structured as follows:

Part I Background

This part addresses diseases linked to unfolding of the proteins or amyloidosis. Further, it gives an explanation of how the protein TTR is linked to it, and a general background of the protein itself. This section will provide information necessary to understand the motivation of experimenting and uncover more information and data about the protein.

The literature also covers theoretical background behind the physics of light and the physics of the methods and experiments used to gather information about the protein and fluorescent probes. This is an important part of the thesis to understand what is going on on an atomic level.

The advantages and drawbacks of each theoretical method are assessed. Information gained from these methods is further elaborated and discussed, to understand the complexity of the system and how different system components will influence the outcome of the results.

Finally, the methodology of the approach and methods used to perform the experiments and get the results are presented. Also in this section, treatment of errors are discussed and defined.

Part II Results

Part II contains the assessed experiments, presenting a selection of the results in relevant figures, tables and pointing out interesting and important factors. It will also address changes that were made, in terms of methodology and materials, and obstacles that were met along the way, if any.

Further, the report gives an overview of the analysis of the results.

Part III Discussion

This part includes a discussion of the chosen approach, methodology, limitations, and results. It will also include discussion and comparison with similar studies and methods. This leaves the final conclusion and elaboration of further work to be assessed to support the rationale.

Chapter 2

Theoretical Background

One of the most fundamental interactions that occur in nature is the interaction between electromagnetic waves (or light) and matter. The study of how atoms and molecules react when irradiated with light is called spectroscopy (Campbell & Dwek 1984). Depending on how the molecules change the light with time and wavelength as they interact with each other, information about optical, structural, dynamic, and energetic properties of the molecules can be determined (Hecht 2016). In this chapter, several photo-physical properties are presented.

2.1 Optical Absorption

The electrons in an atom or a molecule have certain defined discrete energies, dependent on the type of atom, molecular structure and number of electrons in the complete system (Hemmer 2005). The total energy of the molecule is always as low as possible when there is no external interaction interacting with the molecule. If the system were to be given more energy, there exists a set of higher energies that the electrons may occupy. A molecule can gain this amount of energy needed to raise or change its energy from one discrete level to a higher discrete energy level. This can for instance happen by absorbing a photon from a light beam passing through the system. The electron is then excited to the higher energy level. Since the discrete energy levels are defined for different molecules (atoms, molecular structure and number of electrons in the complete system), the absorption energy spectra one can create acts therefore as fingerprints of the molecules under study.

In an absorption measurement the amount of absorbed energy is found by measuring and comparing the incoming intensity I_0 and the transmitted intensity I through a sample at different light frequencies. The absorbance, or optical density, of a sample is then defined as (Lakowicz 1999):

$$A(\omega) \equiv \log \left[\frac{I_0(\omega)}{I(\omega)} \right] = \epsilon(\omega)cl, \quad (2.1)$$

where c is the molar concentration in mol/l or M , l is the path length of the solution (thickness of the sample) usually given in cm, and $\epsilon(\omega)$ is the molar extinction coefficient. Equation (2.1) is also famously known as Beer-Lambert's law. The molar extinction coefficient is the molecular property given in units $M^{-1}\text{cm}^{-1}$, and is a measure for how strongly a chemical substance absorbs light at a particular wavelength, and is given by $\epsilon(\omega) = \sigma N_{Av} 10^{-3} \log e$. σ is the absorption cross section, and N_{Av} is Avogadro's constant. In a sample containing N molecules per unit volume, the beam passing through a slice dz of the sample, is reduced by the amount (Rutherland 2003):

$$\frac{dI}{dz} = -\sigma NI. \quad (2.2)$$

Integrating over the thickness of the sample (l) gives (Birks 1970):

$$I = I_0 e^{-\sigma Nl}, \quad (2.3)$$

which is an exponential decay of the transmitted intensity.

2.2 Emission of Light

Just as atoms and molecules are capable of absorbing light, they are also capable of emitting light. The interaction with radiation of for example an incoming photon, produces a transition probability between two energy levels of the molecule. The energy of an electronically excited state may be transferred in a variety of ways. A common fate is a non-radiative decay where the the excess energy is transferred into for example vibration, rotation and translation to other surrounding molecules. However, an electron in an upper energy level can also go through a radiative decay process, where the excited electron jump to the available lower level, emitting the excess excitation energy as a photon.

This emission of light form from electronically excited states is in general called luminescence. In all cases, the emission is a response to a particular form of input energy. If the input comes from said radiation, the emission is called photo-luminescence. The two most important types of photo-luminescence are fluorescence and phosphorescence. (Lakowicz 1999)

2.2.1 Luminescence

In fluorescence, the singlet state electron in the excited orbital is paired up to a second electron in the ground-state orbital through opposite spin. This makes the excited electron return rapidly to the ground state, leading to an emission of a photon, and the atom is fluorescing. The emission rates of fluorescence are typically in the order of 10^8 s^{-1} , which

means that the typical fluorescence lifetime is near 10 ns (10×10^{-9} s). The lifetime (τ) of a fluorophore is the average time between its excitation and its return to the ground state. This rapid emission of light is from historical reasons called fluorescence. Although, this relaxation time back to ground state seems very short, it is much longer than the stimulated transition time between electronic states, which is around 10^{-15} s. The lifetime will be further assessed in section 2.4. (Lakowicz 1999)

The fluorescent light usually have slightly lower energy than the absorbed photons. This is caused by the vibrational structure in the electronic energy levels. These processes between absorption and emission of light are usually presented as a Jabłoński diagram. A simple and typical diagram is shown in figure 2.1. This illustrates the electronic states of a molecule and transitions between them. The horizontal lines represented by S_0 , S_1 and S_2 , are the singlet ground, first, and second electronic states respectively. Each of these electronic states can be divided into a number of vibrational energy levels. These are denoted by 0, 1, 2, etc. The vertical lines represents the transitions between states, and illustrate the rapid nature of light absorption. (Lakowicz 1999)

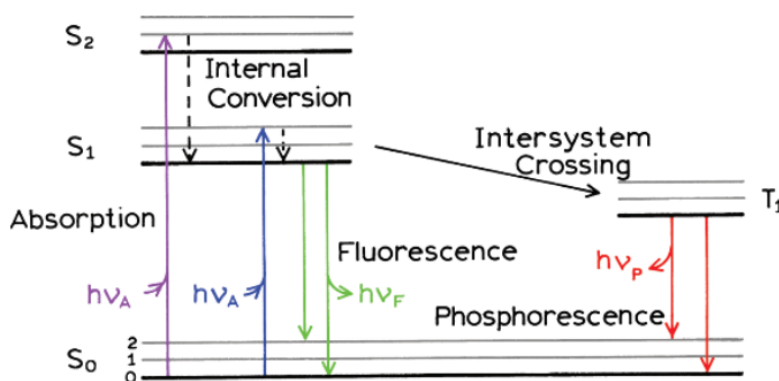


Figure 2.1: One typical simplified example of a Jabłoński diagram. The figure shows the different electronic states and the vibrational energy levels within them. The subscripts A , F and P stand for Absorption, Fluorescence and Phosphorescence respectively.

The transitions of light absorption happens in about 10^{-15} s, which is a short amount of time for a significant displacement of the nuclei. The rapid electron transition within the molecule gives rise to a change in the Coulomb force acting on the nuclei because of the redistribution of charge. This results in a change of vibrational state of the molecule and is called the Franck-Condon Principle. Figure 2.2 illustrates this principle. Since the electron is lighter and faster than the nuclei, we assume that the electron transitions are happening in the presence of a static nuclei (Born-Oppenheimer approximation) (Hemmer 2005). The Franck-Condon Principle states that the vibrational transitions between certain levels are favored when their wave functions overlap. Thus, the probability for the nuclei

to find itself in a position with minimum deviation from its initial location is higher. These transitions across vibrational states of the molecule is why we can observe the difference between the absorbed and the emitted energy.

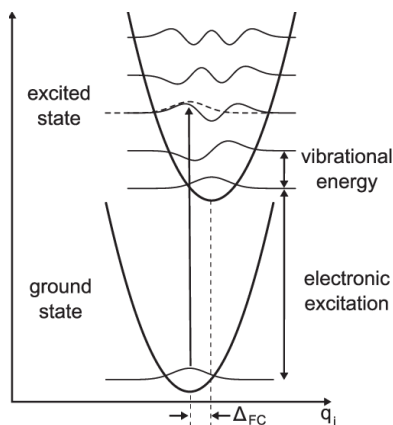


Figure 2.2: The Franck-Condon principle. This figure shows the vibrational transitions, and how some of these transitions are favored when their wave functions overlap. This is the reason for why the difference between absorbed and emitted energy is observed.

The molecule can be excited into several of the possible excited states with different energies. At room temperature the molecules will usually be at their lowest vibrational energy level because there is not enough thermal energy to significantly populate the excited vibrational levels. Therefore excitation or absorption may occur from ground state to any of the vibrational levels in either of the energy states. After being excited, the molecule goes through vibrational relaxation to its lowest vibrational level of that energy state. If the molecule is excited to a higher electronically excited state (for example S_2), the molecule will quickly relax to the first excited state (S_1), followed by vibrational relaxation of this state. This process is called internal conversion and generally occurs in 10^{-12} s or less. In this process the molecule rapidly dissipates its vibrational excitation energy as heat to the surroundings. Since this occurs much faster than the fluorescence lifetime of 10^{-8} s, the internal conversion is generally complete prior to the fluorescence. Therefore, fluorescence emission generally occurs from the lowest energy vibrational state of S_1 . The molecule may also relax to the ground state without emitting any light. This is due to collisions and energy transfer to the surroundings, known as quenching. This process is similar to the internal conversion process. Quenching will be further assessed in section 2.2.2.

Fluorescence spectral data are usually and preferably presented as both emission and excitation (absorption) spectra. Such spectra can be seen in figure 2.3. A fluorescence emission spectrum is a plot of the fluorescence intensity as a function of wavelength, measured at a single constant excitation wavelength. At the same time, a fluorescence excitation spectrum is the dependence of emission intensity as a function of excitation wavelength, measured at a single emission wavelength.

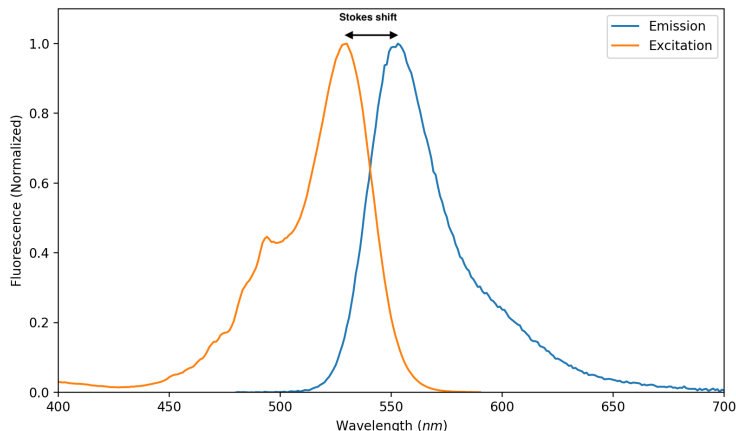


Figure 2.3: Normalized absorption (excitation) and fluorescence emission spectra of the fluorophore Rhodamine-6G as a function of wavelength. One can easily see the Stokes shift in the figure. Raw data are produced in lab at NTNU and plotted in Python.

The Stokes shift is the difference in wavelength between the peaks of the absorption (excitation) and emission spectra (Figure 2.3). It represents the energy loss due to a change in the vibrational states. The shift is typically the result of vibrational relaxation and solvent reorganization as mentioned earlier. It can be observed from the Jablonski diagram that most fluorophores display emission at lower energies (and longer wavelengths) than their absorption.

It is important to note that a fluorophore is a dipole which is surrounded by solvent molecules. Most fluorophores have larger dipole moments in the excited state than in the ground state. In solvent relaxation, rapid rotational motions of small molecules in a fluid solution reorient around the excited-state dipole. This lowers the energy of the molecule and shifts the emission to longer wavelengths. In fluorescence microscopy, a large Stokes shift is advantageous, because it makes it easier to distinguish between the excitation and emission light. (Lakowicz 1999)

Historical note

This phenomenon was first observed in a series of experiments published in 1852 by Sir G.G. Stokes. He examined a solution of sulfate of *quinine* (the ingredient in tonic water that gives it a bitter taste), which he noted was colorless due to its ability to absorb ultraviolet light. By using sunlight as a UV source and a blue stained glass window as a low-pass filter, he selectively transmitted light of wavelengths below 400 nm into the liquid solution. The incident light was high-pass filtered by a yellow glass of wine, allowing emission light from quinine fluorescence (~ 450 nm) to reach the detector. Though Stokes was able to observe the ‘beautiful celestial blue color’ that arose from the excitation of quinine, he found that ‘after passing through this [series of lens and filters], the incident light had lost the power of producing the same effect, and may therefore be considered *qualitatively different* from the original light.’ This energy loss has been attributed to the rapid decay of quinine to the lowest vibrational of S1.

2.2.2 Quenching

The intensity of fluorescence can be temporarily decreased by a wide variety of processes. Such decreases in intensity are called quenching, as briefly mentioned earlier. Quenching can also occur in different forms. Collisional quenching occurs when the excited state of a fluorophore is deactivated upon contact with another molecule in solution. This occurs through electron transfer, spin-orbit coupling and/or intersystem crossings. Inter-system crossings can be seen in the modified Jablónski diagram in figure 2.1. Here, the molecule will undergo a transition to another electronic state with different states spin multiplicity, before it undergoes phosphorescence. Phosphorescence is a much slower process, and there are many competing relaxation phenomena, such as collisions with e. g. oxygen. Therefore, in room-temperature with the solute molecules in a solvent there will not be any radiation for the equipment to pick up. Therefore, the molecule is quenched, giving out no intensity to the detectors.

Another type of quenching is the formation of nonfluorescent complexes. This is also referred as static quenching, as it occurs in the ground state and does not depend on collision or diffusion. Fluorophores bind with a quencher, or another molecule in solution, making the whole molecule nonfluorescent. It should not be confused with photobleaching, where the fluorescent molecules are irreversibly damaged.

A third form of quenching is called self-quenching, which is a subform of collisional quenching. This occurs between two identical molecules where the one molecule is initially in an excited state. This exchanges energy with second molecule that is initially in the ground state, changing both molecules simultaneously to excited states that are intermediate in energy between the two initial states. The drop in energy in the first molecule is equal to the increase in energy of the second molecule, conserving energy in so called self-quenching.

2.3 The Quantum Efficiency

When a photon is absorbed and an energetically excited state is formed, the molecule can undergo several different fates as the molecule relaxes down to ground state. These are all dependent on the nature of the molecule or fluorophore, surroundings (for example solvent) or other properties that contributes to the deactivation, or the loss of energy, and the return down to ground state. The fluorescence quantum yield, or quantum efficiency, is therefore the ratio of photons absorbed to the ratio of photons emitted through fluorescence. In other words, it gives the probability of the excited state to be emitted by fluorescence. With that said, the molecule has normally only the possibility to emit one photon for each absorbed photon. If the molecule emits one photon for each photon absorbed, we say that the molecule has a quantum efficiency of 1. The quantum yield of a process p (e. g. fluorescence) competing with N other processes is given by the rate constants as:

$$\Phi_p = \frac{k_p}{k_p + \sum_{n=1}^N k_n}. \quad (2.4)$$

Substances with the largest quantum yield, approaching unity, such as rhodamines, display the brightest emission.

The easiest way to estimate the quantum yield of a fluorophore is by comparison to known quantum yield values of well-characterized standard samples. (Brouwer 2011) Essentially, it can be assumed that solutions of the standard and test samples with identical absorbance at the same excitation wavelength will absorb the same amount of photons. Therefore, a simple ratio of the integrated fluorescence intensities of the two solutions will give the ratio of quantum yield values. The standard and test sample must have to be recorded under identical conditions. Hence, we arrive at the equation:

$$\Phi_X = \Phi_R \frac{I_X}{I_R} \frac{OD_R}{OD_X} \frac{\eta_X^2}{\eta_R^2}, \quad (2.5)$$

where the subscripts R and X denote the standard (or reference) and test samples respectively. I is the integrated fluorescence intensity, OD is the optical density, and η is the refractive index of the solvent.

2.4 Excited State Lifetime

Fluorescence lifetime is the characteristic time that a molecule remains in its excited state before returning to the ground state. Simply stated, this measure ranges from the moment that energy is absorbed by a molecule (excitation) to the moment a photon is released from said molecule (emission). As mentioned in previous sections (Stokes shift), the photon emitted will be of lower energy due to internal conversion between the vibrational energy states of the molecule. The lifetime can range from picoseconds to a few hundred nanoseconds. The formula for the lifetime of an excited molecule is given by the average time that the molecule spends in the excited state:

$$\tau = \frac{1}{k_p + \sum_{n=1}^N k_n}, \quad (2.6)$$

where k_p is the decay rate of photon emission, and k_n is the decay rate for non-radiative processes. We can see that this equation is closely related to equation (2.4), giving the quantum yield of a process.

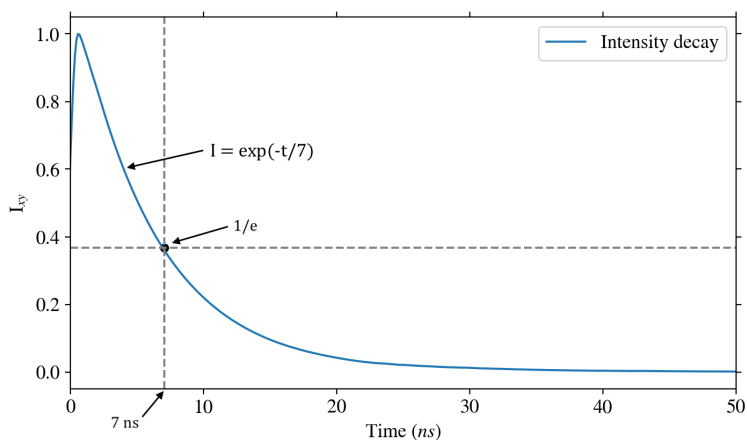


Figure 2.4: Intensity decay figure normalized. The fluorescence lifetime, τ , is the time at which the intensity has decayed to $1/e$ of the original value. The decay of the intensity with time is given by relation (2.7). This figure features the decay of the fluorescent probe Py2SA, which has a lifetime of about 7 ns, and will be discussed in later chapters.

In the impulse (or pulse) method for measuring the lifetime of fluorophores, the sample is illuminated with a short pulse of light and the intensity I of the emission versus time is recorded. Modern laser sources can generate pulses with widths on the order of picoseconds or shorter. Lifetime in this case is given by the time needed for the intensity to go down to $1/e$ or 37% of its initial value. The rate of the intensity decay is given by:

$$I(t) = I_0 e^{-\frac{t}{\tau}}, \quad (2.7)$$

where I_0 is the intensity at the initial moment $t = 0$, $I(t)$ is the intensity at time t , and τ is the lifetime. If one plots the intensity counts as logarithmic as a function of time, one can easily see that the lifetime will be proportional to the slope of the curve. If, however, the curve is of multi-exponential decays consisting of e. g. rapid and slow components, the average lifetime has to be calculated. This can be calculated by (Lakowicz 1999):

$$\tau_{avg} = \frac{\sum_i \alpha_i \tau_i^2}{\sum_i \alpha_i \tau_i}, \quad (2.8)$$

where α is the relative amplitude of the components at $t = 0$, and τ is the estimated decay time. It is summed over i , which is the degree of exponential decay.

2.5 Fluorescence Anisotropy

When a sample is excited with polarized light, many samples also tend to give out polarized emission. The extent of polarization of the emission is described in terms of the anisotropy (r). Samples that display anisotropies that are nonzero, also display polarized emission. This is based on the existence of transition moments for absorption and emission which lie along specific directions within the probes' structure. In a homogeneous solution the ground-state fluorophores are randomly oriented. When exposed to polarized light, the fluorophores that have its orientation along the electric field of the incident light, will preferentially be excited, making the excited-state population not randomly oriented (Lakowicz 1999).

Depolarization of the emission can be caused by a number of reasons, but the relative importance depends on the sample under investigation. Rotational diffusion of the fluorophores is a common cause. The anisotropy measurements reveal the average angular displacement of the fluorophore that occur between the absorption and emission of a photon, and is therefore dependent on the rate and extent of rotational diffusion during the lifetime of the excited state. These, again, depend on the viscosity of the solvent and the size and shape of the rotating molecule under investigation. For a fluorophore, a change in viscosity of its solvent, will therefore change the fluorescence anisotropy, as will be shown later.

Fluorescence anisotropy and its dependence on rotational motion has resulted in numerous application in biomedical research. For example, quantification of protein denaturation, protein association with other macromolecules, and internal dynamics of proteins, where the latter is of interest.

When one measures fluorescence anisotropy, a sample is excited with vertically polarized light, and the electric vector of the excitation light is oriented parallel to the vertical or z-axis. One can then measure the the intensity of the emission through another polarizer.

When the emission polarizer is oriented parallel (\parallel) to the excitation polarizer, the observed intensity is called I_{\parallel} . Likewise, when it is perpendicular (\perp) to the excitation polarizer, the intensity is called I_{\perp} . With these, it is possible to calculate the anisotropy (Jabłoński 1960):

$$r = \frac{I_{\parallel} - I_{\perp}}{I_{\parallel} + 2I_{\perp}} = \frac{(I_{\parallel}/I_{\perp}) - 1}{(I_{\parallel}/I_{\perp}) + 2}, \quad (2.9)$$

where the anisotropy (r) is a dimensionless quantity, and the total intensity is given as $I_T = I_{\parallel} + 2I_{\perp}$. Since also measurements of anisotropy follow pulsed excitations, as lifetime measurements in section 2.4 do (see figure 2.4), the decay of fluorescence anisotropy [$r(t)$] of a sphere is given by:

$$r(t) = r_0 e^{-t/\tau_r}, \quad (2.10)$$

where r_0 is the anisotropy at the initial moment $t = 0$, and τ_r is the rotational correlation time of the sphere. Here, the rotational correlation time of the fluorophore (τ_r) is given by:

$$\tau_r = \frac{\eta V}{RT} = \frac{\eta M}{RT} (\bar{v} + h), \quad (2.11)$$

where η is the viscosity, T is the temperature in kelvin (K), R is the gas constant, and V is the volume of the rotating unit. If it is a protein under investigation, the volume is approximately related to the molecular weight (M), the specific volume ($\bar{v} = 0.73 \text{ ml/g}$), and hydration ($h = 0.23 \text{ g of } H_2O \text{ per gram of protein}$) of the protein.

The theory of fluorescence anisotropy can be derived considering a single spherical molecule (Weber 1965). We can for a brief moment assume that the absorption and emission transition moments are parallel. We can also assume that a single molecule is oriented with some angles θ relative to the z -axis and angle ϕ relative to the y -axis. And of course, the molecule will be randomly oriented in an isotropic solvent. The goal is to calculate the anisotropy that would be observed for this oriented molecule in the absence of rotational diffusion. The conditions of parallel dipoles, immobility, and random ground-state orientation simplify the derivation.

It is also known that fluorescing fluorophores behave like radiation dipoles (Selényi 1939). With this, the intensity projections can be described by:

$$I_{\parallel}(\theta, \phi) = \cos^2 \theta, \quad (2.12)$$

$$I_{\perp}(\theta, \phi) = \sin^2 \theta \sin^2 \phi. \quad (2.13)$$

In an experiment there will be many fluorophores with a random distribution. The anisotropy is therefore calculated by performing the appropriate average based on excitation photo-selection. This meaning, how the selected molecules contribute to the measured intensity. Since excitation polarized along the z -axis yields the equal probability of excitation for all

molecules having an angle ϕ on the y-axis, the ϕ dependence can be eliminated since the average value of $\sin^2 \phi$ equals:

$$\langle \sin^2 \phi \rangle = \frac{\int_0^{2\pi} \sin^2 \phi d\phi}{\int_0^{2\pi} d\phi} = \frac{1}{2}, \quad (2.14)$$

and simplifies equation (2.13) and gives:

$$I_{\perp}(\theta) = \frac{1}{2} \sin^2 \theta. \quad (2.15)$$

If we now assume that we are observing a collection of fluorophores which are oriented relative to the z-axis with a probability $f(\theta)$, the measured intensities for this selection of molecules are going to be:

$$I_{\parallel} = \int_0^{\pi/2} f(\theta) \cos^2 \theta d\theta = k \langle \cos^2 \theta \rangle, \quad (2.16)$$

$$I_{\perp} = \frac{1}{2} \int_0^{\pi/2} f(\theta) \sin^2 \theta d\theta = \frac{k}{2} \langle \sin^2 \theta \rangle, \quad (2.17)$$

where $f(\theta) d\theta$ is the probability of a fluorophore being oriented between θ and $\theta + d\theta$, and k is an instrumental constant. By inserting these into equation (2.9), and using the identity $\sin^2 \theta = 1 - \cos^2 \theta$, one finds that:

$$r = \frac{3 \langle \cos^2 \theta \rangle - 1}{2}, \quad (2.18)$$

which means the anisotropy is determined by the average value of $\cos^2 \theta$, where θ is the angle of the emission dipole relative to the z-axis. If a single fluorophore is oriented along the z-axis, with collinear transitions, $\theta = 0$ and $r = 1.0$, where the average value of $\langle \cos^2 \theta \rangle = \frac{1}{3}$. In practice, it is not possible to obtain a perfectly oriented excited-state population with optical excitation of homogeneous solutions, and the anisotropies are therefore always less than 1.0. For most fluorophores the transition moments are rarely collinear, and the maximum anisotropy is found to be in fact 0.4 for higher population of fluorophores ($\langle \cos^2 \theta \rangle = \frac{3}{5}$). This is considerably smaller than the what is possible for a single fluorophore. The reason for this is the photoselection of the excited fluorophores. When a sample is illuminated with polarized light, the molecules with their absorption transition moments aligned with the electric vector of the polarized incident light have the highest probability of absorption. The dipole need not be exactly aligned to be absorbed. Therefore, a symmetrical probability distribution of excited fluorophores is formed around the z-axis, which determines the maximum photoselection that can be obtained using one-photon excitation of an isotropic solution.

2.6 Fluorescence Resonance Energy Transfer (FRET)

Fluorescence (Förster) Resonance Energy Transfer (FRET) is transfer or radiationless transmission of excited-state energy from a initially excited donor (D) molecule to an acceptor (A) molecule. This means that the donor molecules typically emit at a shorter wavelength which overlap with absorption spectrum of the acceptor molecules. As said, this transmission is radiationless, and occurs without the appearance of a photon. It is a result of long dipole-dipole interactions between the donor and acceptor. The transfer of energy leads to a reduction in the donor's fluorescence intensity, the excited state lifetime of the donor, and an increase in the acceptor's emission intensity. For the rate of energy transfer, there are a couple of conditions that need to be met. It depends on the extent of spectral overlap between emission spectrum of the donor and the absorption spectrum of the acceptor (see Figure 2.5). It also depends on the quantum yield of the donor. The orientation of the donor and acceptor transition dipoles needs to be approximately parallel. And of course the distance between the donor and acceptor molecules must be in close proximity of each other for them to interact. This is typically $10 - 100 \text{ \AA}$.

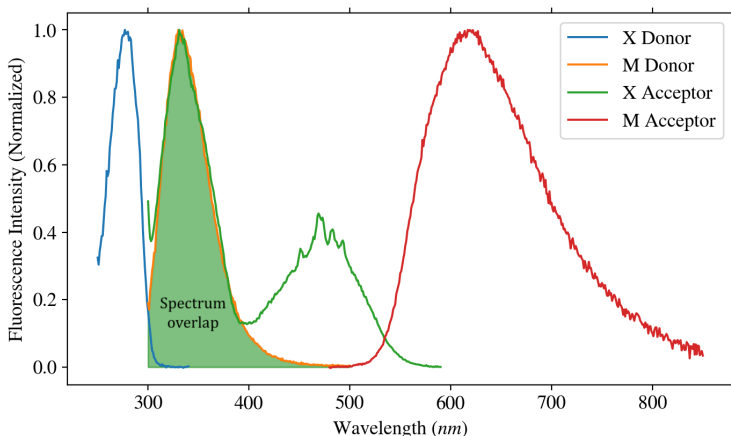


Figure 2.5: Fluorescence spectra of a donor and acceptor. *X* stands for the absorption (excitation) spectrum, and *M* stands for the emission spectrum. One can clearly see the spectra overlap between the donor's emission spectrum and the acceptor's excitation spectrum. Here, there is almost a full overlap! The donor in this case is the native protein TTR, and the acceptor is the fluorophore BTD-SB. These will be further discussed in later sections.

The distance dependence has resulted in the method of FRET being used more and more in biomedical research, for example to measure distances between donors and acceptors and investigate molecular interactions. Typically, a protein is labeled with with a donor and an acceptor. The donor is typically a tryptophan residue, and a ligand can be atypical acceptor. If there is a single D-A pair, and if the distance between the donor and acceptor does not change during the excited-state lifetime, the distance can be determined from the efficiency of energy transfer. The transfer-efficiency can be determined by the quenching

of the donor due to addition of the acceptor. Theodor Förster demonstrated that the transfer efficiency depends on the inverse sixth-distance between donor and acceptor by (Förster 1948):

$$E = \frac{R_0^6}{R_0^6 + r_F^6}, \quad (2.19)$$

where E is the transfer efficiency of the process, and therefore also the quantum yield of the energy transfer transition. R_0 is the Förster distance, which is the distance where the energy transfer is 50% efficient. r_F is the actual distance from the donor to acceptor, and one can see that if $r_F = R_0$, then the transfer efficiency is equal to 50%. The Förster distance is typically and most useful around 20 – 90 Å, which is comparable to the dimensions of biological macromolecules. These distances are comparable to the diameter of several proteins, thickness of biological membranes, and distances between sites on multisubunit proteins, such as TTR. Any process that affect the distance between donor and acceptor, affects the transfer rate, allowing the process to be quantified through FRET measurements. This has resulted in FRET being referred to as a "spectroscopic ruler" (Stryer 1978).

The Förster distance (R_0) is dependent on a number of factors, such as fluorescence quantum yield of the donor in the absence of the acceptor (Φ_D), the refractive index of the solvent or medium (η), the dipole angular orientation of each molecule (κ), and the spectral overlap integral of the donor and acceptor ($J(\lambda)$) (See figure 2.5). This is expressed by:

$$R_0 = 9.78 \times 10^3 [\kappa^2 \eta^{-4} \Phi_D J(\lambda)]^{\frac{1}{6}}, \quad (2.20)$$

in Ångströms (Å). Together with equation (2.19), it is possible to draw some lines and examples with equation (2.20). If, say, R_0 is arbitrarily set to 1, and the distance between donor and acceptor is also equal to 1, then $r_F = R_0$, and the transfer efficiency is 50% by equation (2.19). If the distance between donor and acceptor is ten times closer than the Förster length ($r_F = 0.1R_0$), then the transfer efficiency equals to $E = 0.999999$, and is considerably more efficient. However, if the distance is twice the Förster distance ($r_F = 2R_0$), then the transfer efficiency is $E = 1.56\%$, and is considerably decreased. The efficiency quickly increases to 1.0 as the D-A distance decreases just below R_0 , and at the same time quickly decreases to zero if r_F is greater than R_0 . As a result, this extreme sensitivity for distance is what allows FRET to be used for proximity experiments.

The transfer efficiency can be calculated from the lifetimes in the absence (τ_D) and presence of acceptor (τ_{DA}) (Lakowicz 1999):

$$E = 1 - \frac{\tau_{DA}}{\tau_D}. \quad (2.21)$$

Generally, when conditions for FRET to occur are met, both the excited state of the donor and the energy transferred to the now excited acceptor, will compete for the decay of

excitation energy. With resonance energy transfer, the photon is not emitted, but rather the energy is transferred to the acceptor molecule, whose electrons in turn become excited as described for the donor molecule. The subsequent return to the ground state emits a photon.

2.7 Computational Molecular Docking

Molecular docking is a computational procedure that attempts to predict noncovalent binding of macromolecules or of a macromolecule (receptor) and a small molecule (like a ligand) efficiently. This can be directly from their unbound structures, structures obtained from MD simulations, or homology modeling. The main goal of molecular docking is to predict the bound conformations and the binding affinity. The prediction of binding of small molecules to proteins is of practical importance when it comes to trying to predict the bound conformations of known binders, when the experimental structures are unavailable. (Trott & Olson 2010)

Docking generally assumes that much or all of the receptor is rigid, and that the covalent lengths and angles are constant, all while considering a chosen set of covalent bonds that are freely rotatable (or active rotatable bonds). While molecular dynamics directly deals with energies, docking focuses on reproducing chemical potential, which determine the bound conformation preference and the free energy of binding. With this, the concept is influenced by the minima in the energy profile, the shape of the energy profile, and the temperature (Gilson et al. 1997, Chang et al. 2007).

Molecular docking programs usually use a scoring function that can be used to approximate the standard chemical potential of the system under investigation. When the superficially physics-based terms like the 6–12 van der Waals interactions and Coulomb energies are used in the scoring function, they need to be empirically weighted, to account for this difference between energies and free energies (Gilson et al. 1997, Chang et al. 2007). The scoring function are therefore tuned to recognize the promising conformations and predict the binding affinity as best as possible.

The general functional form of the conformational-dependent part of the scoring function generally used, for example in the program *Autodock Vina* which is used here (Trott & Olson 2010), can be expressed as:

$$c = \sum_{i < j} f_{t_i t_j}(r_{ij}), \quad (2.22)$$

where the summation is over all of the pairs that can move relative to each other, normally excluding 1–4 interactions, for example atoms separated by 3 consecutive covalent bonds. Here, each atom i is assigned a type t_i . A symmetric set of interaction functions $f_{t_i t_j}$ of the interatomic distance r_{ij} is also defined. This value, c , can also be seen as a sum of intermolecular and intramolecular contributions:

$$c = c_{inter} + c_{intra}. \quad (2.23)$$

The optimization algorithm, which will be further assessed, attempts to find the global minimum of c and other low-scoring conformations, which it then ranks. The interaction functions $f_{t_i t_j}$ are defined relative to the surface distance $d_{ij} = r_{ij} - R_{t_i} - R_{t_j}$ (Jain 1996):

$$f_{t_i t_j}(r_{ij}) = h_{t_i t_j}(d_{ij}), \quad (2.24)$$

where R_t is the van der Waals radius of atom type t . In the scoring function, $h_{t_i t_j}$ is a weighted sum of steric interactions identical for all atom pairs, hydrophobic interaction between hydrophobic atoms, and hydrogen bonding.

In Autodock Vina, an Iterated Local Search global optimizer is implemented as the optimization algorithm (Abagyan et al. 1994). Here, a succession of steps consisting of a mutation and a local optimization are taken, with each step being accepted according to a Metropolis criterion. In this implementation, Broyden-Fletcher-Goldfarb-Shanno (BFGS) (Nocedal & Wright 1999) method is used. This local optimization is an efficient quasi-Newton method. Like other quasi-Newton optimization methods, BFGS uses both the value of the scoring function and the gradient, the derivatives of the scoring function with respect to its arguments that is. In this case, the arguments are the position and orientation of the ligand, as well as the values of the torsions for the active rotatable bonds in the ligand and flexible residues.

Materials and Methods

The methodical approach will be influenced by both qualitative and quantitative research. The information gathered will provide insights, while at the same time it is necessary to collect measurable data and statistics to formulate facts. The following sections presents the important aspects of the methods applied to assess the experiments and analysis. Irradiating atoms and molecules with electromagnetic radiation such as light, and then studying the resulting reaction is a method that is known as spectroscopy. Spectroscopy is a useful method to determine structural and dynamical properties of atoms and molecules.

3.1 Fluorescent Probes and Protein

The fluorescent probes were synthesised and sent from the University of Linköping. The university used an automatic liquid chromatography system for the purification of a TTR wild type. The software UNICORN 7.0.1 was used to run the system and analyse the results, where the software is provided by GE Healthcare. To concentrate the protein, they used a Centriprep Centrifugal filter device with Ultracel 10K membrane. For the determination of the protein concentration, a Nanodrop Spectrophotometer wave-scan function was first used to obtain the absorbance at 280 nm where tyrosine and tryptophan absorb. PBS was used as reference and an absorbance spectrum ranging from 450 to 250 nm. The obtained absorbance was then calculated by using Beer-Lambert's law, seen in equation (2.1), using an extinction coefficient of $18450 \text{ M}^{-1} \text{ cm}^{-1}$ for TTR monomer. (Duong 2019)

Monomeric TTR in human consists of 127 amino acids. TTR mainly exists as a homotrimer *in vivo* with a molecular weight of approximately 55 kDa. The monomeric subunits consists of 8 β -strands forming 2 β -sheets, and a small α -helix of 9 amino acids. The four subunits of the tetramer form a β -barrel structure. See figure 3.1 for a representation of the tetrameric structure. The central channel going through the protein, or the tetrameric TTR, has two thyroxine binding sites.

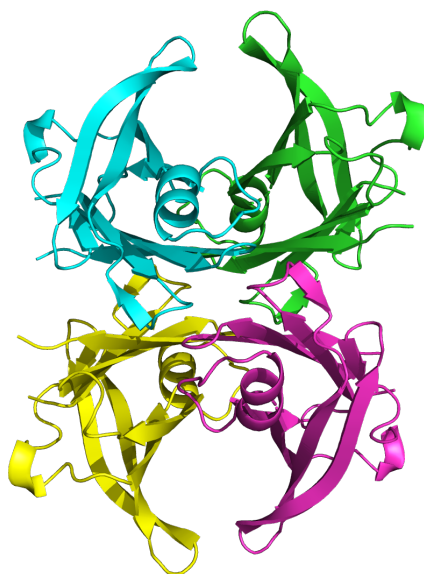


Figure 3.1: Structural representation of the native tetrameric TTR used, characterized and investigated on in this thesis. Each monomer chain is colored differently to easily distinguish the monomeric and the tetrameric structure. PDB file of the structure was forwarded from the research group at Linköping University. Figure was generated in the software PyMOL (Schrödinger, LLC 2020).

The probes, or the small fluorescent molecules, used in this project are there to stain the protein for further inspections, and can be powerful tools. In this thesis, three probes belonging to the group called Luminescent Conjugated Oligothiophenes (LCO's) are investigated, which include pentameric-, hexameric- and heptameric forms of formyl thiophene acetic acid (*p-FTAA*, *hx-FTAA* and *h-FTAA* respectively) (Klingstedt, Åslund, Simon, Johansson, Mason & Nyström 2011). Two pyrene based trans-stilbene salicylic acids (*Py1SA* and *Py2SA*) are also characterized. The salicylate bis-styrylbenzene (*X-34*), and its benzothiadiazole stilbene derivative (*BTD-SB*), are also included in the project. Also, the pentameric thiophene version with a central BTD moiety (*HS-169*), is included in the characterization. Lastly, the probe 1-amino-8-naphtalene sulfonate (*ANS*) is included in the thesis. See figure 3.2 for a chemical representation of the fluorescent probes. It is interesting to look at these probes because of their previous study with amyloid- β proteins and tau fibrils. They have here been used to characterize these proteins and have shown great potential (Zhang et al. 2019, Lindgren et al. 2005, Campos et al. 2016).

The fluorescent probes and the protein were then retrieved and transported to the laboratory at NTNU for investigations. The stock solutions of the probes had a concentration ranging from 0.5 mM to 1.5 mM, while the protein had a tetrameric concentration of 24 μ M and therefore a monomeric concentration of 96 μ M. The concentrated samples were further diluted into stock solutions used for further inspections.

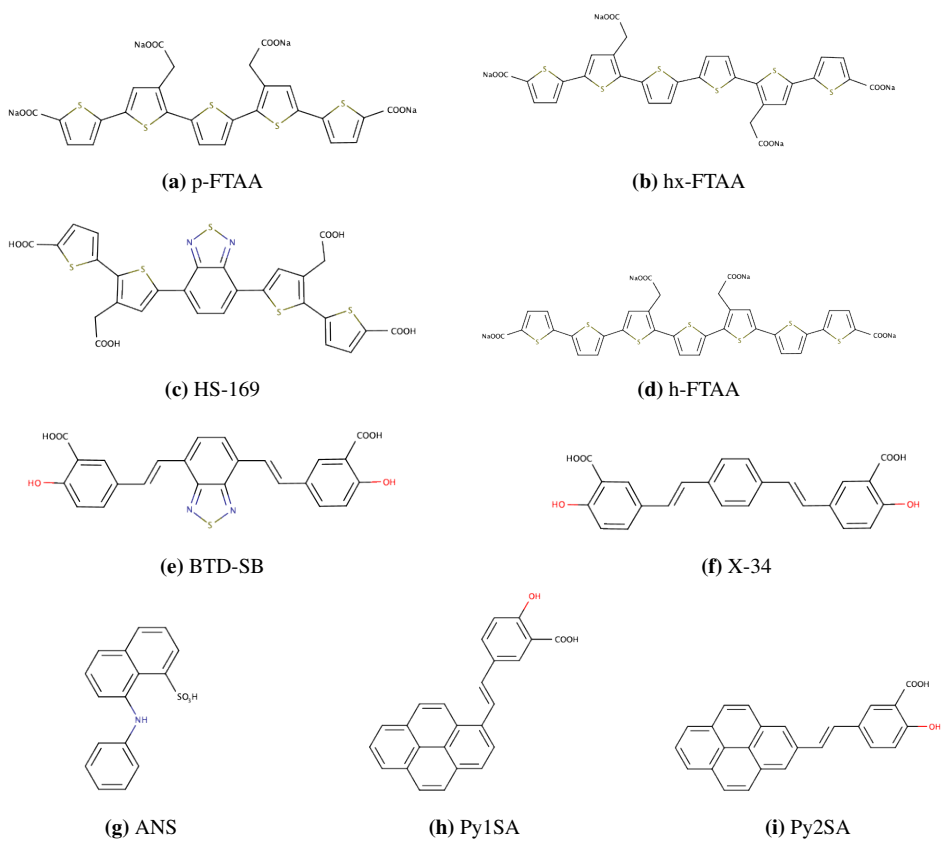


Figure 3.2: Chemical representation of the fluorescent probes used and investigated on in this thesis. The sketches were drawn with the chemical editor MarvinSuite (ChemAxon 2020)

3.2 Absorption Spectroscopy

Absorption is measured by varying the frequency of the applied radiation and measuring the absorbed energy at each frequency or wavelength. The absorption spectrum is gathered as the absorbance, A , as a function of the wavelength, λ . It can then either be plotted as this, or plotted as the extinction coefficient, ϵ , as a function of wavelength, λ , or wavenumber. This can be done by using equation (2.1). From the $\epsilon(\lambda)$ -function, two parameters are often extracted to characterize molecular absorption band. This being the position of the maximum (λ_{max}) and the value of the extinction coefficient at λ_{max} .

The studied molecules were dissolved or diluted in organic and inorganic solvents, which include phosphate-buffered saline (PBS), ethanol (EtOH) and methanol (MeOH). The solvents and molecules were measured by using 10 mm quartz cells, or cuvettes, suitable for spectroscopy and the spectrophotometers used. Quartz cells are used for their high transparency and low absorption, particularly at the UV-side of the spectrum. There will still be some absorption from both the solvent and the cell, so a reference sample also has to be prepared to account for this. The reference sample contains pure solvent and uses an equal quartz cell as the sample. Then, a measurement of the sample and the reference can be obtained at the same time, and the molecular absorbance compared and calculated from the transmitted intensity. The specific spectrophotometer setup can be seen in figure 3.3 (Glimsdal 2009).

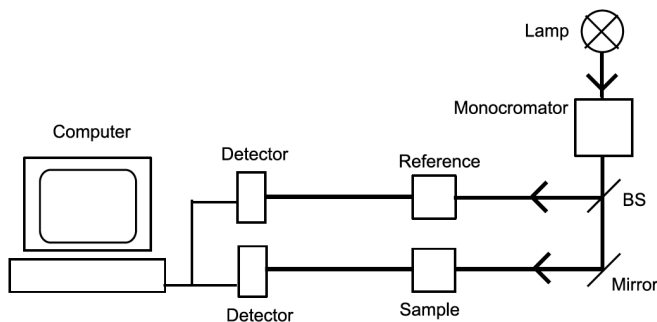


Figure 3.3: A schematic setup of the absorption spectrophotometer. The monitoring wavelength is set by the monochromator. A beamsplitter (BS) and a mirror splits and aligns the lightbeam into two beams going to the reference solution and the sample. The detectors then detect the transmitted optical density.

If a cell has an absorption A_c , the solvent has a absorption A_s and the sample an absorption of A , then the total observed absorbance is given by:

$$A_{tot} = A + A_c + A_s, \quad (3.1)$$

where the the subscripts stands for cell and solvent respectively. Therefore, to account for the difference in beam intensity in the two paths, a baseline has to be found. By using the reference together with the sample, we are therefore able to use this as a baseline and

collect the difference in transmitted intensity. The reference contains pure solvent and have an equal glass cell. The molecular absorbance for each wavelength we are interested in, is therefore obtained and calculated by:

$$A = A_{tot} - A_{ref} = (A + A_c + A_s) - (A_c + A_s). \quad (3.2)$$

The absorbance is normally measured in the visible light (400 – 700 nm) and the UV (200 – 400 nm) regions, as the photon energy needed to excite these molecule into a higher electronic state is here (Campbell & Dwek 1984).

To achieve steady state optical absorption, the absorbance were recorded after waiting 30 minutes for the spectrophotometer to warm up. For steady state conditions, the measurements were also done in room-temperature. The samples are also diluted enough so that the absorbance will be lower than 1.0 to give optimized results. The concentration of the probes were all diluted down to 5 μ M solutions, which are all in the acceptable interval. The optical absorbance were measured using a Shimadzu UV-1601PC UV-Visible Spectrophotometer with the software UV-Probe. For measurements where samples have the protein in it, the spectrophotometer of the type Hitachi U-3010 with an integrating sphere were used. The integrating sphere are there to collect the transmitted light. This to overcome the angular dependence of spread light. With this spectrophotometer, the software UV-Solutions were used.

3.3 Fluorescence Spectroscopy

With emission and excitation spectroscopy we are able to study new features with the molecules, such as the time dependence, binding properties, and polarisation properties of the transitions. We can further with the emission spectra compare them with the newly gathered absorption spectra, at for which wavelengths the excited molecules emit light (photons). The strengths of the emissions at different wavelengths can also be measured. As mentioned, the fluorescence usually occurs at longer wavelengths than that of the absorption. The maximum of the fluorescence intensity is characteristic for the fluorescence spectrum giving the position and wavelength at which the molecule will fluoresce.

In the fluorescence spectroscopy the method is quite similar to the absorbance spectroscopy, however the setup and output is different. Instead of looking at the transmitted optical density, we are now looking at the fluorescence or the emission of light. See figure 3.4 for a simple overview of the setup (Glimsdal 2009). Here, the quartz cuvettes mentioned in section 3.2 are used, but also quartz cuvettes with length 4 mm. This is done to reserve some of the solvents and samples, as it is of limited supply. A reference for a baseline is not required, as the collection geometry is usually at the right angle from the excitation direction, minimizing any background signal. A reference sample of the solvent is, however, desired to have to get an accurate result. These are weak scattering processes detectable with a sensitive spectrometer. Also, some solvents can have some residual impurities that might contribute. These effects are readily accounted for by subtracting the 'baseline' of the reference solvent. Compared to the absorption spectroscopy, it is not necessary to do a new measurement for the solvent for a new sample, if both samples have the same solvent.

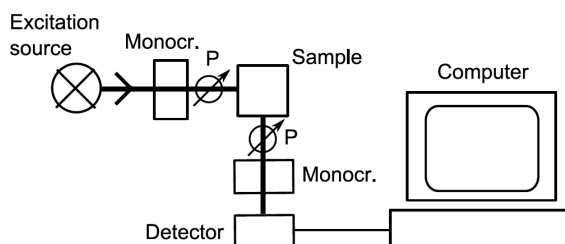


Figure 3.4: A schematic setup of the fluorescence spectrometer. For emission spectroscopy, the detection angles are set to 90° . Excitation source is a lamp, laser or similar. Polarizer and monochromators can be used and inserted where shown. The emission intensity is then detected and sent to the computer.

For the probes with the protein measurements, the protein and probes are diluted down to $1 \mu\text{M}$ having a 1 : 1 relationship in concentration. These are not strict concentrations to follow, but they give a high enough intensity for the fluorescence and affinity analysis. For the samples without the protein, the concentration for the probes are kept the same. These samples are further used in the quantum yield measurements.

The same settings are used for each set of probe and protein measurement. This to assure approximately same conditions when it comes down to comparing the sample with and without the protein. These settings include excitation wavelength, slit widths, scan speed, etc. The steady-state fluorescence spectra were recorded using a HORIBA Scientific PTI QM-8075-22 fluorescence spectrophotometer equipped with a Xe-lamp. For measurements done below an excitation wavelength of 350 nm, the long-pass filter GG055 was used to block spurious signals from the UV-region. The software used was FelixGX Data Analysis.

3.4 Measuring the Quantum Yield

As mentioned earlier, the most reliable and easiest way to measure the quantum yield of an unknown sample is by using the comparative method. This involves using well characterised standard samples (previously recorded and therefore known quantum yields of other samples), and careful and precise methods. Measuring the quantum efficiency is a sensitive measurement, so all settings and methods and measurements must be done carefully.

First, the standard samples need to be chosen, where these should absorb at the same excitation wavelength as the test sample, and preferably emit in a similar region as the test sample. The next thing one has to think about is the concentration range of the reference and test samples. To minimize re-absorption effects, absorbance should not exceed 0.1 for a 10 mm cuvette at the excitation wavelength. (Lakowicz 1999) Over this limit the non-linearity will appear and the calculated quantum efficiency may be incorrect. The cuvettes should be kept clean and the solvent should be of spectroscopic grade and should be subtracted as the background in the calculations.

The next step will be to measure the quantum efficiency. This is easiest done by using the concentrations as when measuring the emission and excitation, where the start concentration is in the range we are after. The absorbance spectrum of the chosen sample is then recorded, and the value of absorbance for the excitation wavelength is then noted. Then, the fluorescence spectrum of the same sample (same concentration) is recorded. The integrated intensity (area) of the fluorescence spectrum is then calculated and noted down. Here it is important that one has taken the solvent into account, and it is the corrected fluorescence spectrum that is analysed. After this the concentration of the sample is increased. The measuring of the absorbance and integrated fluorescence is repeated for 3–5 concentrations (See figure 3.5). The absorbance of the last solution, or the sample with the highest concentration, should preferably be lower or around 0.1. Then these data points are plotted together, and the result should approximately be a straight line with a gradient and the intercept at 0. The same measurements are then taken for the reference and remaining samples, and it is therefore possible to compare the measurements and calculate the quantum efficiency of the sample of interest. This is done by using equation (2.5), where I/OD is the same as the gradient of the measurements of the different samples. (Beeby 2019)

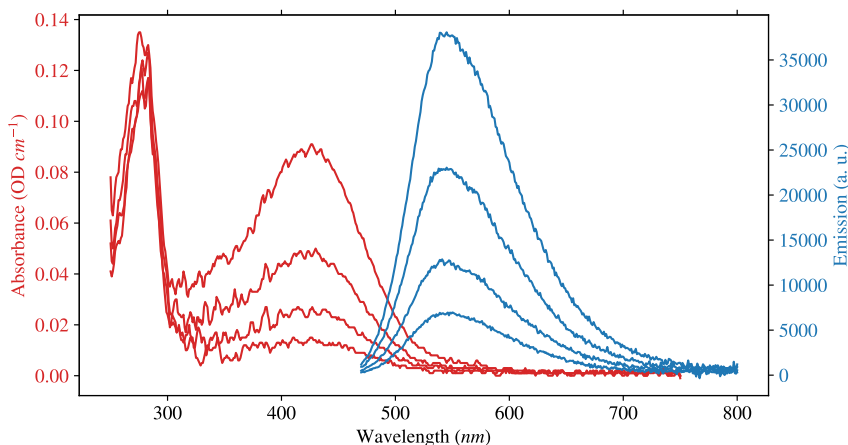


Figure 3.5: Typical measurements of the quantum efficiency. Here, four different concentrations are measured. The sample under investigation in this figure is the probe h-FTAA together with TTR as one can see from the absorption peak around 280 nm. These data are further analysed.

All the settings of the equipment have to be kept constant for the samples and concentrations one wants to compare. This to be sure the samples have the same conditions and do not vary in intensity. Also, for steady state measurements, the samples were measured in room-temperature. If for example a change in slit happens, the fluorescence intensity will change compared to what it would originally have. This will make the measurements wrong and lead to an error in the quantum efficiency.

Following equation (2.5), refractive indices (η) are needed to calculate the quantum yield

of a given sample. Since it is assumed that the refractive index does not change by the presence of a solute, the refractive indices of the solvents can be used. The following refractive indices were used (Daimon & Masumura 2007, Kozma et al. 2005) for room temperature measurements:

- PBS: $n = 1.34$
- MeOH: $n = 1.34$
- EtOH: $n = 1.37$

The standard reference samples with known quantum yields are also needed to calculate the absolute quantum efficiencies. Several standards have been investigated, but the quantum yields sometimes differ between authors (Rurack & Spieles 2011, Melnikov et al. 2017). It is therefore important to do proper research and investigations on standard to use and trust. In order to characterize the studied samples, the standards Rhodamine-6G and Coumarin-102 has been used as references. These were obtained from the company Sigma Aldrich, and came in solid powdered state. They reference samples were made by dissolving these powders in appropriate solvents and concentration. Sometimes the probes themselves have also proven to be reliable, when they have been characterized previously. The quantum yield for Rhodamine-6G is given by Brouwer (2011), and for Coumarin-102 is given by Rurack & Spieles (2011), and are:

- Rhodamine-6G in EtOH: $\Phi_R = 0.94 \pm 0.015$
- Coumarin-102 in EtOH: $\Phi_R = 0.764 \pm 0.041$
- Coumarin-102 in MeOH: $\Phi_R = 0.77 \pm 0.060$

For measuring the quantum yield, the same spectrophotometer was used as for the absorption spectroscopy in section 3.2. The same fluorometer was also used as in the fluorescence spectroscopy in section 3.3.

3.5 Lifetime measurements

The setup of the lifetime measurements are quite similar to the fluorescence spectroscopy. The additions to the setup will be the pulsed light-source, a trigger/sync, a delay, a multi-channel analyzer (MCA) and a separate software (See figure 3.6).

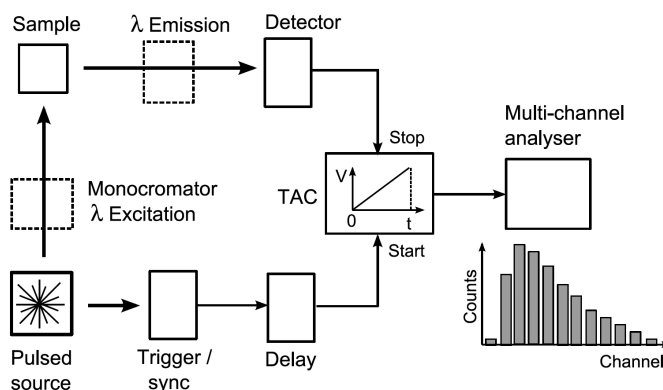


Figure 3.6: A schematic setup of the TCSPC measurements. The top part of the setup is pretty similar to the fluorescence setup in figure 3.4 and also works in the same way. What is introduced is the delay due to the different path-lengths of the start and stop signal. See the text for more details.

The most used method for lifetime measurements, and photon counting in general, is the Time-Correlated Single-Photon Counting (TCSPC) technique (Lakowicz 1999). This technique is based on the principle that the statistical probability distribution of a single emitted photon is equal to the distribution of the actual intensity as a function of time for all photons emitted. The pulsed light-source will generate a short excitation pulse, exciting the sample. The same pulse will be the start of measurement or the system controls and will trigger the the excitation source internally in the sample. After the sample is excited, the sample will emit photons based on the probability for spontaneous emission. The TCSPC technique is using a time-to-amplitude converter (TAC), meaning it is producing a voltage amplitude which is proportional to the time between the start and end of measurement signal. The voltage can then be converted to a time channel by a multi-channel analyser (MCA). The sample is repetitively excited, making a histogram of counts as a function of time, and it is possible to analyse it for the lifetime of the sample by fitting a curve by equation (2.7).

Even though the short pulsed excitation is used, and the system has a short response time in TCSPC mode, the excitation pulse can not be considered a δ -function (Lakowicz 1999). This requires an additional recording of the instrumental response function of the excitation pulse, frequently called the prompt. We need to know the prompt in order to analyze the decay curve and fit a decay model to it (either single or double exponential). See figure 3.7 for an example of a decay created by the instrument. The prompt signal also contain some time-uncertainties from other sources in the detector elements. The prompt is usually measured with a solution of nanoparticles, or the solvent itself if it is of spectroscopic

grade.

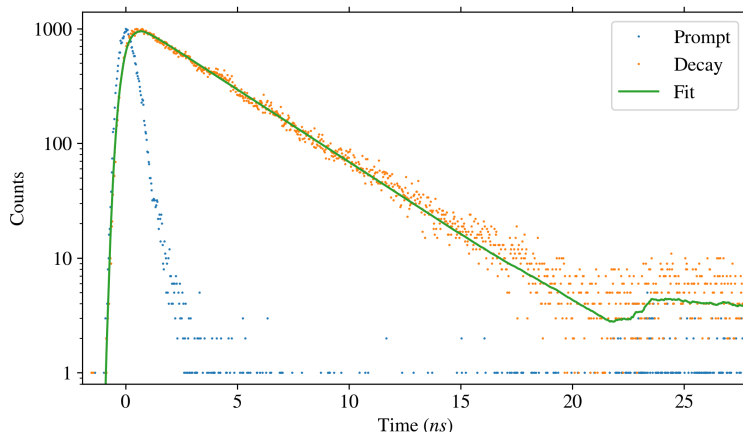


Figure 3.7: Prompt, decay curve and model of TTR in PBS, excited at 278 nm using the NanoLED. Emission measured at 340 nm. Single exponential decay fit with a lifetime of $\tau = 3.42$ ns.

For excitation sources, Horiba NanoLEDs of suitable wavelength were chosen. This is dependent of the sample under investigation. The fluorescence lifetime measurements were obtained using a Jobin Yvon IBH FluoroCube photon-counting spectrometer with a TBX-PS photon detection module, and all samples were measured in room-temperature conditions. The software used was IBH Data Analysis. In the fitting procedure of this software, the convolution of the prompt-signal was included. This gives rise to the odd feature at the end of the decay trace of the fitted signal (> 22 ns) in figure 3.7, as the resulting decay fit-function is convoluted with the prompt signal in the presentation of the fitted curve and can be written as (Birch & Imhof 1999):

$$F(t) = \int_0^t P(t')i(t-t')dt', \quad (3.3)$$

where $F(t)$ is the actual measured relaxation curve, $P(t)$ is the instrumental response function, $i(t)$ being the theoretical response function (with δ -function excitation), and the integral goes over the excitation response function.

3.6 Fluorescence Anisotropy measurements

For the measurements of Fluorescence Anisotropy, the same setup, instruments and software can be used as for the lifetime measurements in section 3.5. An addition to the setup are the two very important polarizers. One excitation polarizer and one emission polarizer. The setup is therefore a combination of figure 3.4 and figure 3.6, where one can see the

polarizers placed correctly in the fluorescence setup. It is easy to see that rotation of the emission polarizer changes the intensity when measuring.

So by equation (2.9), one would want to measure the intensities of I_{\parallel} and I_{\perp} . I_{\parallel} is given by vertically polarized excited light and vertically polarized emitted light. For simplicity, the notation I_{VV} is going to be used, where the two subscripts VV stands for vertical-vertical (in the order of excited-emitted). The same goes for I_{VH} , where it corresponds to the intensity given by vertically polarized excitation and horizontally polarized emission. However, for vertically polarized excitation, the observed polarized intensities are:

$$I_{VV} = kS_V I_{\parallel}, \quad (3.4)$$

$$I_{VH} = kS_H I_{\perp}, \quad (3.5)$$

where S_V and S_H are the sensitivities of the emission channel for the vertically and horizontally polarized components, respectively, and k is a proportionality factor to account for the quantum yield of the fluorophore and other instrumental factors. By dividing the two equations (3.4) and (3.5), we get:

$$\frac{I_{VV}}{I_{VH}} = \frac{S_V}{S_H} \frac{I_{\parallel}}{I_{\perp}} = G \frac{I_{\parallel}}{I_{\perp}}, \quad (3.6)$$

where the G -factor is introduced as the ratio of sensitivities of the detection system for vertically and horizontally polarized light. To get the actual intensity relationship (I_{\parallel}/I_{\perp}), the G -factor has to be determined. This is easily measured using horizontally polarized excitation. This is because both polarizers orientations are perpendicular to the polarization of the excitation. Therefore, any measured difference between I_{HV} and I_{HH} must be due to instrumental factors. We get:

$$\frac{I_{HV}}{I_{HH}} = \frac{S_V}{S_H} \frac{I_{\perp}}{I_{\perp}} = \frac{S_V}{S_H} = G. \quad (3.7)$$

By using the equation of anisotropy (2.9) together with equation (3.7) of the G -factor, and equation (3.6), the ratio anisotropy can be found by:

$$R = \frac{I_{VV} - GI_{VH}}{I_{VV} + 2GI_{VH}}, \quad (3.8)$$

As in section 3.5 for the lifetime measurement, the TCSPC technique is used. Here, four measurements have to be taken, one for each intensity (I_{VV} , I_{VH} , I_{HV} and I_{HH}). See figure 3.8. One then calculate the anisotropy (R) from equation (3.8), and plots it as a function of time. One can then fit a single exponential as in equation (2.10) and get the parameters for rotational correlation time of the sample. Since measuring anisotropy is delicate, and is fragile to noise, one should take measurements with as many counts as possible. Here, measuring times are pre-set, and are ranging from 600 s (10 min) to 2100 s (35 min), depending on the signal from the sample.

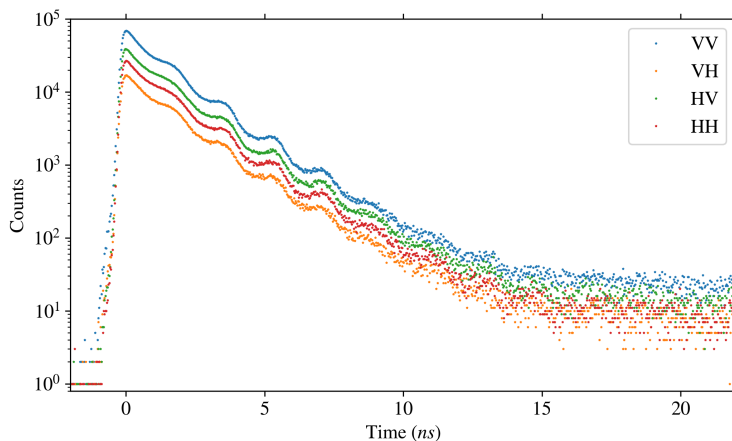


Figure 3.8: Time dependent steady state lifetime measurements for different polarization. These are further used to calculate and plot the anisotropy by equation (3.8). Here, the sample is X-34, excited at 403 nm, emission measured at 460 nm, and the measuring time was pre-set to 600 s.

3.7 FRET methods

Another characterization of TTR and probes, is to measure the FRET effects and check if they apply to certain D-A pairs. To measure FRET effects between the donor molecule (TTR) and the acceptor molecules (probes), the method of time-resolved measurements is used. For D-A pairs, the time-resolved data can be used to recover the conformational distribution or distance distribution between the donor and acceptor (Grinvald et al. 1972, Haas et al. 1975, 1978).

For measuring the FRET effects, the lifetimes of the donor is measured separately, and then with different concentrations of the acceptor molecule. Here, the concentration relationships 0.5 : 1, 1 : 1, 2 : 1 and 4 : 1 are used, as the relationship being acceptor to donor concentrations. The concentration of tetrameric TTR (D) was kept around 1 μM . This means that for each probe, four lifetime measurements needs to be taken in addition to the donor itself. These time-resolved intensity decay data were taken and gathered with the same setup, instrument, software and methods as the lifetime measurements in section 3.5. The NanoLED with excitation wavelength of 278 nm was chosen, as TTR (the donor) that contain tryptophan residues, is excited at this wavelength. The emission was measured around 350 nm as this is where TTR is emitting light.

The fluorescence spectra of the samples also need to be taken after every concentration change. With this, one can observe the quenching of the donor, and see if the spectra get shifted. The emission and excitation spectra were gathered with the setup, instruments, software and methods from the fluorescence spectroscopy in section 3.3.

3.8 Docking and Simulation measurements

As mentioned in the theoretical methods section of computational molecular docking (section 2.7), the program Autodock Vina is frequently used for molecular docking calculations and predictions. There exists other programs as well, but for the necessity in this thesis, Autodock Vina is more than good enough. The input files of Autodock Vina is in the format .PDBQT, so the program *AutodockTools* from the package *MGLTools* (Sanner 1999, Morris et al. 2009) must be used to prepare the samples for the docking calculations. To view the output files and docking results from Autodock Vina, a graphical molecular viewer, or a GUI, has to be used. Here, the molecular visualization program *PyMOL* is used (Schrödinger, LLC 2020).

With molecular docking simulations, there is a general workflow that is followed:

1. Downloading/creating ligands and preparing them for docking
2. Downloading protein structures from e. g. the protein database.
3. For Autodock Vina, converting and preparing the gathered .PDB files of the ligands and protein to .PDBQT files
4. Assigning a grid box / search space for the target protein, i. e. the area where the docking procedure will generate poses
5. Running the docking procedure in Autodock Vina
6. Evaluating the results using PyMOL

For the first and second point, the most common way is to download ligands and proteins from the free and open repository containing information about 3D structures of both large and small biological molecules in the standard .PDB format, but it is also possible to draw and prepare the molecules oneself. The native TTR (protein) file was sent from the research group at Linköping University. However, since there were trouble finding the right ligands or probes in the Protein Data Bank, the probes were made. The ligands were drawn and optimized with the chemical editor *MarvinSuite* (ChemAxon 2020), and specifically with the program *MarvinSketch*. In *MarvinSketch*, it is possible to 3D optimize the molecules, but one has to be careful with the protonation states as well eventual chiral centers and tautomeric states when drawing the molecules. With *MarvinSketch*, it is possible to export the file directly as a .PDB file. Before the ligands are loaded into *AutodockTools* and used for the docking process, they need to be energy minimized, so that they contain correct angles and bond lengths, etc. This can be done using the PRODRG server (Schüttelkopf & van Aalten 2004).

Since Autodock Vina only takes the .PDBQT format as input files, the .PDB files have to be converted. The protein and ligands are loaded into *AutodockTools* to further prepare the files and convert them. First the protein file is loaded in. Most .PDB structures do not have hydrogens, so they have to be added because it is required by the .PDBQT format. With *AutodockTools*, it is possible to add polar hydrogens. Now the grid box, or the area of the receptor where the docking program will be looking for docked information of the ligand, has to be defined. The more extended the search space is, the longer the calculations will

take. For the native TTR, the area was chosen to be large, almost covering the whole protein. Now the protein and ligands can be exported as .PDBQT files and run in Autodock Vina. Autodock Vina creates a log file, where all the calculations are made, and new output .PDBQT files with the calculated conformations that be generated and viewed in PyMOL.

3.9 Treatment of Errors

A part of doing experimental work is to take errors and uncertainties into account. Errors can be calculated manually for example from a dataset of measurements, it can already be implemented in the software the data is gathered from, or it can be a combination of the two. Here, both are considered. The errors in fluorescence are not of particular importance except for the integrated values gathered when calculating the quantum yields. The error of associated with these measurements will be included in the calculations of quantum yield. The fluorescence lifetime software (IBH Data Analysis) provides the standard deviation of the calculations and the fitted curves. However, for the anisotropy measurements this has to be calculated manually. For the molecular docking and simulation calculations, Autodock Vina provides uncertainty calculations as well in terms of binding affinity, and gives the root mean square deviation.

3.9.1 General Propagation of Uncertainty

All experimental measurements have some uncertainty to them. Sources of uncertainty can be (Kirchner 1995):

- statistical error / random variation of replicate measurements
- spatial and temporal variability
- systemic errors (bias)
- imprecise definitions or unrepresentative samples
- uncertainty in the form of the function relating y to x_1, x_2, x_3 , etc.

A quantity y is given by other variables x_1, x_2, x_3 , etc., such that:

$$y = f(x_1, x_2, x_3, \dots). \quad (3.9)$$

To find the uncertainty of y , and how it is related to x_1, x_2, x_3 , etc., a function g has to be found such that the uncertainty of y can be computed from the uncertainties of its components parts:

$$s_y = g(s_{x_1}, s_{x_2}, s_{x_3}, \dots). \quad (3.10)$$

The uncertainty can be estimated by the average value of y , or the *standard error* of y , from the standard values of the individual components means. The uncertainty can also be calculated in individual estimates of y , or the *standard deviation*, using the same principle,

but where the inputs are already the standard deviations of the variables, rather than the standard errors of their means. The standard deviation is given by (Squires 2001, Fornasini 2008, Ku 1966):

$$s_x = \sqrt{s_x^2} = \sqrt{\frac{\sum (x - \bar{x})^2}{n - 1}}, \quad (3.11)$$

where \bar{x} is the mean and s_x^2 is the variance. The standard error of the mean is given by:

$$s_{\bar{x}} = \frac{s_x}{\sqrt{n}}. \quad (3.12)$$

Some important, but simple rules when it comes to calculating uncertainty include:

$$\frac{s_{\bar{y}}}{\bar{y}} = \sqrt{\left(\frac{s_{\bar{x}_1}}{\bar{x}_1}\right)^2 + \left(\frac{s_{\bar{x}_2}}{\bar{x}_2}\right)^2 + \left(\frac{s_{\bar{x}_3}}{\bar{x}_3}\right)^2 + \dots}, \quad (3.13)$$

which is the rule when calculating sums and differences, in a combination for when calculating products and ratios. You can also have a function f that is non-linear and the standard error is then approximated by the Gaussian error propagation rule:

$$s_{\bar{y}} \approx \sqrt{\left(\frac{\delta y}{\delta x_1} s_{\bar{x}_1}\right)^2 + \left(\frac{\delta y}{\delta x_2} s_{\bar{x}_2}\right)^2 + \left(\frac{\delta y}{\delta x_3} s_{\bar{x}_3}\right)^2 + \dots}, \quad (3.14)$$

where $\delta y/\delta x_1$, etc. are the partial derivatives of y with respect to its component variables.

3.9.2 Error calculations for Quantum Yield

When analysing the quantum efficiency data, it is based on a gradient of a straight line starting in the origin and passing through several data points. The straight line, $y = ax + b$, is fitted to the data points to find the best line which passes as closely as possible through all the points. This is usually done through the least squares method (Squires 2001). If the n data points come in pairs (x_i, y_i) the best values for a and b are found by taking the minimum of the function:

$$S = \sum_n (y_i - ax_i - b)^2. \quad (3.15)$$

It then follows that the best values for a and b are found from:

$$a = \frac{\sum (x_i - \bar{x})y_i}{\sum (x_i - \bar{x})^2}, \quad (3.16)$$

and

$$b = \bar{y} - a\bar{x}, \quad (3.17)$$

where \bar{x} and \bar{y} are the mean values given by $\bar{x} = \frac{1}{n} \sum x_i$ and $\bar{y} = \frac{1}{n} \sum y_i$ respectively.

The standard errors, or uncertainties, of the fitted data are then given by equations (3.11), (3.12), (3.16), (3.17) and (3.13), giving:

$$(\Delta a)^2 = \frac{1}{n-2} \frac{\sum (y_i - ax_i - b)^2}{\sum (x_i - \bar{x})^2}, \quad (3.18)$$

and

$$(\Delta b)^2 = \left(\frac{1}{n} + \frac{\bar{x}^2}{\sum (x_i - \bar{x})^2} \right) \frac{\sum (y_i - ax_i - b)^2}{(n-2)}. \quad (3.19)$$

The measured data, the best fit, including the uncertainty is presented as $\Phi = a \pm \Delta a$. The total uncertainty in a new quantum efficiency value is, however, also dependent on the uncertainty of the quantum efficiency value of the reference, so this has to be taken into consideration.

Part II

RESULTS

TTR-Probe Characterization

Several probes were tested and experimented on in this master's thesis. The photophysical properties were characterized by employing the methods described in Chapter 2 and 3, for both the probes and for the probes bound to native TTR. With this characterization, the compounds can be compared and the TTR-probe interaction can be analysed. The compounds showing the most amount of interest and change, can further be analysed in other methods such as TTR dynamics, Anisotropy, etc. The purpose was to set up a database for further studies of amyloid structures involving the TTR protein.

4.1 Absorption Spectroscopy

The first step of the spectroscopic characterization of the probes is to gather the absorption spectra. These were measured, and can be seen in figure 4.1, figure 4.2 and figure 4.3. Also, the absorption spectra for TTR and L-Trp were measured, and are displayed in figure 4.4. By looking at these absorption spectra, it is possible to determine the excitation wavelength, or for which wavelengths of light the samples are absorbing. These wavelengths can then be used to gather fluorescence data that will be further elaborated in the next sections.

As mentioned earlier, all probes have a concentration of 5 μM for their absorption characterization. By this, it is possible to use equation (2.1), and plot the absorbance as the molar extinction coefficient, ϵ .

To have such a similar molecular structure, the pyrenes, Py1SA and Py2SA, are quite different when it comes to the absorption characteristics and spectral identities, as one can see in figure 4.1. Py2SA got for example its characteristic twin peaks at 320 nm and 340 nm, while Py1SA got a single broad peak at around 350 nm. X-34 got a more normal and broad peak around 360 nm, while BTD-SB has two sharp spectral absorption peaks at 330 nm and 470 nm with a relatively high molar extinction coefficient and absorption,

especially for the peak at higher energy transition.

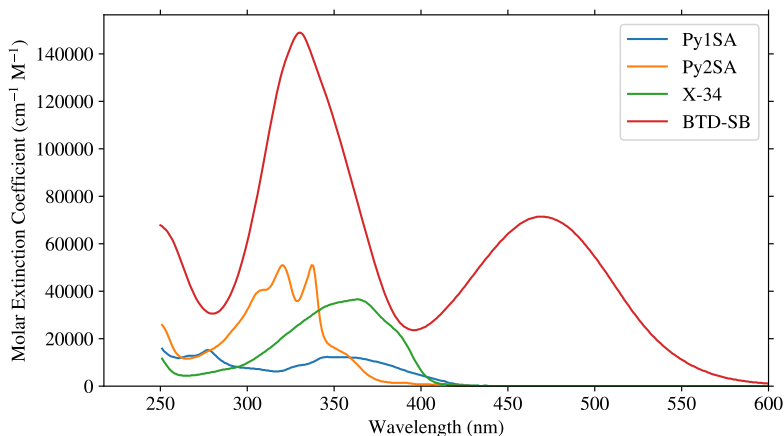


Figure 4.1: Absorption spectra of some of the fluorescent probes used and investigated on in this project. All the probes, except the Pyrenes, are diluted in PBS, while the Pyrenes are diluted in MeOH. The absorption spectra have clear peaks for their excitation wavelength. See table 4.1 for more details. It is plotted as the molar extinction coefficient, ϵ , as a function of wavelength, λ .

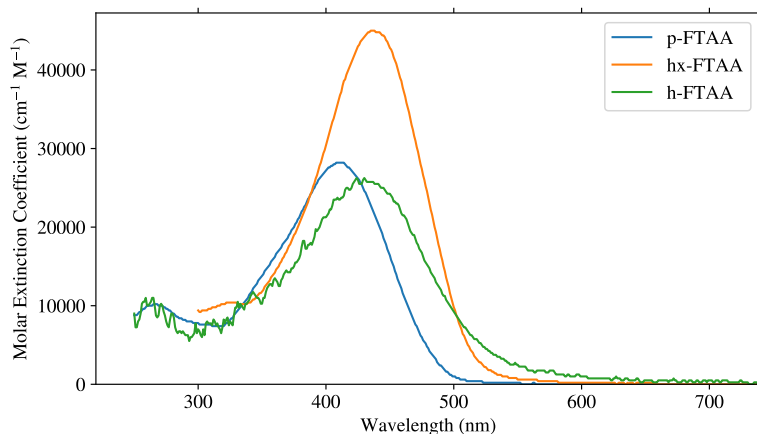


Figure 4.2: Absorption spectra of the fluorescent Oligothiophenes used and investigated on in this project. All of the probes with PBS as solvent. The absorption spectra have clear peaks for their excitation wavelength. See table 4.1 for more details. It is plotted as the molar extinction coefficient, ϵ , as a function of wavelength, λ .

The Oligothiophenes in figure 4.2, show quite the same spectral identities with only small shifts of the peaks in the spectra. p-FTAA, hx-FTAA and h-FTAA having peaks at 410 nm, 440 nm and 420 nm respectively, making them quite similar in spectral peak position (Klingstedt, Åslund, Simon, Johansson, Mason, Nyström, Hammarström & Nilsson 2011). Interestingly, the hexamer has an absorption with higher extinction coefficient at a lower photon energy.

HS-169 were diluted in two solvents, as figure 4.3 shows. Both samples show quite similar spectral characteristics by having two peaks at around 360 nm and 500 nm, where the higher energy peak is slightly blue-shifted for the sample diluted in MeOH.

Figure 4.4 shows the absorbance spectrum of TTR and L-Trp. They both show an expected absorbance peak around 280 nm (Suzuki et al. 2009, Chen 1972). Notice also how the peak is quite sharp, and depletes to zero almost right over the 300 nm mark. The extinction coefficient of TTR and L-Trp were found to be around $77300 \text{ M}^{-1}\text{cm}^{-1}$ and $5400 \text{ M}^{-1}\text{cm}^{-1}$ for tetrameric TTR and L-Trp respectively at $\lambda = 280 \text{ nm}$, and correlates well to previous studies (Mangrolia & Murphy 2018, Du et al. 1998). Figure 4.4 compares the tetrameric TTR that contains 8 Trp per tetramer TTR, with a single Trp.

For more details about the spectral peaks, molar extinction coefficient and solvent for the different samples, it is referred to table 4.1.

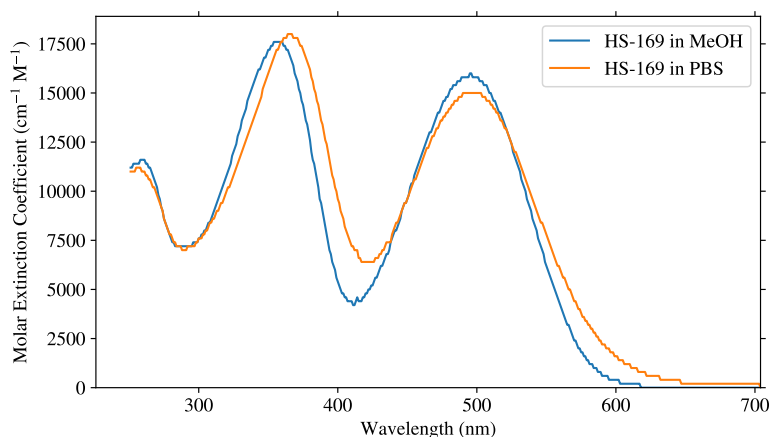


Figure 4.3: Absorption spectra of all the fluorescent probe HS-169 used and investigated on in this project. Here, two different solvents are used. The absorption spectra have clear peaks for their excitation wavelength, and figure show two distinct peaks for both solvents. See table 4.1 for more details. It is plotted as the molar extinction coefficient, ϵ , as a function of wavelength, λ .

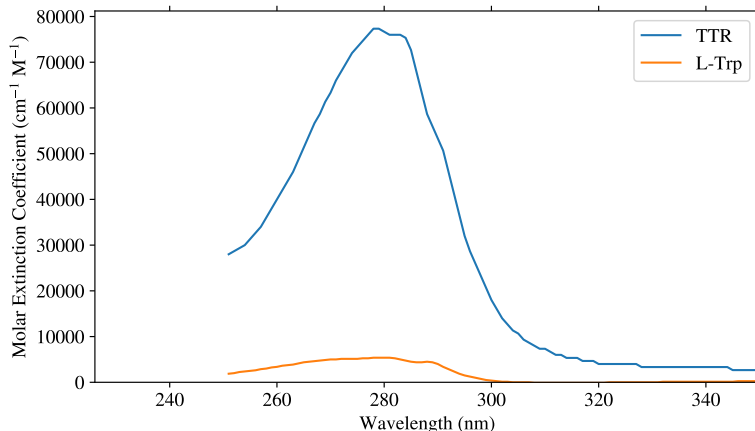


Figure 4.4: Absorption spectrum of tetrameric TTR, the protein investigated on in this project, and L-Tryptophan. The absorption spectra has clear expected peaks at an excitation wavelength around $\lambda_{abs} = 280$ nm. This absorption band is associated with the tryptophans in the protein. It is plotted as the molar extinction coefficient, ϵ , as a function of wavelength, λ .

Table 4.1: Absorption characteristics, and calculated Molar Extinction Coefficient for the fluorescent probes investigated. λ_{abs} is the wavelength where the absorption was maximum, and from which ϵ is calculated.

Sample	λ_{abs} (nm)	ϵ ($10^4 \text{ M}^{-1} \text{ cm}^{-1}$)	Solvent
p-FTAA	410	2.82	PBS
hx-FTAA	436	4.50	PBS
h-FTAA	424	2.63	PBS
Py1SA	346	1.24	MeOH
Py2SA	320	5.10	MeOH
Py2SA	337	5.10	MeOH
X-34	363	3.66	PBS
BTD-SB	330	14.9	PBS
BTD-SB	469	7.14	PBS
HS-169	365	1.80	PBS
HS-169	496	1.50	PBS
HS-169	356	1.76	MeOH
HS-169	495	1.60	MeOH
TTR	279	7.73	PBS
L-Trp	280	0.54	PBS

4.2 Fluorescence Spectroscopy

By using the new information it is possible to measure fluorescence spectroscopy data of the samples as well. Here, emission and excitation spectra are taken of all the probes, with and without the protein. For the emission spectrum, the excitation wavelength is chosen to be the maximum absorption wavelength, λ_{abs} , measured from the previous results. In this section, the results that were of most interest are displayed. To see the results from the other probes that are not displayed in this section, it is referred to appendix A.1.

In figure 4.5 we see the excitation and emission spectra of X-34, with and without TTR. The spectra are normalized to 1. This to get a good representation of the differences or spectral shifts that occur when adding TTR. As expected, the excitation maximum is about the same as in the absorption spectroscopy. The excitation spectrum is measured by the emission maximum, which is found to be around 510 nm. When TTR is added, the whole spectrum shifts substantially towards the ultraviolet side of the visible spectrum, by almost 50 nm. We can also see the excitation spectrum gets red-shifted. More details of the results are in table 4.2.

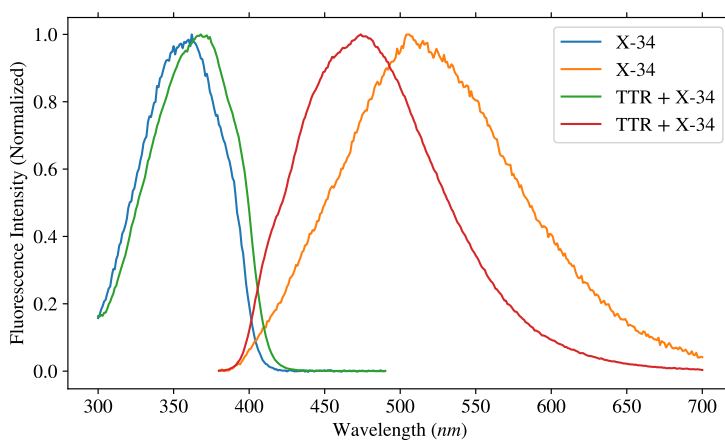


Figure 4.5: Excitation (green and blue) and emission (yellow and red) spectra of the fluorescent probe X-34, with and without the protein TTR.

Figure 4.6 shows the excitation and emission spectra of PyISA, with and without the protein. Also here the excitation maximum shows similar traits as in the absorption spectroscopy. The emission maximum is found to be around 525 nm, with two small twin peaks at 390 nm and 410 nm. When adding the TTR, the excitation spectrum is red-shifted. The emission maximum stays the same and the spectrum does not shift. However, the two small twin peaks disappear, and do not give the same intensity as they used to. More details are in table 4.2.

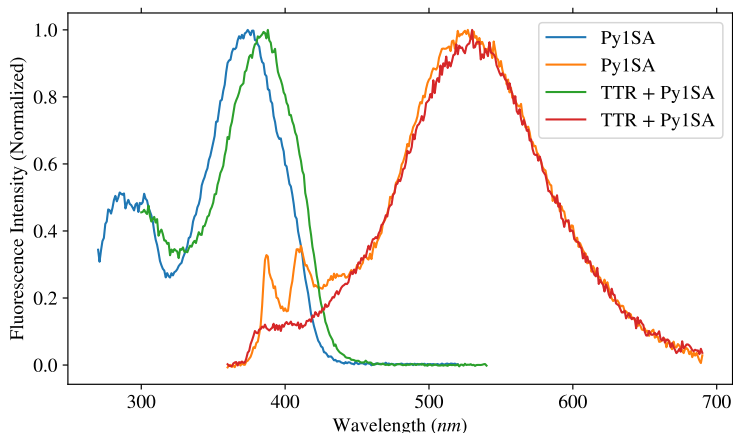


Figure 4.6: Excitation (green and blue) and emission (yellow and red) spectra of the fluorescent probe Py1SA, with and without the protein TTR. Notice how two of the emission maxima around 380 nm and 410 nm disappear when bound to TTR.

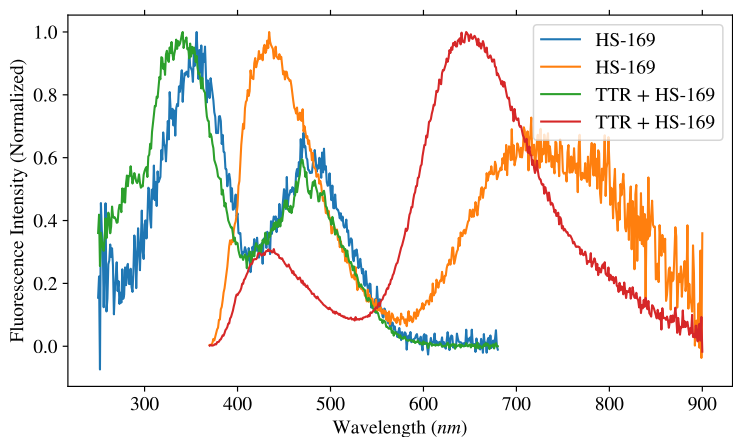


Figure 4.7: Excitation (green and blue) and emission (yellow and red) spectra of the fluorescent probe HS-169, with and without the protein TTR. Here a long-pass filter was used.

The excitation and emission spectra for HS-169 diluted in PBS, with and without TTR, are displayed in figure 4.7. HS-169 are one of the probes that are diluted both in PBS and MeOH for the characterization. The fluorescence spectra of HS-169 diluted in MeOH can be seen in appendix A.1. The signal to noise ratio (S/N) is low using PBS as solvent, as also observed in figure 4.7. From the absorption spectroscopy, HS-169 was found to have two absorption peaks. HS-169 was therefore excited two times, one for each wavelength

equal to these peaks. What was found, was that the probe also has two peaks for the emission of light, around 440 nm and 720 nm. Notice how the peak around 440 nm is in between the two absorption peaks, while also being in the absorption band or excitation band.

For HS-169 bound to TTR, the results were quite similar with the higher energy transition peak being slightly shifted towards the UV region. The peak with a lower transition energy, however, got substantially blue-shifted and significantly stronger, if one compares it with the spectrum of the probe alone.

4.3 The Quantum Efficiency

The quantum efficiency (QE) is a measure of how efficient a fluorophore emits upon excitation. It is also a good indicator of quenching mechanisms that may impair the QE. The fluorescence spectra and the absorption spectra were used to determine quantum yield of the respective compounds. It is therefore interesting to look at the quantum efficiency, and how it will change when adding the protein. The proximity of charged groups, hydrophobic regions and solvent water, can have an impact on the quenching efficiency. For many of the samples, the probe itself can be used as a reliable characterized standard sample (Brouwer 2011). This is an advantage, because of the maximum excitation wavelength being somewhat constant. The emission will also happen in the similar region, as seen in previous results. Equation (2.5) is used to calculate the quantum efficiency for all the samples of interest. Also here, as in fluorescence spectroscopy section, the measurements that gave the most interesting results are displayed. View appendix A.2 for more results. All the essential parameters of the data are, however, summarized in table 4.2 for easy comparison.

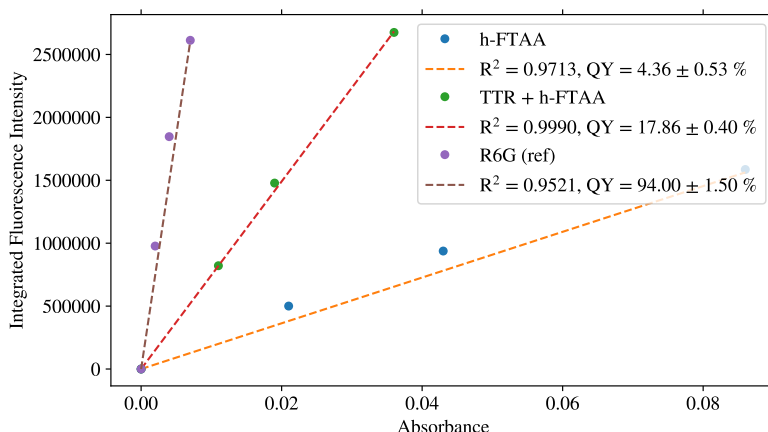


Figure 4.8: Relative quantum efficiency for samples containing the fluorescent probe h-FTAA, with and without the protein TTR. Both samples are diluted in PBS. Here, the highly reliable quantum yield standard for Rhodamine-6G is used as a reference.

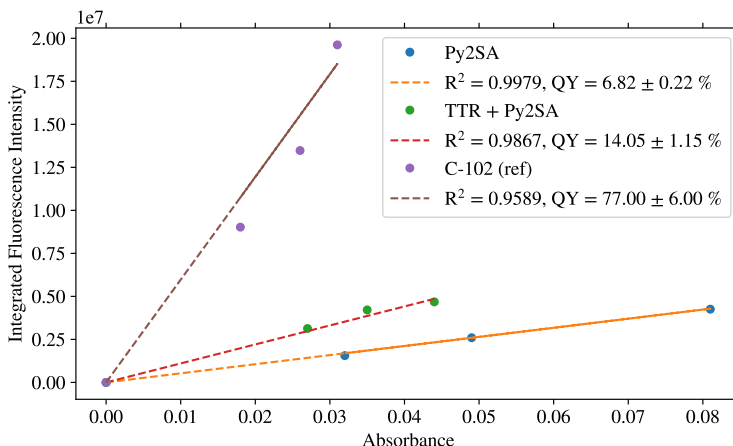


Figure 4.9: Relative quantum efficiency for samples containing the fluorescent probe Py2SA, with and without the protein TTR. The probe without the protein is diluted in MeOH, while with the protein, it is diluted in PBS. Here, the highly reliable quantum yield standard for Coumarin-102 is used as a reference.

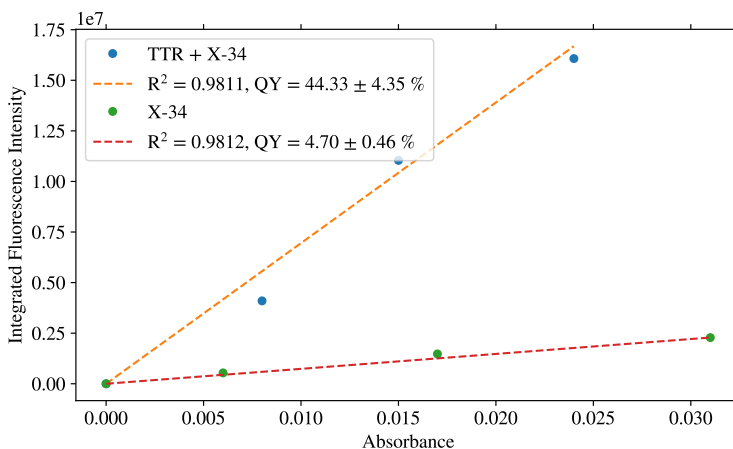


Figure 4.10: Relative quantum efficiency for samples containing the fluorescent probe X-34, with and without the protein TTR. Both samples are diluted in PBS. The probe by itself is here used as the quantum yield standard, where the quantum efficiency is established to be $\Phi_R = 4.70 \%$ (Zhang, Sandberg, Kongsom, Wu, Nyström, Nilsson, Konradsson, LeVine III, Lindgren & Hammarström 2018)

Figure 4.8 shows the results for the measurements done for h-FTAA, with and without the protein. To calculate the relative quantum yield of this probe, with and without the

protein, Rhodamine-6G was used as reference. The reliable and well known reference R6G has quantum yield standard of $\Phi_R = 0.94 \pm 0.015$ (Brouwer 2011). The quantum yields were found to be around 18 % and 4 %, with and without TTR, respectively.

The measurements for quantum efficiency of Py2SA, with and without TTR, are plotted in figure 4.9. This was determined by the the reliable standard sample, Coumarin-102. C-102 has a known quantum yield standard of $\Phi_R = 0.77 \pm 0.06$ (Rurack & Spieles 2011). From this the quantum efficiency of Py2SA is calculated to be around 7 %, and 14 % when bound to TTR.

Finally, figure 4.10 shows the results of the quantum efficiency for X-34, with and without the protein. A literature review reveals a quantum efficiency for X-34 to be $\Phi_R = 5\%$ (Zhang, Sandberg, Kongsmo, Wu, Nyström, Nilsson, Konradsson, LeVine III, Lindgren & Hammarström 2018). With this, and the protein added to the sample, the quantum efficiency is calculated to be $\Phi_X = 44\%$. The increased quantum yield in the probes displayed here means that they have an increase in photons emitted compared to what have been absorbed, when bound to TTR. All results are listed in table 4.2, including fluorescence characteristics.

Table 4.2: Photophysical characteristics of the samples under investigation. λ_{abs} is the wavelength of maximum absorption, λ_{ex} is the wavelength of maximum excitation, λ_{em} is the wavelength of maximum emission, and Φ_X is the calculated quantum yield with its uncertainty.

Sample	λ_{abs} (nm)	λ_{ex} (nm)	λ_{em} (nm)	Stokes' Shift (nm)	Φ_X (%)
p-FTAA	410	411	544	133	20.00 ± 0.46
p-FTAA + TTR	416	409	540	131	16.26 ± 1.10
hx-FTAA	436	433	555	122	15.81 ± 0.30
hx-FTAA + TTR	435	421	548	127	14.24 ± 0.44
h-FTAA	424	409	579	170	4.36 ± 0.53
h-FTAA + TTR	426	427	545	118	17.86 ± 0.40
Py1SA	346	377	388	11	-
"	"	"	411	34	-
"	"	"	525	148	4.15 ± 0.18
Py1SA + TTR	387	388	530	142	9.93 ± 2.74
Py2SA	337	337	416	79	6.82 ± 0.22
"	320	320	444	124	-
Py2SA + TTR	340	340	419	79	14.05 ± 1.15
"	321	323	448	125	-
X-34	363	363	507	144	4.70 ± 0.46
X-34 + TTR	373	368	474	106	44.33 ± 4.35
BTD-SB	330	330	620	290	-
"	469	470	620	150	0.16
BTD-SB + TTR	331	331	617	286	-
"	480	469	617	148	3.86 ± 0.44
HS-169 (PBS)	365	357	436	79	0.07 ± 0.01
"	365	357	716	359	0.13 ± 0.01
"	"	"	"	"	0.20 ± 0.02
"	496	470	716	246	0.10 ± 0.01
HS-169 (MeOH)	356	350	434	84	0.04 ± 0.01
"	356	350	650	300	21.25 ± 1.51
"	"	"	"	"	21.26 ± 1.89
"	492	470	650	180	15.37 ± 1.84
HS-169 + TTR	363	349	424	75	0.09 ± 0.02
"	363	349	657	308	0.55 ± 0.18
"	"	"	"	"	0.65 ± 0.20
"	495	470	657	187	0.81 ± 0.11
ANS	-	306	482	176	-
ANS + TTR	-	278	479	201	-

4.4 Lifetime measurements

Based on the results from section 4.1 and 4.2, the excited state lifetime were determined for the probes with and without TTR. Just as the QE, changes in lifetime can report on quenching mechanisms, such as presence of charged amino residues in proteins, or proximity to a water phase. As for the previous parts, only the most interesting results are displayed. View appendix A.3 for a full overview of the decay traces along with fits.

Figure 4.11 shows the lifetime decay plot of the pyrene Py2SA, with and without TTR, measured at two different emission wavelength, 420 nm and 445 nm. These emission wavelengths are characterized as the two twin peaks one can see in figure A1d. The samples were excited using a NanoLED at 337 nm. The plot shows the prompt, which is a measurement of the instrumental response, the decay data of the samples, and an exponential fit. All the exponential fits are fitted with a double exponential decay, except for the decay of the probe alone measured at emission wavelength 445 nm. By using equation (2.8), the average lifetime for the samples containing a double exponential were calculated. All data and calculations are given in table 4.3. We see that for the sample with the protein, we have a significantly longer lifetime. The pyrene Py2SA is a generally "long-lived" probe (Zhang, Wang, Sandberg, Wu, Nyström, LeVine III, Konradsson, Hammarström, Durbeej & Lindgren 2018), with a measured lifetime at about 31 ns and 7 ns for the 420 nm wavelength, and 27 ns and 6 ns for the 445 nm wavelength, with and without TTR, respectively.

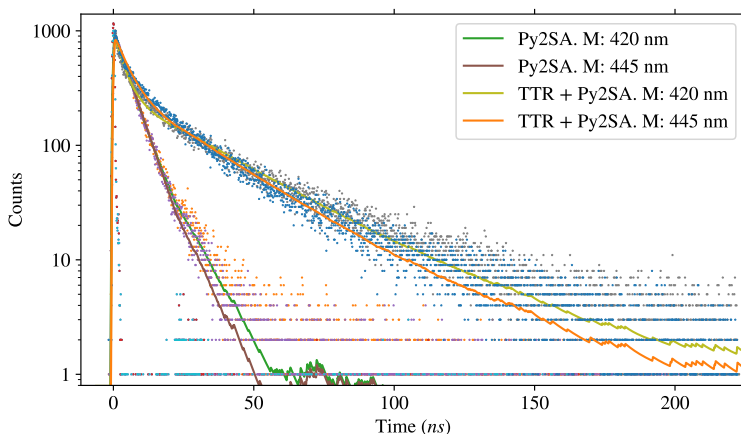


Figure 4.11: Lifetime decay of the fluorescent probe Py2SA, with and without the protein, TTR, in PBS. The samples are excited at 337 nm, and the emission is measured at 420 nm and 445 nm (The two emission maxima). Both single and double exponential decays. The average lifetimes (τ_{avg}) along with the values of its components are given in table 4.3.

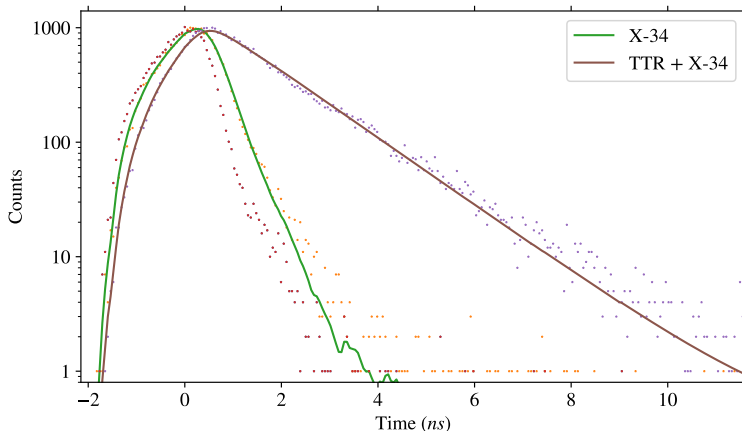


Figure 4.12: Lifetime decay of the fluorescent probe X-34, with and without the protein, TTR, in PBS. The samples are excited at 373 nm, and the emission is measured at 510 nm. Single exponential decays. The average lifetimes (τ_{avg}) are given in table 4.3.

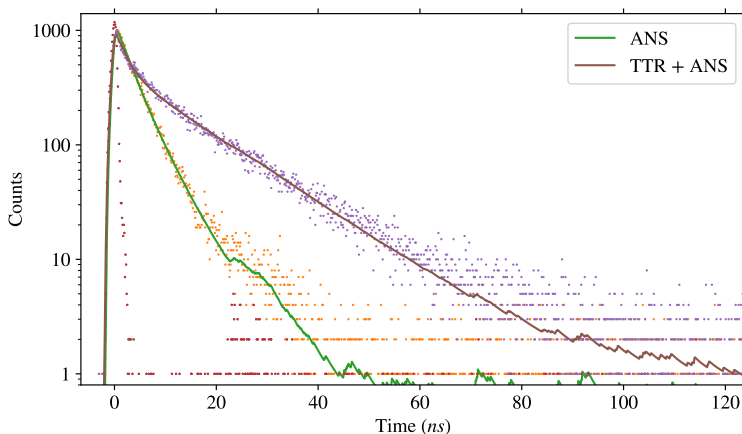


Figure 4.13: Lifetime decay of the fluorescent probe ANS, with and without the protein, TTR, in PBS. The samples are excited at 373 nm, and the emission is measured at 480 nm. Double exponential decays. The average lifetimes (τ_{avg}) along with the values of its components are given in table 4.3.

The lifetime decay data of X-34, with and without TTR, is presented in figure 4.12. The samples were excited with a 373 nm NanoLED, and the emission was measured at 510 nm. Both decays are fitted with single exponential decays which make the calculations for the lifetimes straight forward. Also here we get a significantly longer lifetime for the probe

bound to the protein. The lifetimes were found to be around 1.5 ns and 0.3 ns, with and without TTR respectively. These are not as long times as the pyrene, Py2SA, but the change is significant.

Lastly, the long-lived probe ANS is included in this section. The lifetime decay data is shown in figure 4.13. The samples were excited using the same NanoLED as for X-34 (373 nm), but the emission was here measured at 480 nm. Both samples were fitted with a double exponential decay, and the data for the components are in table 4.3. The lifetimes were found to be around 14 ns and 4.8 ns, with and without the protein, respectively. We can see a general increase in lifetimes of the probes displayed here. This is in agreement with previous studies of e. g., ANS and TTR (Lindgren et al. 2005).

Table 4.3: Lifetime characteristics of the samples investigated in this thesis. τ_1 is the first lifetime component of a multi-exponential lifetime decay, α_1 is the first component's preexponential factor, τ_2 is the second component, α_2 its factor, and τ_{avg} is the average lifetime calculated by the components and equation (2.8). For the probes HS-169 and Py2SA, all excitation and emission peaks are considered, and are chronologically specified.

Sample	τ_1 (ns)	α_1 (%)	τ_2 (ns)	α_2 (%)	τ_{avg} (ns)
p-FTAA	0.64 ± 0.01	100	-	-	0.64 ± 0.01
p-FTAA + TTR	0.60 ± 0.01	100	-	-	0.60 ± 0.01
hx-FTAA	0.74 ± 0.01	100	-	-	0.74 ± 0.01
hx-FTAA + TTR	0.75 ± 0.01	100	-	-	0.75 ± 0.01
h-FTAA	0.17 ± 0.01	100	-	-	0.17 ± 0.01
h-FTAA + TTR	0.30 ± 0.01	73.18	0.95 ± 0.02	26.82	0.65 ± 0.02
Py1SA	0.59 ± 0.02	100	-	-	0.59 ± 0.02
Py1SA + TTR	1.23 ± 0.06	61.71	2.61 ± 0.06	38.29	2.02 ± 0.06
Py2SA	4.88 ± 0.17	64.95	9.24 ± 0.18	35.05	7.08 ± 0.25
	5.97 ± 0.02	100	-	-	5.97 ± 0.02
Py2SA + TTR	3.50 ± 0.12	22.12	32.04 ± 0.24	77.88	31.18 ± 0.27
	4.93 ± 0.16	27.78	28.56 ± 0.21	72.22	27.09 ± 0.26
X-34	0.27 ± 0.01	100	-	-	0.27 ± 0.01
X-34 + TTR	1.47 ± 0.01	100	-	-	1.47 ± 0.01
BTD-SB + TTR	1.69 ± 0.01	100	-	-	1.69 ± 0.01
HS-169 (PBS)	0.70 ± 0.01	61.66	3.01 ± 0.03	38.34	2.38 ± 0.03
	0.12 ± 0.01	97.57	0.71 ± 0.05	2.43	0.20 ± 0.05
	0.003 ± 0.002	100	-	-	0.003 ± 0.002
HS-169 (MeOH)	0.55 ± 0.01	58.18	2.31 ± 0.02	41.82	1.88 ± 0.02
	0.72 ± 0.08	8.46	2.29 ± 0.01	91.54	2.24 ± 0.08
	0.23 ± 0.02	10.52	2.22 ± 0.01	89.48	2.19 ± 0.02
HS-169 + TTR	0.62 ± 0.01	57.36	4.13 ± 0.04	42.64	3.54 ± 0.04
	0.14 ± 0.01	42.42	3.75 ± 0.02	57.58	3.66 ± 0.02
	0.05 ± 0.01	16.88	3.51 ± 0.02	83.12	3.50 ± 0.02
ANS	2.83 ± 0.14	49.55	5.73 ± 0.09	50.45	4.78 ± 0.17
ANS + TTR	2.07 ± 0.10	18.08	14.35 ± 0.08	81.92	13.97 ± 0.13

Probe-TTR Interaction

Going through all the photo-physics of the fluorescent ligands in solvents, we aim on the main objective of the thesis - probe-protein interaction. Since all photo-physical characteristics for the probes with and without TTR are characterized, it is now interesting to have a look at the probe-TTR interaction, and what really happens when the different probes interact with the protein.

5.1 Changes in Spectra

For easy comparison between the different probes with and without TTR protein, the essential changes in the photo-physical parameters are summarized in table 5.1. This table summarizes spectral shifts, and changes in the photo-physical characteristics like the quantum efficiency and lifetimes. To start with, each sample is compared with the same sample, and then we turn to the situation when it is bound to TTR. That means that for a sample with a $\Delta\lambda_{em} = -10$ change, the sample has a spectral shift downwards or is shifted towards the UV side of the spectrum, when the sample is bound to TTR compared to when it is not. The same goes for changes equal to $\Delta\lambda_{em} = +10$. The sample has a spectral change that is red-shifted. For the change in Stokes' Shift (ΔSS), the change is based on the width of the shift. So a negative change, means that the Stokes' Shift is narrower when TTR is introduced to the probe. A positive change means that the width of the Stokes' shift is larger. For the change in lifetimes and quantum yields, the change means there are an increase or decrease, regarding if it is positive or negative. This is also an comparison of before and after adding the TTR.

Some probes that are worth mentioning and highlighting are, but are not limited to, h-FTAA, Py2SA, X-34 and HS-169. h-FTAA got, as one can see from table 5.1 and from figure A1c, both a substantial shift in the excitation and emission spectra. The combination of the excitation peak being red-shifted, and the emission peak being shifted towards the UV region, when the probe is introduced to TTR, makes the Stokes' Shift significantly

narrower. Another significant change with this probe-TTR interaction is the increase in quantum efficiency.

There is not a lot of change in the spectral characteristics of Py2SA, but there is a lot of change when it comes to its lifetime and quantum yield. When TTR is introduced, the quantum efficiency increases by about 7%, and the lifetime with the significant increase of 24 ns, making it very long-lived compared to the other probes. This was the objective to establish these pyrene based amyloid probes as outlined in Zhang, Wang, Sandberg, Wu, Nyström, LeVine III, Konradsson, Hammarström, Durbeej & Lindgren (2018).

Not only is there a notable spectral shift for the X-34 and TTR interaction, but it also got the largest increase in the quantum yield. Furthermore, it increases by nearly 40% when it is bound to TTR, which is almost a factor of 10 from what the quantum yield is for the probe alone.

For HS-169, the probe was diluted in both PBS and MeOH solvents. However, TTR was only added to the sample with PBS, as the protein would have denatured in the extreme environments of MeOH. The sample with MeOH, is therefore compared with the TTR and HS-169 sample that is diluted in PBS. Notice how the spectral shift changes are large for the sample diluted in PBS and small for the sample diluted in MeOH. Another substantial difference between the solvents, are their impact on QE.

Table 5.1: Changes in photo-physical characteristics of the samples under investigation. $\Delta\lambda_{abs}$ is the change in wavelengths of maximum absorption, $\Delta\lambda_{ex}$ is the change in wavelengths of maximum excitation, $\Delta\lambda_{em}$ is the change in wavelengths of maximum emission, ΔSS is the change in the spectra Stokes' Shifts, $\Delta\Phi_X$ is the change in QY, and $\Delta\tau$ is the change in lifetime. Here, the probe is compared with $+/-$ differences against when it is bound to TTR. For example if $\Delta\Phi_X = +5$, the quantum yield increases by 5 when the probe is bound to TTR, compared to when it is not. For the probe HS-169, both excitation peaks are considered, and are chronologically specified. Also, when considering HS-169 (MeOH) it is compared with the TTR in PBS.

Sample (w / wo TTR)	$\Delta\lambda_{abs}$ (nm)	$\Delta\lambda_{ex}$ (nm)	$\Delta\lambda_{em}$ (nm)	ΔSS (nm)	$\Delta\Phi_X$ (%)	$\Delta\tau$ (ns)
p-FTAA	+6	-2	-4	-2	-3.74	-0.04
hx-FTAA	-1	-12	-7	+5	-1.57	+0.01
h-FTAA	+2	+18	-34	-52	+13.50	+0.48
Py1SA	+41	+11	+5	-6	+5.78	+1.43
Py2SA	+3	+3	+3	0	+7.23	+24.1
X-34	+10	+5	-33	-38	+39.63	+1.20
BTD-SB	+11	-1	-3	-4	+3.70	+1.65
HS-169 (PBS)	-2	-8	-12	-51	+0.45	+1.16
	-1	0	-59	-59	+0.71	+3.50
HS-169 (MeOH)	+7	-1	-10	+8	-20.61	+1.66
	+3	0	+7	+7	-14.56	+1.31
ANS	-	-28	-3	+25	-	+9.19

5.2 TTR characteristics

When scrutinizing the probe-TTR interaction, it is important to know the characteristics of the protein itself and its components. Also, when looking at changes in spectra (probes alone, and bound to TTR), characteristics and information about the protein is important to understand what is going on a molecular level when TTR is added. View table 5.2 for a summary of the results.

Table 5.2: Photophysical characteristics of TTR and L-Trp which is a component of TTR. λ_{abs} is the wavelength of maximum absorption, λ_{ex} is the wavelength of maximum excitation, λ_{em} is the wavelength of maximum emission, SS is the Stokes' Shift, Φ_X is the calculated quantum yield with its uncertainty, and τ is the lifetime with its uncertainty.

Sample	λ_{abs} (nm)	λ_{ex} (nm)	λ_{em} (nm)	SS (nm)	Φ_X (%)	τ (ns)
TTR	276	277	330	53	6.35 ± 0.90	3.42 ± 0.01
L-Trp	280	273	350	77	15.00 ± 1.00	2.88 ± 0.01

Figure 5.1 shows the fluorescence spectra for TTR and L-Trp. We can clearly see a comparison between the two, because of TTR's tryptophan residues. As expected, the excitation maximum is about the same for both samples, since the absorption data also showed approximately the same peak. For the emission spectra, however, the TTR spectrum or peak is a little blue-shifted compared to the tryptophan peak. For TTR, the emission maximum is found to be at around 330 nm, while for the L-Trp the peak is at 350 nm.

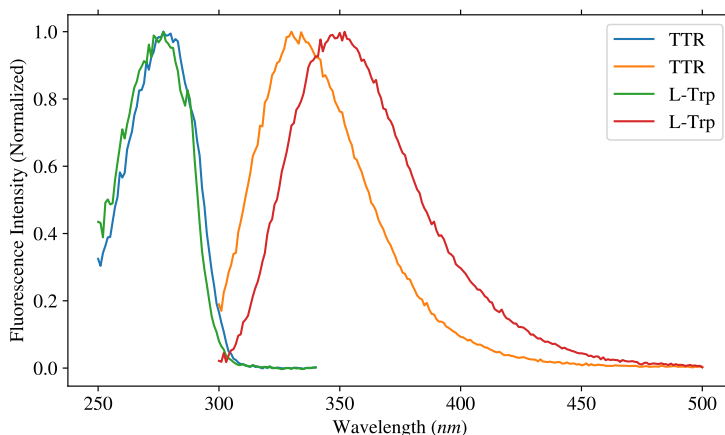


Figure 5.1: Excitation (green and blue) and emission (yellow and red) spectra of TTR and L-Trp

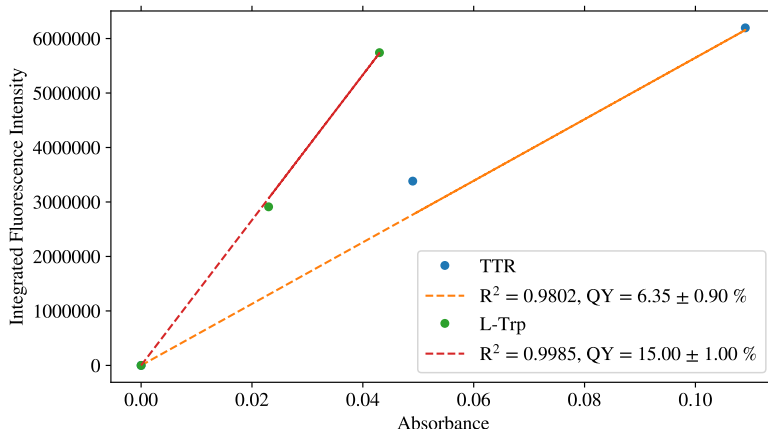


Figure 5.2: Relative quantum efficiency for the samples TTR and L-Trp. Both samples are diluted in PBS. Here, L-Trp itself is used as the quantum yield standard, where the quantum efficiency is established to be $\Phi_R = 0.15 \pm 0.01$ (Suzuki et al. 2009, Chen 1972).

In figure 5.2 the quantum efficiency of TTR and L-Trp are determined. For the relative quantum yield, L-Trp was here used as a reference standard. A literature review revealed that tryptophan has a quantum yield equal to $\Phi_R = 0.15 \pm 0.01$ (Suzuki et al. 2009, Chen 1972), and is also referenced in the reliable article (Brouwer 2011). The quantum yield of TTR was found to be around 6%.

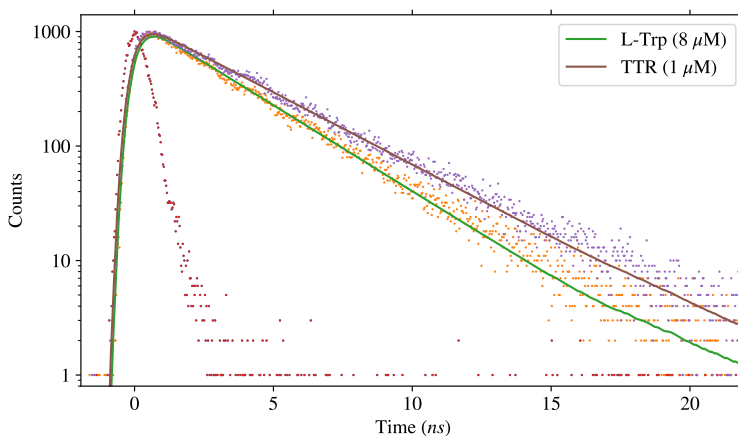


Figure 5.3: Lifetime decay of TTR and L-Trp, in PBS. The samples are excited at 278 nm, and the emission is measured at 340 nm. Single exponential decays.

The lifetimes were also measured, and are displayed in figure 5.3. The samples were here excited using a NanoLED at 278 nm, and monitoring the emission at 350 nm from tryptophans in TTR. Both decays were fitted with a single exponential decay, and the lifetimes were found to be 3.4 ns and 2.9 ns for the TTR and tryptophan respectively. See table 5.2 for more details.

5.3 FRET analysis

Fluorescence Resonance Energy Transfer (FRET) is the transfer of excited-state energy from a donor (D) molecule to an acceptor (A) molecule. This energy transfer leads to a reduction of the donor's excited state lifetime. The rate of energy is for example dependent on the extent of spectral overlap between the donor and acceptor, among other conditions. The donor in this case is the TTR molecule and its tryptophan residues, and the acceptor are the probes. As we have seen in the fluorescence spectra of TTR and L-Trp (figure 5.1) and the fluorescence spectra of the probes (section 4.2), there are several of the probes that are potential candidates of FRET effects. Here, measurements have been performed with all probes, but only the most interesting results are displayed in this section. All samples are excited at 280 nm, which is on the absorption peak of TTR as was found in section 4.1 and 5.2. The emission is measured at 350 nm, as this is where the tryptophan (donor) is emitting light, but as it also can be where the energy is transferred and the probes (acceptor) are excited instead. View appendix A.4 for more results. All measurements are, however, summarized in table 5.3 and table 5.4.

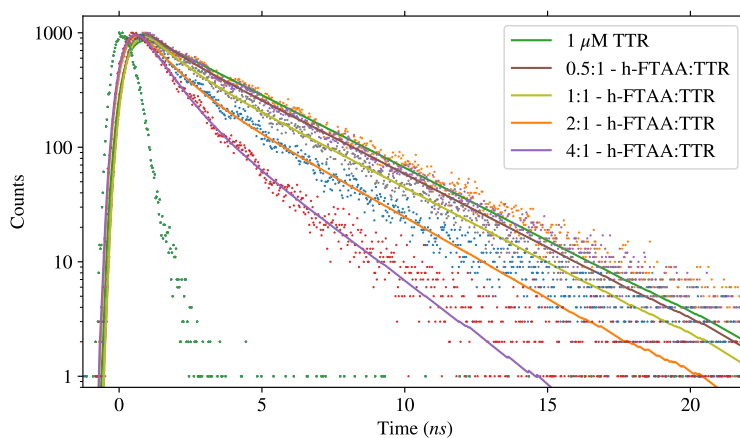


Figure 5.4: FRET measurements for the acceptor h-FTAA together with the donor TTR, using time-resolved method. The NanoLED with excitation wavelength of 278 nm is used, and the emission is observed at 350 nm.

In figure 5.5 we see the decays of TTR and h-FTAA as the acceptor molecule. The decays are fitted with double exponential curves. h-FTAA has an absorption peak at around

420 nm, but has a broad absorption band also absorbing for wavelengths near the TTR peak of emission. It is therefore reason to believe that FRET effects occur. As one can see in the figure, the intensity of the decay decreases as the concentration of h-FTAA (acceptor) increases, and we get decreasing lifetimes of TTR. Details for the lifetimes are summarized in table 5.3.

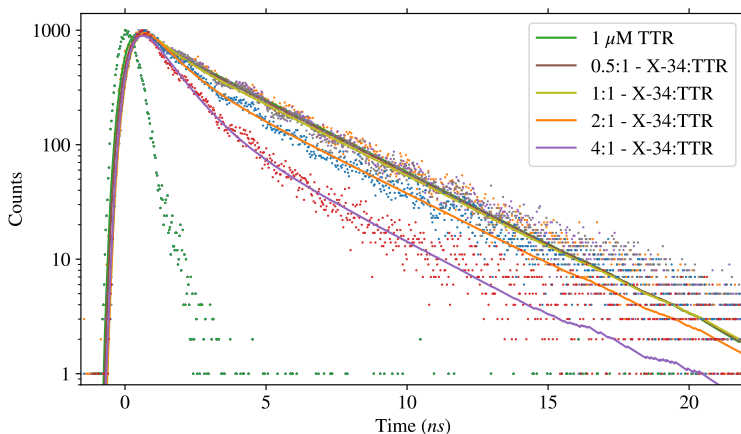


Figure 5.5: FRET measurements for the acceptor X-34 together with the donor TTR, using time-resolved method. The NanoLED with excitation wavelength of 278 nm is used, and the emission is observed at 350 nm.

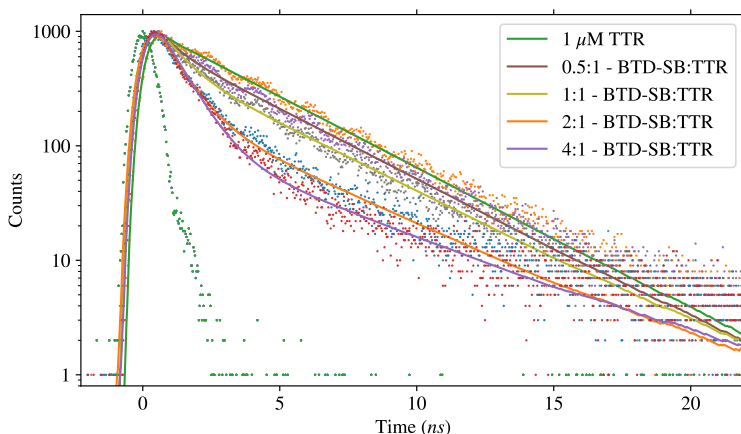


Figure 5.6: FRET measurements for the acceptor BTD-SB together with the donor TTR, using time-resolved method. The NanoLED with excitation wavelength of 278 nm is used, and the emission is observed at 350 nm.

Another probe that contributes to FRET is the probe X-34, where the results can be viewed in figure 5.5. X-34's absorption peak is at around 360 nm, where this contributes to a lot of spectral overlap with the donor's (TTR) emission spectrum. As figure 5.5 shows, the intensity of excited state lifetime decreases as the concentration of X-34 increases. Details of the results can be viewed in table 5.4.

Finally, in figure 5.6 BTD-SB is introduced as an acceptor of FRET for TTR. The spectral overlap between the emission of TTR and absorption of BTD-SB were introduced in section 2.6 in figure 2.5, and it is clear that the overlap is substantial. As with the other probes displayed here, the excited lifetime of TTR decreases significantly when the concentration of BTD-SB is increased. From the results in table 5.4 and equation (2.21), the transfer efficiency passes 50 % somewhere between the concentration ratios of 2 : 1 and 4 : 1. As we recall from the theory in section 2.6, the Förster distance of donor and acceptor is achieved when the energy transfer is equal to 50 %. By looking at the tables of results (table 5.3 and table 5.4), BTD-SB is the only acceptor that passes this energy transfer limit.

Table 5.3: FRET results for the Oligothiophenes under investigation. c-ratio is the ratio of concentration between the probe and tetrameric TTR, λ_{em} is the wavelength of maximum emission. As in table 4.3, the different components of the multi-exponential lifetime decay are given as τ_i with their respective preexponential factor (α_i) in paranthesis, if applicable. τ_{avg} is the average lifetime calculated by the components and equation (2.8).

Sample	c - ratio	λ_{em} (nm)	τ_1 (α_1) (ns)	τ_2 (α_2) (ns)	τ_{avg} (ns)
TTR	1 μ M	330	3.42 (100 %)	-	3.42 \pm 0.01
L-Trp	8 μ M	350	2.87 (100 %)	-	2.87 \pm 0.01
p-FTAA : TTR	0.5 : 1	334	3.30 (100 %)	-	3.30 \pm 0.01
	1 : 1	332	3.20 (100 %)	-	3.20 \pm 0.01
	2 : 1	331	2.99 (100 %)	-	2.99 \pm 0.01
	4 : 1	331	2.84 (100 %)	-	2.84 \pm 0.02
hx-FTAA : TTR	0.5 : 1	334	3.45 (100 %)	-	3.45 \pm 0.01
	1 : 1	331	3.37 (100 %)	-	3.37 \pm 0.01
	2 : 1	336	3.37 (100 %)	-	3.37 \pm 0.01
	4 : 1	332	3.29 (100 %)	-	3.29 \pm 0.01
h-FTAA : TTR	0.5 : 1	331	0.65 (10 %)	3.39 (90 %)	3.33 \pm 0.05
	1 : 1	334	0.86 (19 %)	3.33 (81 %)	3.19 \pm 0.05
	2 : 1	332	0.88 (33 %)	3.05 (67 %)	2.77 \pm 0.04
	4 : 1	330	0.80(52 %)	2.31 (48 %)	1.90 \pm 0.03

Table 5.4: Continuation of table 5.3. FRET results for the probes under investigation. c-ratio is the ratio of concentration between the probe and tetrameric TTR, λ_{em} is the wavelength of maximum emission. As in table 4.3, the different components of the multi-exponential lifetime decay are given as τ_i with their respective preexponential factor (α_i) in parenthesis, if applicable. τ_{avg} is the average lifetime calculated by the components and equation (2.8).

Sample	c - ratio	λ_{em} (nm)	τ_1 (α_1) (ns)	τ_2 (α_2) (ns)	τ_{avg} (ns)
TTR L-Trp	1 μ M	330	3.42 (100 %)	-	3.42 ± 0.01
	8 μ M	350	2.87 (100 %)	-	2.87 ± 0.01
Py1SA : TTR	0.5 : 1	333	3.49 (100 %)	-	3.49 ± 0.01
	1 : 1	332	3.34 (100 %)	-	3.34 ± 0.01
	2 : 1	333	3.37 (100 %)	-	3.37 ± 0.01
	4 : 1	332	3.15 (100 %)	-	3.15 ± 0.01
Py2SA : TTR	0.5 : 1	332	3.46 (100 %)	-	3.46 ± 0.01
	1 : 1	332	3.38 (100 %)	-	3.38 ± 0.01
	2 : 1	331	3.37 (100 %)	-	3.37 ± 0.01
	4 : 1	332	3.28 (100 %)	-	3.28 ± 0.02
X-34 : TTR	0.5 : 1	332	0.51 (9 %)	3.48 (91 %)	3.43 ± 0.04
	1 : 1	334	0.61 (14 %)	3.49 (86 %)	3.41 ± 0.06
	2 : 1	331	0.86 (31 %)	3.52 (69 %)	3.26 ± 0.04
	4 : 1	335	0.93 (60 %)	3.28 (40 %)	2.58 ± 0.04
BTD-SB : TTR	0.5 : 1	333	3.20 (100 %)	-	3.20 ± 0.01
	1 : 1	331	2.84 (100 %)	-	2.84 ± 0.02
	2 : 1	331	1.84 (100 %)	-	1.84 ± 0.02
	4 : 1	328	1.38 (100 %)	-	1.38 ± 0.02
HS-169 : TTR	0.5 : 1	332	3.40 (100 %)	-	3.40 ± 0.01
	1 : 1	333	3.43 (100 %)	-	3.43 ± 0.01
	2 : 1	331	3.43 (100 %)	-	3.43 ± 0.01
	4 : 1	333	3.35 (100 %)	-	3.35 ± 0.01
ANS : TTR	0.5 : 1	331	3.41 (100 %)	-	3.41 ± 0.01
	1 : 1	332	3.36 (100 %)	-	3.36 ± 0.01
	2 : 1	333	3.38 (100 %)	-	3.38 ± 0.01
	4 : 1	332	3.31 (100 %)	-	3.31 ± 0.01

Chapter 6

TTR Dynamics from Fluorescence Anisotropy

Anisotropy measurements provide information on the size and shape of proteins or the rigidity of molecular environments. As mentioned in the theory in section 2.5, rotational diffusion of fluorophores is a common cause of depolarization of emission. Anisotropy measurements can therefore reveal the average angular displacement of the fluorophore that occur between excitation and emission of a photon. It is therefore dependent on the rotational diffusion during the lifetime of the excited state, and for example viscosity of the solvent. Therefore, to get reliable results for the TTR dynamics, a fluorophore with a long excited state lifetime is preferable. Here, based on the results in the earlier chapters, Py2SA is chosen as the fluorophore, as it shows to have the longest lifetimes, both unbound and bound to TTR.

6.1 Polarized Intensities

First the vertically and horizontally polarized light intensities have to be measured, as mentioned in section 2.5 and section 3.6. In total four different intensities were measured for each sample, that is one for each polarization needed to calculate and plot the anisotropy (equation (3.8)). The time dependent steady state lifetime measurements for Py2SA bound to TTR for different polarized light are displayed in figure 6.1. Since it is the rotational diffusion coefficient of the fluorophore it is focused on, as this is the one that binds to TTR and displays a long lifetime, the sample is excited with a NanoLED at 337 nm and the emission measured at 416 nm. Anisotropy is, as mentioned in section 3.6, a delicate process, and is prone to noise. As polarizers are used, the intensity is drastically reduced, both for the excitation and emission. Long measurement times are therefore needed, in favor of getting a solid and precise signal. With the fluorophore bound to TTR, the measuring time were pre-set to 1200 s, or 20 min, for all four measurements.

Measurements were also taken of the probe (Py2SA) alone, both in PBS and in 75 % Glycerol. Glycerol have a higher viscosity than PBS, and will essentially make the probe move around slower. However, a higher viscosity fluid use a long time reaching steady state conditions when mixed with other molecules. When Py2SA was mixed with 75 % Glycerol, the sample therefore rested for the duration of the Py2SA in PBS measurements to be completed. The measurements for the polarization intensities for Py2SA alone diluted in both different fluids, can be found in appendix A.5.

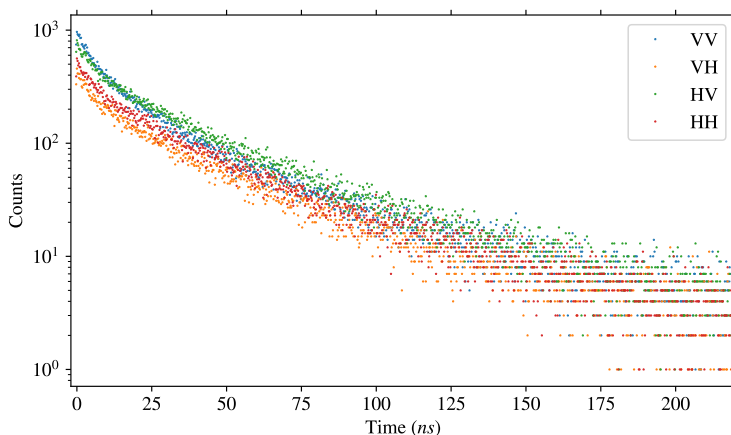


Figure 6.1: Time dependent steady state lifetime measurements for different polarization of Py2SA bound to TTR. These are further used to calculate and plot the anisotropy by equation (3.8). Here, the sample is excited at 337 nm, emission measured at 416 nm, and the measuring time was pre-set to 1200 s (20 min).

6.2 Calculated Anisotropy

Figure 6.2 show the results of analysing the polarized intensities by equation (3.8), and plotting it as a function of time. Even for long measuring times, one can see there is a wide spread in data points. However, it is possible to see a trend of the points. A moving average over five data points were implemented, to more easily see the results and fit an exponential decay to the data. The exponential fit is merely there to guide the eye, but is of good help to determine the results for the dynamics of different conformational states of TTR. For the probing of TTR, the fitted rotational correlation time using Py2SA was found to be 19 ns.

The fitted rotational correlation time for Py2SA in Glycerol is shown in figure 6.3. Here the data points are noticeably more assembled. With long measuring times, it is generally difficult to measure a good instrumental factor, or G , from equation (3.7). This is because with long measuring times, the longer the instruments are exposed to noise. This is visible in the figure, as there is a dip or an offset in the data points along the whole transient. A

baseline is therefore also fitted with the exponential decay. The fitted rotational correlation time for Py2SA diluted in 75 % glycerol was found to be 4 ns.

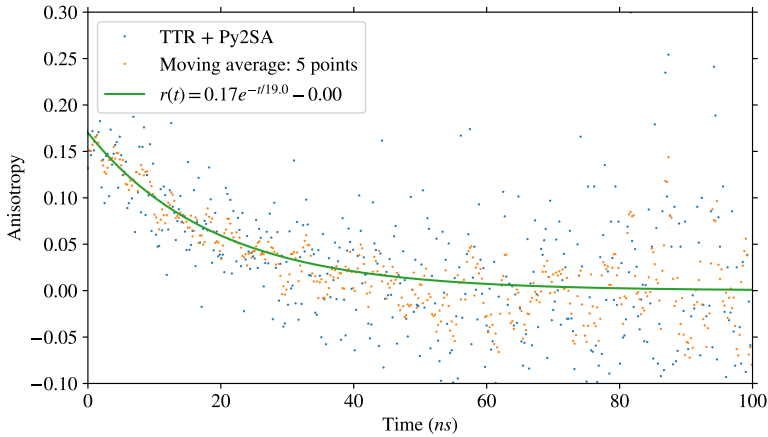


Figure 6.2: Results of anisotropy based on the polarization intensities from figure 6.1 and calculations from equation (3.8). There is also calculated a moving average, where the average of 5 points are taken for each point. A single exponential decay was fitted with the data using equation (2.10), yielding the rotational correlation time to be $\tau_r = 19.0 \pm 4.0$, with $r_0 = 0.17$.

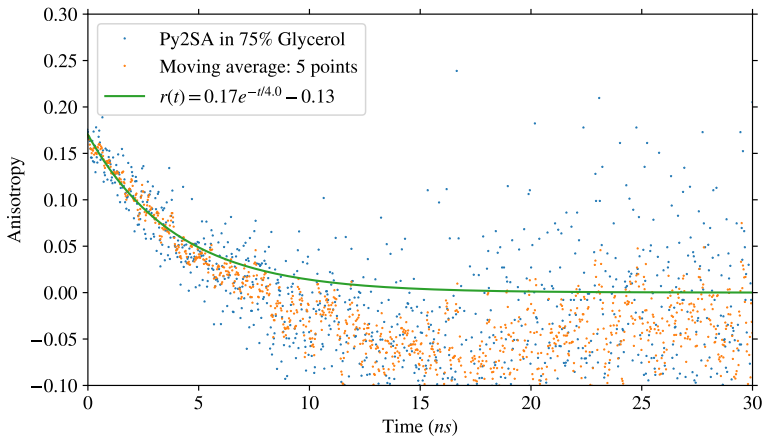


Figure 6.3: Results of anisotropy based on the polarization intensities from figure A8 and calculations from equation (3.8). There is also calculated a moving average, where the average of 5 points are taken for each point. A single exponential decay was fitted with the data using equation (2.10), yielding the rotational correlation time to be $\tau_r = 4.0 \pm 0.5$, with $r_0 = 0.17$. A baseline was also fitted, where this was found to be $y_0 = -0.13$.

In figure 6.4, the fitted rotational correlation time for Py2SA diluted in PBS is shown. Here the data points are spread, and not as precise. Py2SA diluted in PBS is generally low in signal and intensity as one can see in figure A9. The lower QE when using water based solvents, such as PBS, results in a weaker signal. This lead to long measuring times, and a fitted baseline, as for the probe diluted in glycerol. Here a moving average were also performed, and a single exponential decay fitted. The rotational correlation time was found to be around 0.5 ns. Notice how this is much shorter than the measurements done for the same probe in glycerol, which is a more viscous fluid.

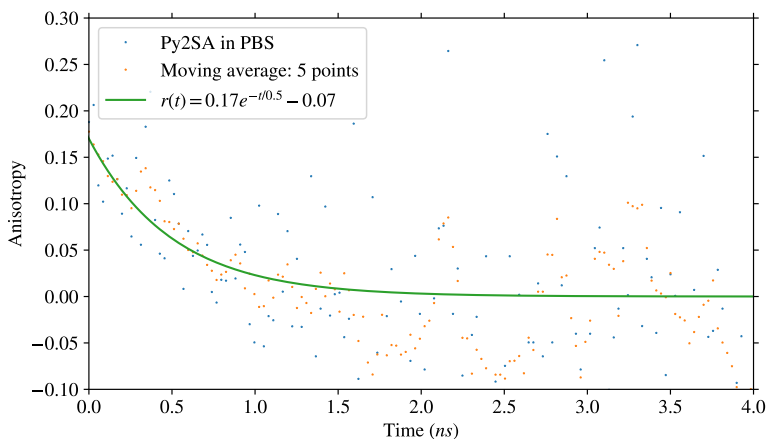


Figure 6.4: Results of anisotropy based on the polarization intensities from figure A9 and calculations from equation (3.8). There is also calculated a moving average, where the average of 5 points are taken for each point. A single exponential decay was fitted with the data using equation (2.10), yielding the rotational correlation time to be $\tau_r = 0.5 \pm 0.2$, with $r_0 = 0.17$. A baseline was also fitted, where this was found to be $y_0 = -0.07$.

Molecular Docking Calculations

Molecular docking calculations is a computational procedure that attempts to predict non-covalent binding of a macromolecule and a ligand. In this case a protein, and a fluorescent probe. It will calculate properties such as binding affinities, predict the best conformations for the ligand, and simulate the docking process itself.

7.1 Results of Docking

Here, Autodock Vina was used to calculate nine different binding modes or affinities, and rank them accordingly for each probe docked to TTR. The other modes are then compared to the first one in terms of binding affinity. The root-mean-square deviation (rmsd) from the best mode is also calculated, and given in Ångström (Å). The rmsd values are calculated relative to the first or best mode and use only movable heavy atoms, meaning ignoring for example hydrogens. The rmsd upper bound (u. b.), matches each atom in one conformation with itself in the other conformation, ignoring any symmetry. The rmsd lower bound (l. b.) matches each atom in one conformation with the closest atom of the same element in the other conformation. In this section, only the most interesting docking results are displayed. For more data and information of the docking results, it is referred to the results in appendix A.6.

Figure 7.1 shows the lowest energy conformation of the fluorescent probe h-FTAA docked to TTR for each binding site. Table 7.1 shows other calculations for similar conformation of the probe. Left binding site in this case means the binding site closest to the reader, while the right binding site is furthest away. Notice how the h-FTAA molecule binds to TTR almost as a belt around the molecule, instead of being angled inwards as seems to be the trend with the other probes (See appendix A.6).



Figure 7.1: Best docking, best conformation and best binding affinity of the probe h-FTAA docked to native tetrameric TTR. Each monomer of TTR is colored differently. Results calculated with Autodock Vina (Trott & Olson 2010). The chemical representation generated in the software Py-MOL (Schrödinger, LLC 2020).

Table 7.1: Docking results calculated from docking h-FTAA to tetrameric TTR with Autodock Vina (Trott & Olson 2010). Left- and right binding sites relative to what figure 7.1 is showing. Here, nine different binding modes or affinities are calculated, and ranked accordingly. The root-mean-square deviation is also displayed.

Mode	Left binding site			Right binding site		
	Affinity (kcal / mol)	Dist. from best mode rmsd l.b.	rmsd u.b.	Affinity (kcal / mol)	Dist. from best mode rmsd l.b.	rmsd u.b.
1	-6.6	0.000	0.000	-6.8	0.000	0.000
2	-6.5	2.332	16.148	-6.7	2.506	16.033
3	-6.1	2.514	3.656	-6.5	1.627	16.066
4	-6.0	1.479	16.140	-6.5	2.198	15.941
5	-6.0	2.775	15.961	-6.5	7.009	10.613
6	-5.6	1.593	1.880	-6.5	1.986	2.441
7	-5.2	2.150	2.685	-6.4	7.286	11.513
8	-5.1	2.103	16.121	-6.4	6.382	15.355
9	-4.8	2.868	4.008	-6.4	7.325	15.513

Figure 7.2 shows the the lowest energy conformation of the fluorescent probe Py1SA docked to TTR for each binding site. Calculations for the nine binding modes or conformation are shown in table 7.2, with left and right binding sites being relative to figure

7.2 and the reader. Notice the higher affinity for Py1SA compared to h-FTAA.

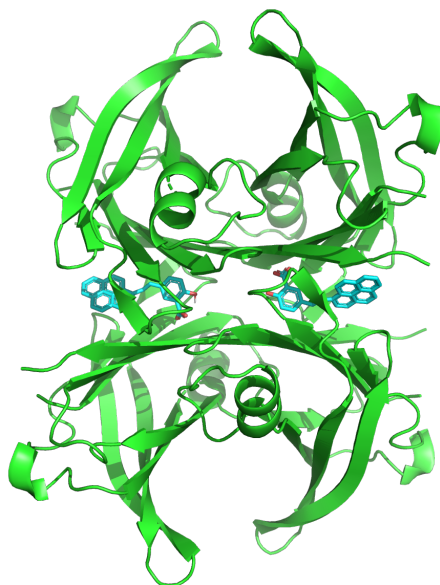


Figure 7.2: Best docking, best conformation and best binding affinity of the probe Py1SA docked to native tetrameric TTR. Results are calculated with Autodock Vina (Trott & Olson 2010). The chemical representation generated in the software PyMOL (Schrödinger, LLC 2020).

Table 7.2: Docking results calculated from docking Py1SA to tetrameric TTR with Autodock Vina (Trott & Olson 2010). Left- and right binding sites relative to what figure 7.2 is showing. Here, nine different binding modes or affinities are calculated, and ranked accordingly. The root-mean-square deviation is also displayed.

Mode	Left binding site			Right binding site		
	Affinity (kcal / mol)	Dist. from best mode rmsd l.b.	rmsd u.b.	Affinity (kcal / mol)	Dist. from best mode rmsd l.b.	rmsd u.b.
1	-10.2	0.000	0.000	-10.2	0.000	0.000
2	-10.2	5.183	6.968	-10.2	1.322	2.046
3	-10.1	18.872	23.226	-10.2	1.505	3.677
4	-10.1	18.877	23.269	-10.2	1.082	3.147
5	-9.9	4.788	8.705	-10.0	1.534	3.534
6	-9.9	4.977	9.069	-9.9	1.395	3.181
7	-9.9	4.691	8.847	-9.9	1.054	2.139
8	-9.9	5.044	8.983	-9.9	0.953	1.808
9	-9.7	19.199	23.515	-9.8	1.017	2.769

7.2 Comparison with X-ray Crystallography

The rmsd values are only a comparison to the binding mode that the scoring function predicts as the lowest energy. The best way to verify the predictions of the docking results, is to compare them to crystallography structures of the same molecules, which is here done with the probe Py1SA. This is displayed in figure 7.3. This preliminary crystallography structure of Py1SA bound to TTR was created by the research group in Linköping. Notice the similarities of conformation and angles of binding modes of the probe.

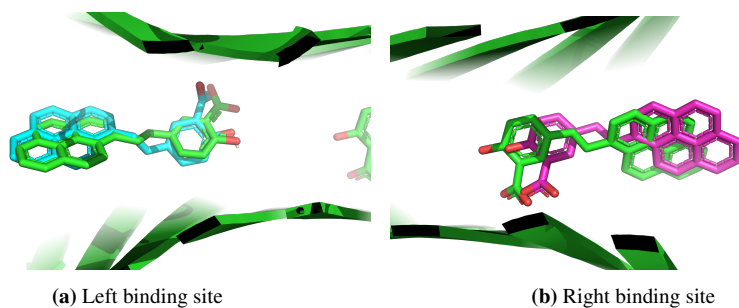


Figure 7.3: Py1SA docking results (blue and pink) with TTR compared with a X-ray crystallography structure of Py1SA bound to TTR, green being the crystallography structure (Full structure: TTR + Py1SA). Crystallography structure made by the research group in Linköping.

Part III

DISCUSSION

Discussion and Limitations

First, absorption spectroscopy was done to determine the wavelength regions accessible for excitation of the fluorescent probes and the protein. With this determined, excitation and emission spectra were gathered through fluorescence spectroscopy. By gathering these spectra of the fluorescent probes, with and without TTR, we can see and compare the different probes. Secondly, with knowledge of the probe feature with TTR it is meaningful to make docking between the probes and amyloid aggregates. With the solvent and native TTR properties at hand, it is then possible to reveal what the spectral characteristics of the amyloid binding sites are. Ultimately, the spectral and other photo-physical parameters will aid in studies *in vitro* cell studies, sections from patients, or even *in vivo* microscopic investigations.

8.1 Evaluation of the TTR-probe characterization

8.1.1 Absorption Spectroscopy

The results of absorption spectroscopy are mainly there to determine the excitation wavelength needed to do further analysis and characterization of the samples under investigation. But in section 4.1 there are a couple of interesting factors happening. As one can see in figure 4.2 the oligothiophenes show quite the same spectral identities, with only small shift in the spectra. They have quite the same position where the peaks are situated at 410 nm 440 nm and 420 nm for the pentameric, hexameric and heptameric thiophene respectively. Interestingly, the hexamer has an absorption with higher extinction coefficient and at a lower photon energy. As the band-gap usually gets smaller and the transition dipole moment larger for longer conjugation lengths, it suggests that the heptamer takes a more folded structure of its back-bone (Klingstedt, Åslund, Simon, Johansson, Mason, Nyström, Hammarström & Nilsson 2011).

Two other interesting results were the absorption spectra of BTD-SB and HS-169 showing

two distinct peaks at two different energy transitions (See figures 4.3 and 4.1. Since BTDSB is almost completely quenched in PBS (See figure A2c), the two peaks of HS-169 was further investigated with the other photo-physical properties.

8.1.2 Fluorescence properties

All of the probes show some difference in spectral shift. As also pointed out in section 4.2, the probes showing the largest spectral shifts, discrepancies and potential are X-34, Py1SA and HS-169. We can see from both the figures and table 4.2 that the fluorescence spectra tend to slightly shift towards the blue/UV region when the probes are bound to the protein. By comparing them and looking at their Stokes' Shift, it can be noted that h-FTAA (Figure A1c), HS-169 (Figure 4.7) and X-34 (Figure 4.5) have the largest spectral shift, with a difference of 34 nm, 33 nm and 59 nm when they are bound to TTR. It is also worth mentioning that the excitation spectra of h-FTAA is drastically red-shifted when introduced to TTR. More than many of the other fluorescent probes. Similar results have been reported by Sjölander et al. (2016). Fluorescent probes that give substantial differences in spectral shifts are useful in spectral imaging. For example for molecules with a large spectral shift, it is possible to distinguish the probe from the probe attached to the protein when looking at it through fluorescence microscopy, or other sorts of imaging. This can be crucial when it comes to determination of protein, or protein fibrils, such as TTR depositions. It can therefore be useful for diagnosis of the types of diseases mentioned earlier related to amyloidosis, or TTR depositions.

Py1SA does not change a lot in terms of spectral shift when bound to TTR. However, the fluorescence spectra show an interesting discrepancy. When bound to the protein, the twin peaks at around 390 nm and 410 nm completely disappear, as one can see in figure 4.6. This can also be an interesting factor to look at when it comes to imaging, and also the lifetime of this molecule. Changes like these are important when it comes to characterization of the protein and the probe (Zhang, Sandberg, Konsmo, Wu, Nyström, Nilsson, Konradsson, LeVine III, Lindgren & Hammarström 2018, Lindgren & Hammarström 2010).

When it comes to ranking the probes in terms of their spectral shifts, and with a quick look at tables 4.2 and 5.1, the ranking would be as follows:

1. HS-169, 2. h-FTAA, 3. X-34, 4. ANS, 5. p-FTAA, 6. Py1SA, 7. hx-FTAA, 8. BTDSB, 9. Py2SA.

Here, none of the probes are bad, but rather there are some very good ones. This list is as mentioned based off of the difference in spectra (spectral shift), but also change in Stokes' Shift after the addition of TTR to the probe. It is worth mentioning again, the interesting discrepancy happening with Py1SA, and should not be ignored. Similar traits was seen in a study of the Py2SA bound to amyloid- β and tau fibrils (Zhang, Wang, Sandberg, Wu, Nyström, LeVine III, Konradsson, Hammarström, Durbeej & Lindgren 2018, Zhang et al. 2017). Such optical properties will expand the number of fluorescent probes available for targeting a variety of protein aggregates.

8.1.3 Quantum Yield properties

The measurements of the quantum yield is a delicate, but powerful method of characterization. Also from the quantum efficiency measurements, we see that X-34 is an interesting candidate, with an increase in quantum yield from 4.7 % to 44.3 %! All the other probes also show potential, where the quantum efficiency is increasing, except for the two oligothiophenes p-FTAA and hx-where the quantum efficiency is actually decreasing. What is also interesting here, is that h-FTAA is one of the probes with the highest increases in quantum yield, besides from X-34. It went from having a quantum efficiency of 4.4 % to 18 % when bound to TTR. That is a change of almost 14 % and by a factor of 4. This can further explain that h-FTAA interact with TTR in another way than what the other thiophenes do. For example with what was mentioned earlier, with suggesting that the heptamer takes a more folded structure. All the oligothiophenes are highly relevant for studies of Amyloid- β Fibrils studies on Alzheimers (Bäck et al. 2016).

The quantum efficiency of the probe BTD-SB (Table 4.2) was determined from previous studies (Zhang et al. 2019, Zhang, Sandberg, Konsmo, Wu, Nyström, Nilsson, Konradsson, LeVine III, Lindgren & Hammarström 2018), since the probe was self-quenching (See figure A2c). From previous study, and with the measurements done on this probe, it shows a general increase in quantum efficiency as well. When it comes to ranking the probes in terms of changes in their quantum efficiencies when bound to TTR (by looking at table 4.2), that ranking would be as follows:

1. X-34, 2. h-FTAA, 3. Py2SA, 4. Py1SA, 5. BTD-SB, 6. HS-169, 7. hx-FTAA, 8. p-FTAA.

These are merely based on the change in quantum efficiency, and how efficient the fluorophore will emit upon excitation after binding to TTR. What all these results say something about, is the binding affinity of TTR. The fact that the probes give a higher quantum efficiency when TTR is added to the sample, shows that the probes actually bind to the protein. This can be due to solvent effects on the probes and protein. Generally, PBS was used as solvent for all probes, because this is what TTR has to be diluted in to not denature. HS-169 was, however, measured for both PBS and MeOH. This was mainly done to look at general characteristics, but turned out to reveal some interesting factors. For the case of this thesis, the first interesting change was in the fluorescence spectra, and the probe's spectral shift. With a quick glance at table 4.2 and the figures 4.7, A2a, A3a and A3b, one can quickly see the similarities of spectral characterization of HS-169 bound to TTR and HS-169 diluted in MeOH, while there is a more significant red-shift for HS-169 diluted in PBS. With MeOH having a different polarity than PBS, and the quantum yield of HS-169 diluted in MeOH being relatively high compared to when it is diluted in PBS, it is reason to believe that PBS/water acts like a quencher for the probe. Since PBS also is a polar molecule, and the binding sites of TTR being hydrophobic, give the results more reliability in terms of binding affinity and that the probes actually binds and penetrates the membrane of TTR.

Another interesting feature of the HS-169 probe is the appearance of an extra high energy emission. Normally, fluorescence emits only from the lowest singlet state (S_1), and this is referred to as "Kasha's rule" (Kasha 1950). Using advanced quantum chemical calcula-

tions transition oscillator strengths for such "forbidden" transitions can be calculated.

All the quantum efficiency results can also be of help when it comes to diagnosis and to distinguish probe from probe bound to protein.

8.1.4 Excited State Lifetime properties

It is interesting to look at the results for the excited state lifetime of the different samples. Most of the probes did not show a lot of difference when bound to TTR. However, X-34, HS-169, the long-lived pyrene Py2SA, and the probe ANS show some interesting results. As a general remark, most probes show an increase in excited state lifetimes when bound to TTR. However, p-FTAA show a decrease in its excited state lifetime (See tables 4.3 and 5.1). The biggest increase is the long-lived pyrene, Py2SA, which increases its lifetime from 7 ns to 31 ns when bound to TTR. Therefore, a ranking of the probes in terms of general lifetime, but also change when bound to TTR, would be:

1. Py2SA, 2. ANS, 3. HS-169, 4. Py1SA, 5. BTD-SB, 6. X-34, 7. h-FTAA, 8. hx-FTAA, 9. p-FTAA

It is worth noting that the lifetime of the probe BTD-SB diluted in PBS was found to be < 0.05% from Zhang, Sandberg, Konsmo, Wu, Nyström, Nilsson, Konradsson, LeVine III, Lindgren & Hammarström (2018), and was used to calculate the difference in lifetimes.

Longer lifetimes are also of interest when it comes to molecular dynamics. (Lindgren et al. 2005, Campos et al. 2016, Sörgjerd et al. 2008) Here, variables such as rotational diffusion coefficient, size and kinetics of the sample can be calculated. When it comes to longer lifetimes, Py2SA seems to be the best candidate, followed by ANS, as previous studies have shown. This will be discussed in later section about the probe-TTR interaction.

Previous studies have also shown great promise and similar results for the pyrenes, Py1SA and Py2SA, and the salicylate bis-styrylbenzene, X-34, and its derivative, BTD-SB, together with amyloid- β and tau fibrils (Zhang, Wang, Sandberg, Wu, Nyström, LeVine III, Konradsson, Hammarström, Durbeej & Lindgren 2018, Zhang et al. 2017, Zhang, Sandberg, Konsmo, Wu, Nyström, Nilsson, Konradsson, LeVine III, Lindgren & Hammarström 2018, Zhang et al. 2019). This shows how great these fluorescent probes can potentially be for characterization of not just TTR, but other proteins linked to neurodegenerative diseases.

As with the spectral data, the lifetime can also be measured through imaging. By using the Fluorescence Lifetime Imaging (FLIM) method, it is possible to take the analysis and determination of TTR or amyloid fibril to the next level. Fluorescence microscopy, compared to solution spectroscopy, allows the analysis of specific objects in the object plane, rather than the average of the whole sample. With the data gathered from this project, especially of probes showing a difference in lifetime, it is possible to compare these with data gathered from the FLIM method. By using these two methods to gather precise information about the amyloid binding probes, it can be of help for further studies towards diagnosis of amyloidosis. There have been a lot of interesting research in this field to, that also these probes can contribute to (Berezin & Achilefu 2010, Arja et al. 2013).

8.2 Evaluation of the Probe-TTR Interaction

8.2.1 FRET properties

With the FRET measurements it is possible to get a qualitative understanding of distances and interactions between probe (A) and protein (D). By previous studies, and the TTR characteristics measurements done in 5.2, it is safe to say that the tryptophan residues influence the photo-physical properties of TTR. The tryptophan residues are also considered to be affiliated to the binding sites of TTR. Since many of the probes absorb or are excited near where TTR and tryptophan emit photons, FRET effects may occur. By investigating table 5.3 and table 5.4, one can conclude by the results that h-FTAA, X-34 and BTD-SB are the most interesting of the probes. There are FRET-effects occurring with some of the other probes too, but not as prominent as for these three. In terms of energy transfer and ranking these three probes based on their FRET properties, the list would be as follows:

1. BTD-SB, 2. h-FTAA, 3. X-34

It is also worth mentioning p-FTAA as an honorable fourth probe which expresses some energy transfer and interaction with TTR. The other probes were hard to rank, as they all expressed similar properties. The Förster distance was mentioned in the theory section as the distance where the transfer efficiency is 50% efficient and can be calculated by equation 2.21 based on the results on D and D-A lifetime decays. BTD-SB is the only probe that passes the Förster distance somewhere between having the concentration ratio of 2 : 1 and 4 : 1 with TTR. Further analysis and work can be done, where distances between donor and acceptor can be better determined and calculated. With the information at hand, this merely gives a qualitative measure of the distance between the fluorescent probes and tryptophans in TTR, but also tells us a lot about the probe-TTR interaction.

8.2.2 Properties of Molecular Docking

Molecular docking calculations are based on computational procedure, and are there to simulate the physics and chemistry that happens in the real microscopic world. Since these are molecules and interactions the human eye cannot observe, this tool is of great help to understand what is happening. It can also be a tool for comparisons and for simulations of the yet unknown.

Two probes that are docked to TTR are of interest, when it comes to the results of the molecular docking. As figure 7.1 shows, the two h-FTAA molecules docked on each available binding site bind almost as a belt around the TTR molecule. This representation is what the scoring function and simulation calculated as the lowest energy conformation, making it the most likely conformation. This is interesting, since the results show that the probes generally angle inwards in the pockets of TTR. This can have to do with the size or backbone of h-FTAA, making it difficult or not energetically favorable to angle inwards. This belt formation can also be an explanation for the spectral differences and differences in other photo-physical properties when comparing it to the other oligothiophenes.

Figure 7.2 shows the best docking, best conformation and the best binding affinity of the probe Py1SA. This probe shows the regular inwards angled conformation. What is inter-

esting, is that the research group at Linköping University made an X-ray crystallography structure of exactly this probe bound to native tetrameric TTR. The comparison between best conformation and the crystallography structure can be viewed in figure 7.3. By looking at the comparison, one can quickly determine that the method of molecular docking is a very accurate method, as it predicts the docking effectively. Since all bonds are made rotatable and that the molecule can move freely inside the large grid box one assigns, the calculations are impressive.

Another interesting discrepancy is the apparent trend that the right binding site got a generally lower binding affinity for all of the probes. This can be seen over all the probes and all the tables, e. g. if one compares table 7.1 and 7.2. See appendix A.6 for more comparisons. Previous studies have shown that the binding affinity of TTR to thyroid hormone T4 is dependent on the length of the N-terminal in TTR monomer, and the number of hydrophilic groups in the N-terminal. However, the evolutionary changes on the C-terminal region has occurred less in comparison to the N-terminal of TTR (Prapunpoj & Leelawatwattana 2009). The accessibility of thyroxine hormone binding sites may depend on the C-terminal region due to the fact that these segments are close to the central channel where, as we can see in the figures, the binding sites are. These small changes, can also be the reason to why there are small differences in the calculated conformations. With this, it is even possible to distinguish the binding sites from one another.

The next step of molecular docking and the calculations would be to combine this method with further studies or calculations of the FRET-effects. By measuring the change in fluorescence spectra of the donor and acceptor molecules, the Förster distance can be determined and the FRET-method can be used as a spectroscopic ruler (Lakowicz 1999, Förster 1948). It can then be compared with distances calculated through the docking simulations.

8.2.3 The dynamics of TTR

Time-resolved fluorescence anisotropy was utilized to probe the dynamics of TTR. Since long excited state lifetimes are desirable in the measurements of anisotropy, Py2SA was used. Long lifetime probes are desired because of the rotational correlation time of TTR also being relatively long. As previously studied in e. g. Lindgren et al. (2005), a short lifetime fluorescent molecule will contribute to the measurements being truncated, leading to inaccurate results. The fitted rotational correlation time for native TTR using bound Py2SA was found to be 19 ns. Lindgren et al. (2005) reported a result of 27 ns, where they used the fluorescent probe ANS. As measured in the article and in this dissertation, the lifetime of ANS bound to TTR is found to be around 14 ns. Since the rotational correlation time were larger than the than the fluorescence lifetime of bound ANS, a direct determination of the rotational time were not reliable for this probe, as concluded in the article. It was also mentioned that the trace from the fluorescence anisotropy decay measurement of the aggregate showed that the anisotropy decay did not reach zero, due to longer rotational correlation time of the aggregate than the fluorescence lifetime of the probe. By looking at figure 6.2, it is evident that the decay goes towards zero without any form of baseline fitting. It is worth mentioning that the signal to noise ratio is still significant, and should not be ignored. Following this, the results measured for Py2SA should therefore be more reliable with the reason being the longer lifetime of the probe.

Time-resolved fluorescence anisotropy measurements were also conducted on Py2SA alone, in two different solvents. In figure 6.3, the trace and anisotropy decay of Py2SA in 75 % Glycerol is shown. In figure 6.4, the trace and anisotropy decay of Py2SA in PBS is shown. As one can see and mentioned earlier, the water-based PBS acts as a quencher for Py2SA giving a poor S/N ratio. Furthermore, the measuring times had to be increased significantly. With increased measuring times, the measure of a good instrumental factor is difficult. With longer measuring times, the longer the instruments are exposed to noise. This can be viewed in the results as there is an offset in the data points along the whole transient. This is seen as a dip in the data points. Since the absorbance and emission of Py2SA in the different solvents are relatively similar to when its bound to TTR, the r_0 also has to be relatively similar. r_0 measures the angle between the excitation- and emission dipole moment, and it is therefore difficult to see physically why it should change much. r_0 was therefore fixed to 0.17, as this was the value of r_0 in the anisotropy decay measurement of TTR. A baseline was then added to make the exponential decay fit to the r_0 value. The figures now show that the decay converges to zero after the offset. The rotational correlation time of Py2SA in Glycerol was then found to be 4.0 ns and 0.5 ns for Py2SA in PBS. Here, the solvent effects are displayed as Glycerol is a more viscous fluid, and therefore will make Py2SA move slower. This gave some proof-of-principle for the method with distinctly different rotational correlation times for the probe in TTR, 75 %, and pure PBS.

Conclusion and Suggested Further Work

The findings have been discussed in the previous chapter, whereas this chapter summarizes the conclusion for the thesis and further work to be conducted to support the rationale.

The objective for the thesis was originally to acquire more knowledge of the protein (TTR), how it forms amyloid structures and can be characterized using several fluorescent binding probes. Due to the corona pandemic during spring 2020, the spectroscopy lab at NTNU, and the protein lab with our collaboration at Linköping University, were closed, or operating with reduced capacity during most of March until May. The initial objective and project plan was altered. Instead, the project's focus was shifted towards a more detailed investigation of the native TTR protein.

Amyloidosis is a group of diseases where normal soluble proteins are triggered to form toxic amyloid fibrils which are highly stable and insoluble. The transport protein TTR is one of these proteins related to some of these diseases such as Alzheimer's disease, Carpal Tunnel Syndrome and heart failures. Due to lack of a direct cure for these diseases, and lack of knowledge about the protein, new strategies for early diagnosis and characterization are implemented. Many biological tools and techniques have been contributing to understanding the protein and the amyloid fibrils at a molecular level. Studies have shown that using photo-physical processes and small fluorescent binding molecules have proven to be a powerful method for characterization of amyloid structure by staining protein aggregates.

Nine different probes with and without TTR protein have been studied in terms of photo-physical parameters and probe-protein interactions, where all of them have given results and shown some sort of interaction with the protein. Data on interactions with TTR, and data on the protein itself, has in this way been properly investigated. With all of the probes showing different kinds of reactions, interactions and optical properties, it is

therefore safe to say that these fluorescent probes have the potential to be used in targeting and characterization of protein aggregates of TTR. They can also potentially be used as fluorescent markers and diagnosis tools for the neurodegenerative diseases that TTR may bring.

9.1 Suggested Further Work

This thesis lay the groundwork and base for what the aim and background the thesis originally had. As said, due to the corona pandemic during spring 2020, the amyloid fibrils could not be produced, retrieved or investigated. Suggested further work, is therefore to investigate on amyloid aggregates, such as ATTR, further characterize them, and compare the results with the characterization of the TTR protein investigated on in this thesis. Therefore, this vast characterization work of TTR is already done, and can be used for comparisons or as a supplement or an assist for when values are needed.

Comparisons by using Confocal Laser Scanning Microscopy (CLSM), or other forms of fluorescence imaging, is also something that can be looked further into. A deeper study on the FRET-effects and determination of the Förster distances can be calculated for relevant probes. This can further be compared with distances calculated from docking results and more advanced quantum chemical calculations.

Secondly, it was discovered a peculiar double emission using HS-169 as probe, that is an apparent deviation from Kasha's rule. Further studies combining spectroscopy and theoretical calculations could reveal more about what interactions governs this phenomenon.

The lifetime changes upon binding for certain fluorescent ligands suggest that FLIM could be useful for investigation of TTR/amyloid deposits.

Bibliography

Abagyan, R., Totrov, M. & Kuznetsov, D. (1994), 'ICM – a new method for protein modeling and design: Applications to docking and structure prediction from the distorted native conformation', *Journal of Computational Chemistry* **15**(5), 488–506.

URL: <https://onlinelibrary.wiley.com/doi/abs/10.1002/jcc.540150503>

Arja, K., Sjölander, D., Åslund, A., Prokop, S., Heppner, F. L., Konradsson, P., Lindgren, M., Hammarström, P., Åslund, K. O. A. & Nilsson, K. P. R. (2013), 'Enhanced fluorescent assignment of protein aggregates by an oligothiophene–porphyrin-based amyloid ligand', *Macromolecular Rapid Communications* **34**(9), 723–730.

URL: <https://onlinelibrary.wiley.com/doi/abs/10.1002/marc.201200817>

Åslund, A., Sigurdson, C. J., Klingstedt, T., Grathwohl, S., Bolmont, T., Dickstein, D. L., Glimsdal, E., Prokop, S., Lindgren, M., Konradsson, P., Holtzman, D. M., Hof, P. R., Heppner, F. L., Gandy, S., Jucker, M., Aguzzi, A., Hammarström, P. & Nilsson, K. P. R. (2009), 'Novel pentameric thiophene derivatives for in vitro and in vivo optical imaging of a plethora of protein aggregates in cerebral amyloidoses', *ACS chemical biology* **4**(8), 673–684.

URL: <https://pubmed.ncbi.nlm.nih.gov/19624097>

Bäck, M., Appelqvist, H., LeVine, Harry, r. & Nilsson, K. P. R. (2016), 'Anionic oligothiophenes compete for binding of x-34 but not pib to recombinant $\alpha\beta$ amyloid fibrils and alzheimer's disease brain-derived $\alpha\beta$ ', *Chemistry (Weinheim an der Bergstrasse, Germany)* **22**(51), 18335–18338.

URL: <https://pubmed.ncbi.nlm.nih.gov/27767229>

Beeby, A. (2019), *A Guide to Recording Fluorescence Quantum Yields*, HORIBA Scientific, Middlesex, UK.

Berezin, M. Y. & Achilefu, S. (2010), 'Fluorescence lifetime measurements and biological imaging', *Chemical Reviews* **110**(5), 2641–2684.

URL: <https://doi.org/10.1021/cr900343z>

Birch, D. J. S. & Imhof, R. E. (1999), *Time-Domain Fluorescence Spectroscopy Using*

-
- Time-Correlated Single-Photon Counting*, Springer US, Boston, MA, pp. 1–95.
URL: https://doi.org/10.1007/0-306-47057-8_1
- Birks, J. B. (1970), *Photophysics of Aromatic Molecules*, Wiley-Interscience, New York, USA.
- Brouwer, A. M. (2011), ‘Standards for photoluminescence quantum yield measurements in solution (iupac technical report)’, *Pure and Applied Chemistry* **83**(12), 2213 – 2228.
URL: <https://www.degruyter.com/view/journals/pac/83/12/article-p2213.xml>
- Campbell, I. D. & Dwek, R. A. (1984), *Biological Spectroscopy*, Benjamin/Cummings Publishing Company, Michigan, USA.
- Campos, R. I., Wu, X., Elgland, M., Konradsson, P. & Hammarström, P. (2016), ‘Novel trans-stilbene-based fluorophores as probes for spectral discrimination of native and protofibrillar transthyretin’, *ACS Chemical Neuroscience* **7**(7), 924–940.
URL: <https://doi.org/10.1021/acschemneuro.6b00062>
- Chang, C.-e. A., Chen, W. & Gilson, M. K. (2007), ‘Ligand configurational entropy and protein binding’, *Proceedings of the National Academy of Sciences* **104**(5), 1534–1539.
URL: <https://www.pnas.org/content/104/5/1534>
- ChemAxon (2020), ‘Marvin was used for drawing, displaying and characterizing chemical structures, substructures and reactions’.
URL: <https://chemaxon.com/products/marvin/>
- Chen, R. F. (1972), ‘Measurements of absolute values in biochemical fluorescence spectroscopy’, *JOURNAL OF RESEARCH of the Notional Bureau of Standards - A. Physics and Chemistry* **76A**(6), 593–606.
URL: https://nvlpubs.nist.gov/nistpubs/jres/76A/jresv76An6p593_A1b.pdf
- Daimon, M. & Masumura, A. (2007), ‘Measurement of the refractive index of distilled water from the near-infrared region to the ultraviolet region’, *Appl. Opt.* **46**(18), 3811–3820.
URL: <http://ao.osa.org/abstract.cfm?URI=ao-46-18-3811>
- Du, H., Fuh, R.-C. A., Li, J., Corkan, L. A. & Lindsey, J. S. (1998), ‘Photochemcad \ddagger : A computer-aided design and research tool in photochemistry’, *Photochemistry and Photobiology* **68**(2), 141–142.
URL: <https://onlinelibrary.wiley.com/doi/abs/10.1111/j.1751-1097.1998.tb02480.x>
- Duong, S. (2019), Evaluation of novel fluorescent probes for in vivo transthyretin amyloid using fibrils generated in vitro under varying conditions, Master’s thesis, Linköping University, Department of Physics, Chemistry and Biology, Linköping, Sweden.
- Fikrle, M., Paleček, T., Kuchynka, P., Němeček, E., Bauerová, L., Straub, J. & Ryšavá, R. (2013), ‘Cardiac amyloidosis: A comprehensive review’, *Cor et Vasa* **55**(1), e60 – e75.
URL: <http://www.sciencedirect.com/science/article/pii/S0010865012001361>
- Fornasini, P. (2008), *The Uncertainty in Physical Measurements: An Introduction to Data*
-

Analysis in the Physics Laboratory, Springer, New York, USA.

URL: <https://doi.org/10.1007%2F978-0-387-78650-6>

Förster, T. (1948), 'Intermolecular energy migration and fluorescence', *Annalen der Physik* **437**(1-2), 55–75.

Gilson, M. K., Given, J. A., Bush, B. L. & McCammon, J. A. (1997), 'The statistical-thermodynamic basis for computation of binding affinities: A critical review', *Biophysical Journal* **72**(3), 1047–1069.

URL: [https://www.cell.com/biophysj/pdf/S0006-3495\(97\)78756-3.pdf](https://www.cell.com/biophysj/pdf/S0006-3495(97)78756-3.pdf)

Glimsdal, E. (2009), Spectroscopic characterization of some platinum acetylide molecules for optical power limiting applications, PhD thesis, Norwegian University of Science and Technology (NTNU), Trondheim, Norway.

Grinvald, A., Haas, E. & Steinberg, I. Z. (1972), 'Evaluation of the distribution of distances between energy donors and acceptors by fluorescence decay', *Proceedings of the National Academy of Sciences* **69**(8), 2273–2277.

URL: <https://www.pnas.org/content/69/8/2273>

Haas, E., Katchalski-Katzir, E. & Steinberg, I. Z. (1978), 'Brownian motion of the ends of oligopeptide chains in solution as estimated by energy transfer between the chain ends', *Biopolymers* **17**(1), 11–31.

URL: <https://onlinelibrary.wiley.com/doi/abs/10.1002/bip.1978.360170103>

Haas, E., Wilchek, M., Katchalski-Katzir, E. & Steinberg, I. Z. (1975), 'Distribution of end-to-end distances of oligopeptides in solution as estimated by energy transfer', *Proceedings of the National Academy of Sciences* **72**(5), 1807–1811.

URL: <https://www.pnas.org/content/72/5/1807>

Hecht, E. (2016), *Optics, Global Edition*, 5 edn, Pearson Education Limited, London, UK.

Hemmer, P. C. (2005), *Kvantemekanikk*, 5 edn, Tapir Akademisk Forlag, Trondheim, Norway.

Jabłoński, A. (1960), 'On the notion of emission anisotropy', *Bull. Acad. Pol. Sci. Ser. A* **2**, 259–264.

Jain, A. N. (1996), 'Scoring noncovalent protein-ligand interactions: A continuous differentiable function tuned to compute binding affinities', *Journal of Computer-Aided Molecular Design* **10**(5), 427–440.

URL: <https://doi.org/10.1007/BF00124474>

Kasha, M. (1950), 'Characterization of electronic transitions in complex molecules', *Discuss. Faraday Soc.* **9**, 14–19.

URL: <http://dx.doi.org/10.1039/DF9500900014>

Kirchner, J. (1995), Data analysis toolkit #5: Uncertainty analysis and error propagation, Technical report, Berkeley Seismology Laboratory, University of California.

URL: http://seismo.berkeley.edu/~kirchner/eps_120/Toolkits/Toolkit_05.pdf

-
- Klingstedt, T., Åslund, A., Simon, R. A., Johansson, L. B. G., Mason, J. J., Nyström, S., Hammarström, P. & Nilsson, K. P. R. (2011), 'Synthesis of a library of oligothiophenes and their utilization as fluorescent ligands for spectral assignment of protein aggregates', *Org. Biomol. Chem.* **9**, 8356–8370.
URL: <http://dx.doi.org/10.1039/C1OB05637A>
- Klingstedt, T., Åslund, A., Simon, R. A., Johansson, L. B. G., Mason, J. J. & Nyström, S. (2011), 'Synthesis of a library of oligothiophenes and their utilization as fluorescent ligands for spectral assignment of protein aggregates', *Org. Biomol Chem.* **9**.
- Kozma, I. Z., Krok, P. & Riedle, E. (2005), 'Direct measurement of the group-velocity mismatch and derivation of the refractive-index dispersion for a variety of solvents in the ultraviolet', *J. Opt. Soc. Am. B* **22**(7), 1479–1485.
URL: <http://josab.osa.org/abstract.cfm?URI=josab-22-7-1479>
- Ku, H. H. (1966), 'Notes on the use of propagation of error formulas', *JOURNAL OF RESEARCH of the National Bureau of Standards - C. Engineering and Instrumentation* **70C**(4), 263–273.
URL: https://nvlpubs.nist.gov/nistpubs/jres/70C/jresv70Cn4p263_A1b.pdf
- Lakowicz, J. R. (1999), *Principles of Fluorescence Spectroscopy*, 2 edn, Kluwer Academic/Plenum Publishers, New York, USA.
- Lindgren, M. & Hammarström, P. (2010), 'Amyloid oligomers: spectroscopic characterization of amyloidogenic protein states', *The FEBS Journal* **277**(6), 1380–1388.
URL: <https://febs.onlinelibrary.wiley.com/doi/abs/10.1111/j.1742-4658.2010.07571.x>
- Lindgren, M., Sörgjerd, K. & Hammarström, P. (2005), 'Detection and characterization of aggregates, prefibrillar amyloidogenic oligomers, and protofibrils using fluorescence spectroscopy', *Biophysical Journal* **88**(6), 4200 – 4212.
URL: <http://www.sciencedirect.com/science/article/pii/S0006349505734706>
- Mangrolia, P. & Murphy, R. M. (2018), 'Retinol-binding protein interferes with transthyretin-mediated β -amyloid aggregation inhibition', *Biochemistry* **57**(33), 5029–5040.
URL: <https://doi.org/10.1021/acs.biochem.8b00517>
- Melnikov, A. S., Serdobintsev, P. Y., Vedyaykin, A. D. & Khodorkovskii, M. A. (2017), 'Two-photon absorption cross section for coumarins 102, 153 and 307', *Journal of Physics* **917**.
- Morris, G. M., Huey, R., Lindstrom, W., Sanner, M. F., Belew, R. K., Goodsell, D. S. & Olson, A. J. (2009), 'Autodock4 and autodocktools4: Automated docking with selective receptor flexibility', *Journal of Computational Chemistry* **30**(16), 2785–2791.
URL: <https://onlinelibrary.wiley.com/doi/abs/10.1002/jcc.21256>
- Murphy, R. M. (2007), 'Kinetics of amyloid formation and membrane interaction with amyloidogenic proteins', *Biochimica et Biophysica Acta (BBA) - Biomembranes* **1768**(8), 1923 – 1934. Amyloidogenic Protein–Membrane Interaction.
URL: <http://www.sciencedirect.com/science/article/pii/S0005273606004913>
-

-
- Nocedal, J. & Wright, S. J. (1999), *Numerical Optimization*, 2 edn, Springer Series in Operations Research, Springer Verlag, Berlin, Germany.
- Prapunpoj, P. & Leelawatwattana, L. (2009), 'Evolutionary changes to transthyretin: structure–function relationships', *The FEBS Journal* **276**(19), 5330–5341.
URL: <https://febs.onlinelibrary.wiley.com/doi/abs/10.1111/j.1742-4658.2009.07243.x>
- Rambaran, R. N. & Serpell, L. C. (2008), 'Amyloid fibrils', *Prion* **2**(3), 112–117. PMID: 19158505.
URL: <https://doi.org/10.4161/pri.2.3.7488>
- Rurack, K. & Spieles, M. (2011), 'Fluorescence quantum yields of a series of red and near-infrared dyes emitting at 600 – 1000 nm', *Analytical Chemistry* **83**(4), 1232–1242.
URL: <https://doi.org/10.1021/ac101329h>
- Rutherland, R. L. (2003), *Handbook of Nonlinear Optics, Revised and Expanded*, 2 edn, Marcel Dekker, Inc., New York, USA.
- Sanner, M. F. (1999), 'Python: a programming language for software integration and development.', *Journal of molecular Graphics & Modelling* **17**(1), 57–61.
URL: <https://pdfs.semanticscholar.org/409d/3f740518eafcfaadb054d9239009f3f34600.pdf>
- Schrödinger, LLC (2020), The PyMOL molecular graphics system.
URL: <https://pymol.org/2/>
- Schüttelkopf, A. W. & van Aalten, D. M. F. (2004), 'ProdrG - a tool for high-throughput crystallography of protein-ligand complexes', *Acta Crystallogr.* **D60**, 1355–1363.
URL: <http://prodrG1.dyndns.org/submit.html>
- Selényi, P. (1939), 'Wide-angle interferences and the nature of the elementary light sources', *Phys. Rev.* **56**, 477–479.
URL: <https://link.aps.org/doi/10.1103/PhysRev.56.477>
- Sjölander, D., Bijzet, J., Hazenberg, B. P., Nilsson, K. P. R. & Hammarström, P. (2015), 'Sensitive and rapid assessment of amyloid by oligothiophene fluorescence in subcutaneous fat tissue', *Amyloid* **22**(1), 19–25.
URL: <https://doi.org/10.3109/13506129.2014.984063>
- Sjölander, D., Röcken, C., Westermark, P., Westermark, G. T., Nilsson, K. P. R. & Hammarström, P. (2016), 'Establishing the fluorescent amyloid ligand h-ftaa for studying human tissues with systemic and localized amyloid', *Amyloid* **23**(2), 98–108. PMID: 26987044.
URL: <https://doi.org/10.3109/13506129.2016.1158159>
- Sörgjerd, K., Klingstedt, T., Lindgren, M., Kågedal, K. & Hammarström, P. (2008), 'Prefibrillar transthyretin oligomers and cold stored native tetrameric transthyretin are cytotoxic in cell culture', *Biochemical and Biophysical Research Communications* **377**(4), 1072 – 1078.
URL: <http://www.sciencedirect.com/science/article/pii/S0006291X08020810>
- Squires, G. L. (2001), *Practical Physics*, 4 edn, Cambridge University Press, Cambridge.
-

-
- Stryer, L. (1978), 'Fluorescence energy transfer as a spectroscopic ruler', *Annual Review of Biochemistry* **47**(1), 819–846. PMID: 354506.
URL: <https://doi.org/10.1146/annurev.bi.47.070178.004131>
- Suzuki, K., Kobayashi, A., Kaneko, S., Takehira, K., Yoshihara, T., Ishida, H., Shiina, Y., Oishi, S. & Tobita, S. (2009), 'Reevaluation of absolute luminescence quantum yields of standard solutions using a spectrometer with an integrating sphere and a back-thinned ccd detector', *Phys. Chem. Chem. Phys.* **11**, 9850–9860.
URL: <http://dx.doi.org/10.1039/B912178A>
- Trott, O. & Olson, A. J. (2010), 'Autodock vina: Improving the speed and accuracy of docking with a new scoring function, efficient optimization, and multithreading', *Journal of Computational Chemistry* **31**(2), 455–461.
URL: <https://onlinelibrary.wiley.com/doi/abs/10.1002/jcc.21334>
- Ueda, M. & Ando, Y. (2014), 'Recent advances in transthyretin amyloidosis therapy', *Translational neurodegeneration* **3**, 19–19.
URL: <https://pubmed.ncbi.nlm.nih.gov/25228988>
- Weber, G. (1965), 'Polarization of the fluorescence of solutions subjected to an electric field', *The Journal of Chemical Physics* **43**(2), 521–524.
URL: <https://doi.org/10.1063/1.1696775>
- Zhang, J., Konsmo, A., Sandberg, A., Wu, X., Nyström, S., Obermüller, U., Wegenast-Braun, B. M., Konradsson, P., Lindgren, M. & Hammarström, P. (2019), 'Phenolic bis-styrylbenzo[c]-1,2,5-thiadiazoles as probes for fluorescence microscopy mapping of $\alpha\beta$ plaque heterogeneity', *Journal of Medicinal Chemistry* **62**(4), 2038–2048.
URL: <https://doi.org/10.1021/acs.jmedchem.8b01681>
- Zhang, J., Sandberg, A., Konsmo, A., Wu, X., Nyström, S., Nilsson, K. P. R., Konradsson, P., LeVine III, H., Lindgren, M. & Hammarström, P. (2018), 'Detection and imaging of $\alpha\beta$ 1-42 and tau fibrils by redesigned fluorescent x-34 analogues', *Chemistry – A European Journal* **24**(28), 7210–7216.
URL: <https://chemistry-europe.onlinelibrary.wiley.com/doi/abs/10.1002/chem.201800501>
- Zhang, J., Sandberg, A., Wu, X., Nyström, S., Lindgren, M., Konradsson, P. & Hammarström, P. (2017), 'trans-stilbenoids with extended fluorescence lifetimes for the characterization of amyloid fibrils', *ACS Omega* **2**(8), 4693–4704.
URL: <https://doi.org/10.1021/acsomega.7b00535>
- Zhang, J., Wang, J., Sandberg, A., Wu, X., Nyström, S., LeVine III, H., Konradsson, P., Hammarström, P., Durbeej, B. & Lindgren, M. (2018), 'Intramolecular proton and charge transfer of pyrene-based trans-stilbene salicylic acids applied to detection of aggregated proteins', *ChemPhysChem* **19**(22), 3001–3009.
URL: <https://chemistry-europe.onlinelibrary.wiley.com/doi/abs/10.1002/cphc.201800823>

Additional Results

A.1 Emission and Excitation Spectroscopy

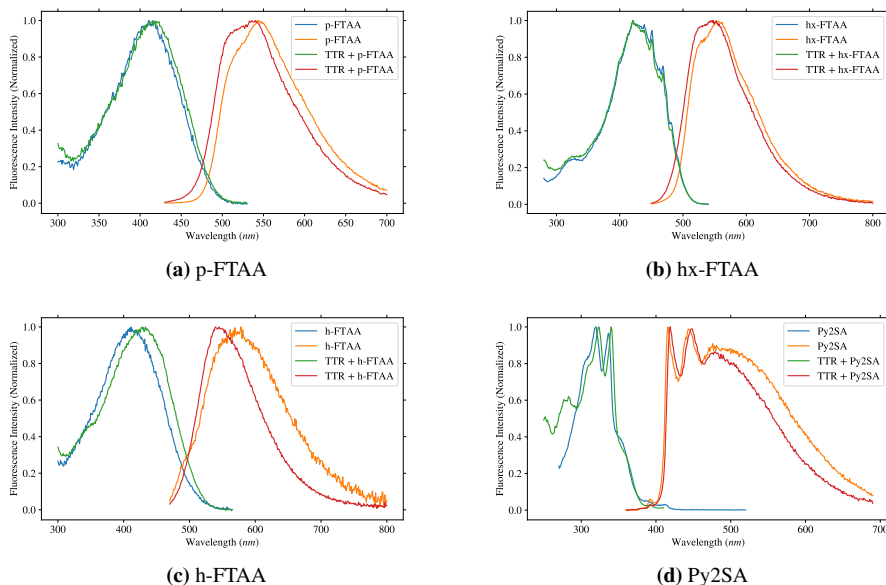
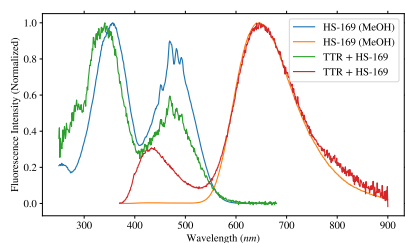
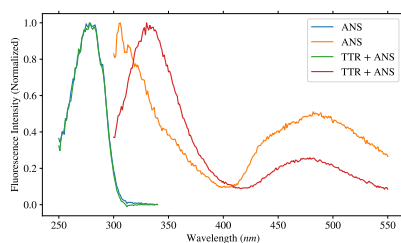


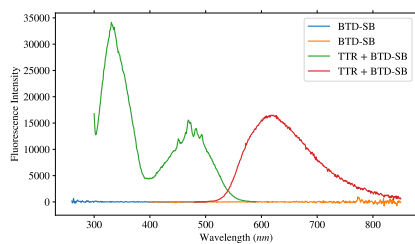
Figure A1: Excitation (green and blue) and emission (yellow and red) spectra of some additional fluorescent probes characterized, with and without the protein TTR. See table 4.2 for more details on each probe, and table 5.1 for changes when the probes are bound to TTR.



(a) HS-169 in MeOH



(b) ANS



(c) BTD-SB. Notice how there are no intensity or signal from the sample containing only the probe and the solvent. The sample is self-quenching.

Figure A2: Excitation (green and blue) and emission (yellow and red) spectra of some additional fluorescent probes characterized, with and without the protein TTR. See table 4.2 for more details on each probe, and table 5.1 for changes in spectra when the probes are bound to TTR.

A.2 The Quantum efficiency

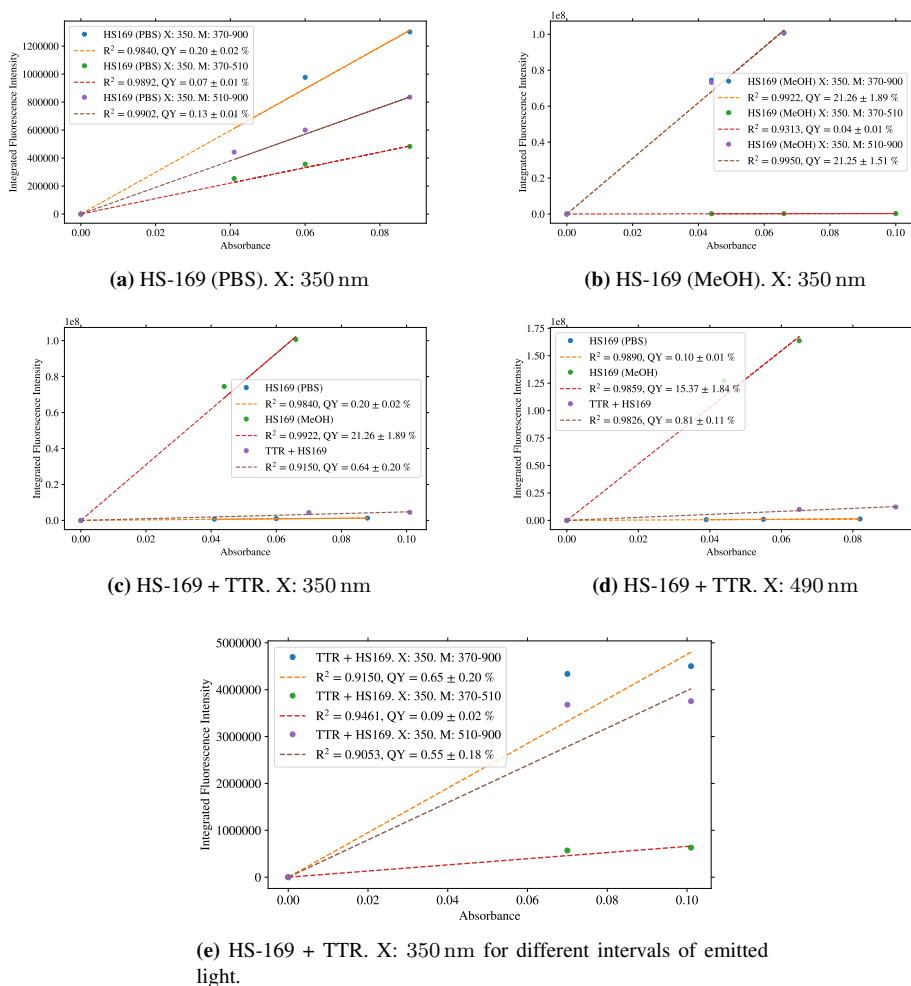
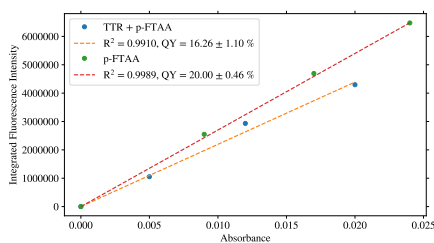
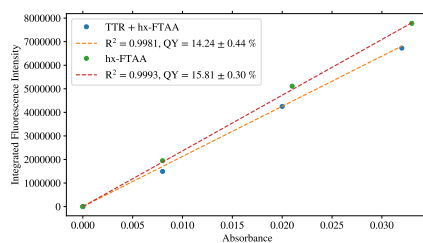


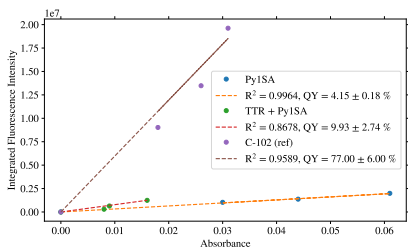
Figure A3: Relative quantum efficiency for samples containing the fluorescent probe HS-169, with and without the protein TTR. HS-169 is both diluted in PBS and MeOH. HS-169 with the protein is diluted in PBS. C-102 and R6G are used as quantum yield standards, depending on the excitation wavelength. See table 4.2 for each figure for the measured and calculated quantum yield, and table 5.1 for the changes when HS-169 are bound to TTR.



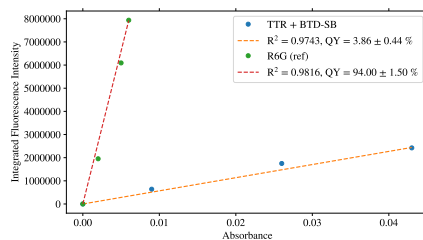
(a) p-FTAA (Aslund et al. 2009)



(b) hx-FTAA



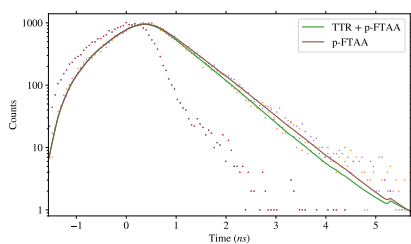
(c) Py1SA



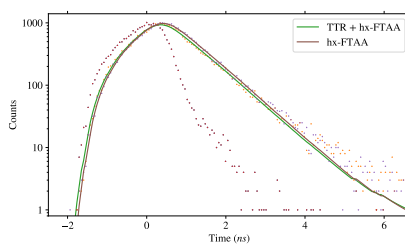
(d) BTD-SB

Figure A4: Relative quantum efficiency for some samples investigated in this thesis, with and without the protein TTR. C-102 and R6G are used as references. See table 4.2 or each figure for the measured and calculated quantum yield. See table 4.2 for more details on each probe, and table 5.1 for the changes in QY when the probes are bound to TTR.

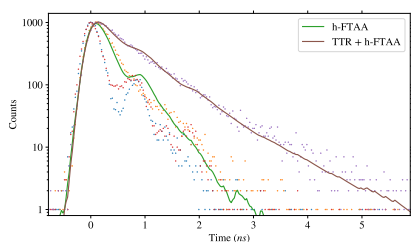
A.3 Lifetime measurements



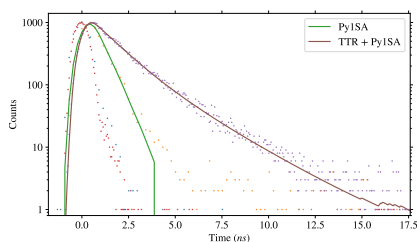
(a) p-FTAA
X: 373 nm, M: 525 nm



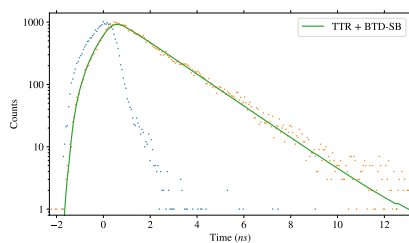
(b) hx-FTAA
X: 373 nm, M: 550 nm



(c) h-FTAA
X: 469 nm, M: 575 nm



(d) Py1SA
X: 337 nm, M: 500 nm



(e) BTD-SB
X: 373 nm, M: 620 nm

Figure A5: Lifetime decay of some fluorescent probes, with and without the protein, TTR, in PBS. The average lifetimes (τ_{avg}) are given in table 4.3. See table 5.1 for the changes when the probe is bound to TTR.

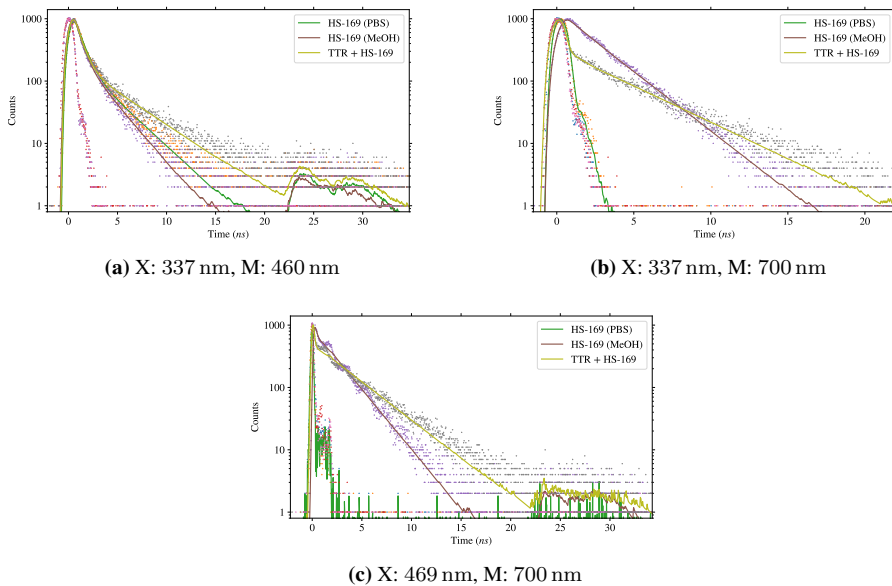


Figure A6: Lifetime decay of the fluorescent probe HS-169 diluted in both MeOH and PBS, with and without the protein, TTR (protein in PBS). The average lifetimes (τ_{avg}) along with the values of its components are given in table 4.3. See table 5.1 for the changes when the probe is bound to TTR.

A.4 FRET measurements

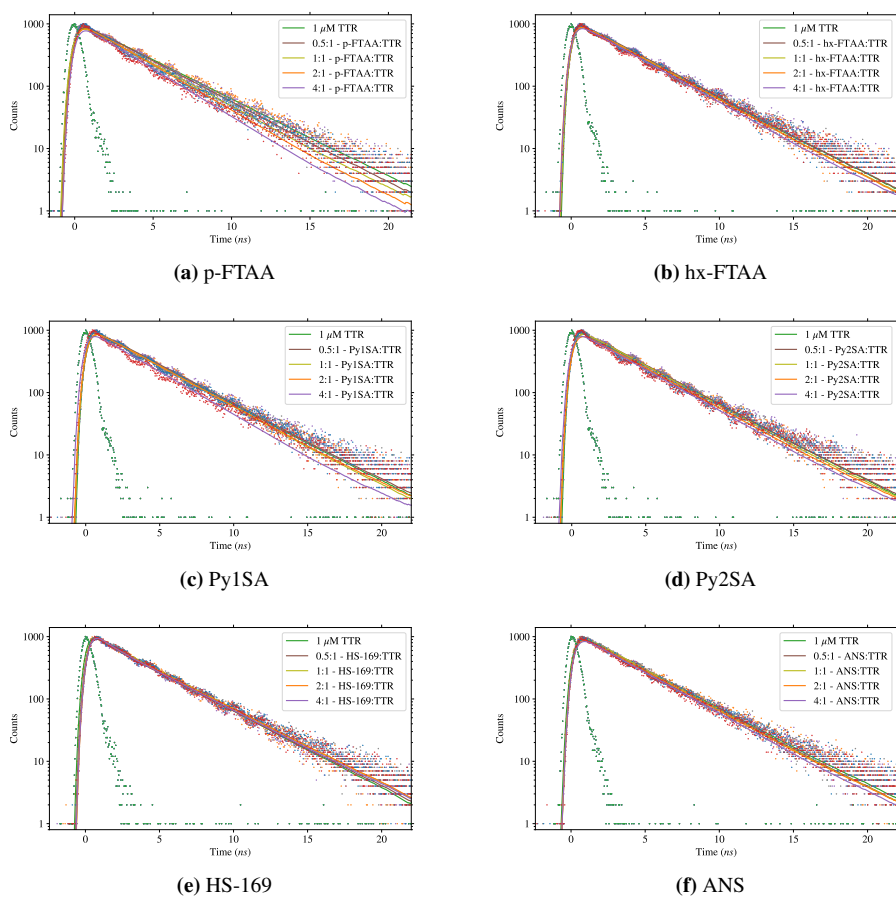


Figure A7: FRET measurements for some of the samples under investigation, using time-resolved method. The donor (D) is TTR and the acceptor (A) is each probe in the figure. The NanoLED with excitation wavelength of 278 nm is used, and the emission is observed at 350 nm. See table 5.3 and table 5.4 for more details regarding the FRET effects for each probe.

A.5 Anisotropy

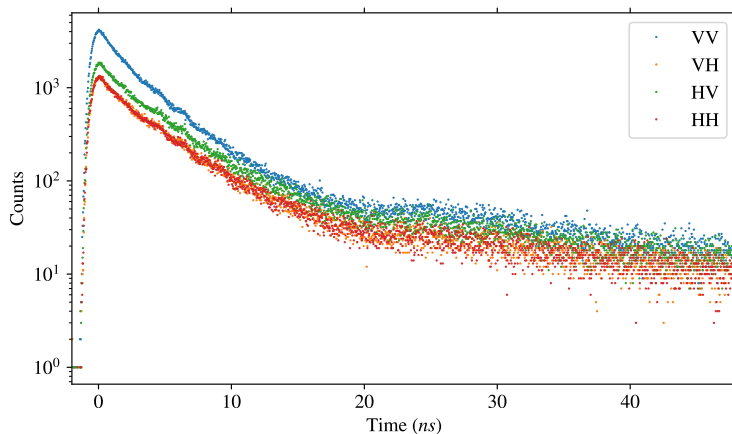


Figure A8: Time dependent steady state lifetime measurements for different polarization of the probe Py2SA diluted in 75 % Glycerol. These measurements are further used to calculate and plot the anisotropy by equation (3.8). Here, the sample is excited at 337 nm, emission measured at 416 nm, and the measuring time was pre-set to 1500 s (25 min). The results of anisotropy can be seen in figure 6.3.

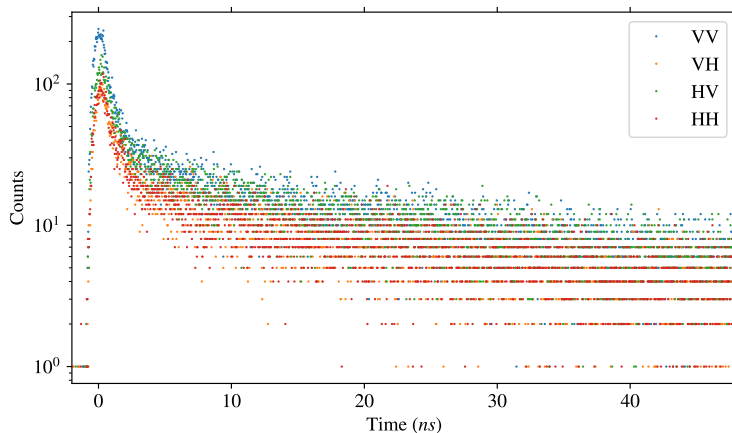


Figure A9: Time dependent steady state lifetime measurements for different polarization of the probe Py2SA diluted in PBS. These measurements are further used to calculate and plot the anisotropy by equation (3.8). Here, the sample is excited at 337 nm, emission measured at 416 nm, and the measuring time was pre-set to 2100 s (35 min). The results of anisotropy can be seen in figure 6.4

A.6 Molecular Docking

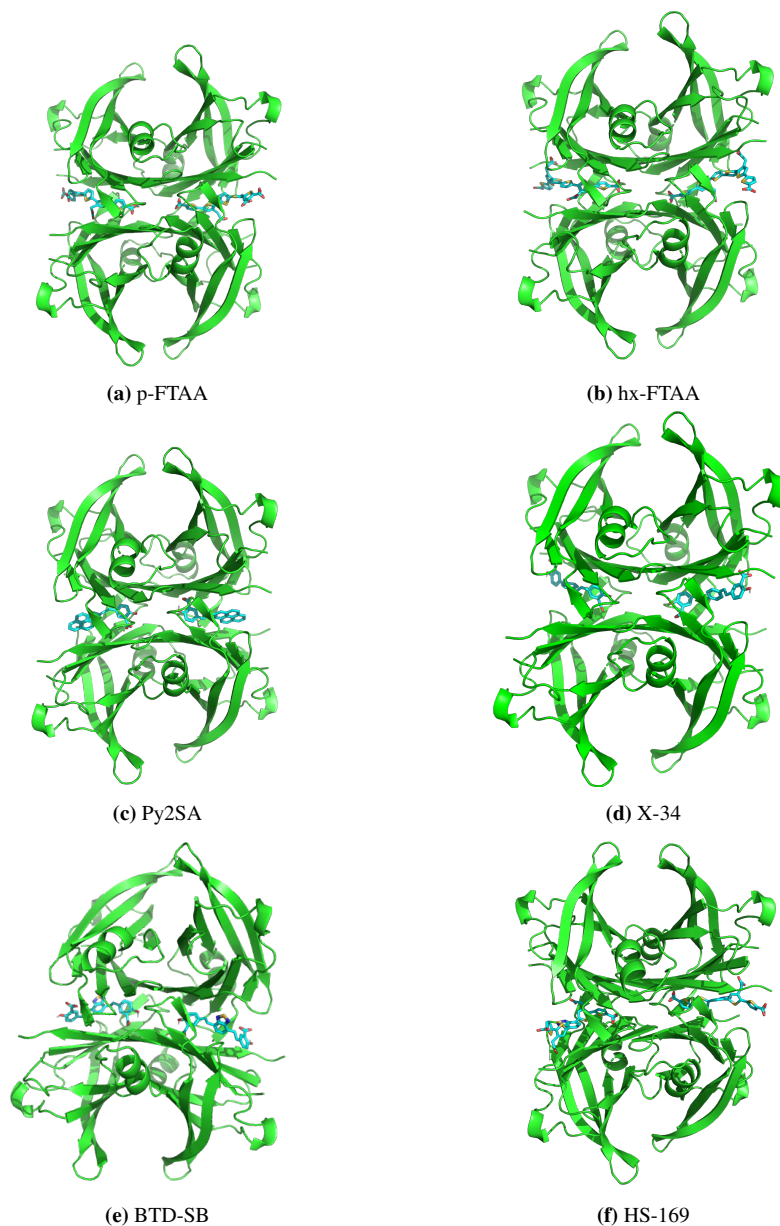


Figure A10: Best docking, best conformation, and best binding affinity of some of the probes docked to the native tetrameric TTR, taken from some different angles. Results calculated with Autodock Vina (Trott & Olson 2010). The chemical representation generated in the software Py-MOL (Schrödinger, LLC 2020).



Figure A11: Best docking, best conformation and best binding affinity of the probe ANS docked to native tetrameric TTR. Results gathered and calculated with Autodock Vina (Trott & Olson 2010). The chemical representation generated in the software PyMOL (Schrödinger, LLC 2020).

Table A.1: Docking results calculated from docking ANS (figure A11) to tetrameric TTR.

Mode	Left binding site			Right binding site		
	Affinity (kcal / mol)	Dist. from best mode rmsd l.b. rmsd u.b.		Affinity (kcal / mol)	Dist. from best mode rmsd l.b. rmsd u.b.	
1	-6.6	0.000	0.000	-6.8	0.000	0.000
2	-6.6	3.035	4.076	-6.8	2.562	3.694
3	-6.4	0.696	1.608	-6.8	0.530	1.188
4	-6.4	2.782	3.775	-6.8	2.603	3.541
5	-6.4	0.877	1.559	-6.5	3.878	7.592
6	-6.3	2.508	5.838	-6.4	3.653	7.169
7	-6.3	2.241	6.107	-6.3	2.396	4.864
8	-6.1	2.444	6.018	-6.3	2.799	5.345
9	-6.1	2.260	5.959	-6.3	3.098	5.600

Table A.2: Docking results calculated from docking p-FTAA (figure A10a) to tetrameric TTR.

Mode	Left binding site			Right binding site		
	Affinity (kcal / mol)	Dist. from best mode rmsd l.b.	rmsd u.b.	Affinity (kcal / mol)	Dist. from best mode rmsd l.b.	rmsd u.b.
1	-7.4	0.000	0.000	-8.2	0.000	0.000
2	-7.3	5.174	10.040	-8.1	4.756	8.776
3	-6.8	7.091	11.786	-7.0	6.841	10.489
4	-6.8	3.948	6.665	-7.0	4.373	11.564
5	-6.7	7.692	13.788	-6.8	4.231	7.149
6	-6.6	5.243	7.426	-6.7	4.053	11.704
7	-6.4	8.394	13.392	-6.7	5.872	9.162
8	-6.1	5.171	7.326	-6.7	6.347	10.014
9	-5.9	7.840	12.856	-6.6	5.413	8.831

Table A.3: Docking results calculated from docking hx-FTAA (figure A10b) to tetrameric TTR.

Mode	Left binding site			Right binding site		
	Affinity (kcal / mol)	Dist. from best mode rmsd l.b.	rmsd u.b.	Affinity (kcal / mol)	Dist. from best mode rmsd l.b.	rmsd u.b.
1	-8.8	0.000	0.000	-9.6	0.000	0.000
2	-8.8	7.350	14.058	-9.6	6.597	13.125
3	-8.8	7.113	14.323	-9.5	6.992	13.241
4	-8.7	7.208	13.307	-9.5	1.237	1.446
5	-8.6	1.699	13.747	-9.2	1.829	2.144
6	-8.2	1.284	13.425	-9.1	7.395	12.632
7	-8.0	7.278	13.213	-8.2	6.358	9.362
8	-7.9	2.391	2.781	-8.1	4.536	13.688
9	-7.7	1.922	13.201	-8.1	3.756	6.831

Table A.4: Docking results calculated from docking Py2SA (figure A10c) to tetrameric TTR.

Mode	Left binding site			Right binding site		
	Affinity (kcal / mol)	Dist. from best mode rmsd l.b. rmsd u.b.		Affinity (kcal / mol)	Dist. from best mode rmsd l.b. rmsd u.b.	
1	-10.0	0.000	0.000	-10.4	0.000	0.000
2	-10.0	0.162	2.274	-10.2	0.241	2.280
3	-9.9	2.026	3.883	-10.2	5.433	6.812
4	-9.8	1.332	3.204	-9.9	5.321	9.009
5	-9.8	1.168	2.157	-9.9	4.304	8.820
6	-9.8	1.674	3.410	-9.9	4.615	9.113
7	-9.7	1.742	2.954	-9.8	5.144	8.678
8	-9.6	0.732	2.832	-9.8	4.310	8.858
9	-9.4	1.444	2.077	-9.7	5.439	8.961

Table A.5: Docking results calculated from docking X-34 (figure A10d) to tetrameric TTR.

Mode	Left binding site			Right binding site		
	Affinity (kcal / mol)	Dist. from best mode rmsd l.b. rmsd u.b.		Affinity (kcal / mol)	Dist. from best mode rmsd l.b. rmsd u.b.	
1	-9.3	0.000	0.000	-9.3	0.000	0.000
2	-9.3	6.498	9.540	-9.3	7.548	11.301
3	-9.2	6.518	9.300	-9.2	7.087	10.987
4	-9.1	6.670	11.380	-9.2	7.006	10.258
5	-9.1	6.614	11.276	-9.1	1.204	11.108
6	-9.1	6.783	11.008	-9.1	1.257	2.036
7	-9.1	1.401	10.997	-9.1	7.081	11.272
8	-9.1	1.741	2.648	-9.0	7.132	11.470
9	-9.1	1.593	2.486	-8.9	1.858	3.062

Table A.6: Docking results calculated from docking BTD-SB (figure A10e) to tetrameric TTR.

Mode	Left binding site			Right binding site		
	Affinity (kcal / mol)	Dist. from best mode rmsd l.b.	rmsd u.b.	Affinity (kcal / mol)	Dist. from best mode rmsd l.b.	rmsd u.b.
1	-8.7	0.000	0.000	-8.8	0.000	0.000
2	-8.7	5.007	7.103	-8.7	4.936	7.201
3	-8.6	1.465	2.734	-8.4	1.412	9.852
4	-8.6	4.918	6.798	-8.4	4.402	11.611
5	-8.5	1.375	9.961	-8.4	4.096	11.899
6	-8.4	0.926	9.803	-8.4	4.941	11.706
7	-8.2	5.416	10.330	-8.3	4.540	12.086
8	-7.8	4.579	9.083	-8.2	4.427	6.754
9	-7.6	5.430	7.282	-8.2	4.058	6.640

Table A.7: Docking results calculated from docking HS-169 (figure A10f) to tetrameric TTR.

Mode	Left binding site			Right binding site		
	Affinity (kcal / mol)	Dist. from best mode rmsd l.b.	rmsd u.b.	Affinity (kcal / mol)	Dist. from best mode rmsd l.b.	rmsd u.b.
1	-9.9	0.000	0.000	-10.0	0.000	0.000
2	-9.9	5.855	11.694	-10.0	5.845	10.439
3	-8.8	16.078	24.823	-9.1	5.862	10.562
4	-8.7	16.840	24.643	-9.0	6.569	10.430
5	-8.6	15.967	25.036	-8.9	5.270	10.285
6	-8.6	16.651	24.647	-8.8	4.932	9.919
7	-7.8	16.237	24.491	-8.8	6.763	10.521
8	-7.7	16.851	24.823	-8.7	3.163	11.631
9	-7.5	6.393	11.887	-8.6	5.118	11.825

